Dissertation

submitted to the

Combined Faculty of Natural Sciences and Mathematics

of the Ruperto Carola University Heidelberg, Germany

for the degree of

Doctor of Natural Sciences

Presented by

M.Sc. Euan Clark

born in: Edinburgh, United Kingdom

Oral examination: 9th December 2019

In Vivo Characterisation of ANKS3

- A New Candidate for Ciliopathic Disease -

Referees: Prof. Dr. Thomas Wieland

Prof. Dr. Hans-Peter Hammes

Aus dem Zentrum für Medizinische Forschung

der Medizinischen Fakultät Mannheim

(Direktor: Prof. Dr. med. Norbert Gretz)

Supervisor: Prof. Dr. Sigrid Hoffmann

FUNDING

This study was supported by the grant of the NIH (5RO1DK100482) to Prof. Dr. Sigrid Hoffmann

Dedication

This thesis is dedicated to my grandfather Robert Burden. From a young age he showed me all the beauty of nature and science and set me on the path I am on.

He is my oldest friend, in age and duration, and I would not be the person I am without him.

TABLE OF CONTENTS

SUMMARY

ANKS3 is an Ank and SAM domain containing protein. It interacts with ciliopathy associated NPHP proteins as well as ANKS6 and the RNA binding protein BICC1 which cause polycystic kidney disease (PKD) when mutated in rodents. The ANKS3 SAM domain is capable of assembling homopolymers and forms large complexes with BICC1. This ANKS3 homopolymerisation is prevented by ANKS6-ANKS3-SAM domain binding. The PKD causing *Anks6*$^{p.R823W}$ mutation prevents ANKS6 from binding to ANKS3 which might result in increased ANKS3-SAM domain homopolymerisation. The function of ANKS3 in mammals is quite unresolved.

This thesis aimed to clarify the role of *Anks3* in rats and the pathophysiological role of ANKS3-SAM domain homopolymerisation in PKD. To this end, we generated novel rat models, using CRISPR/Cas9, carrying either an *Anks3* knockout (*Anks3*^{KO}), an ANKS3-SAM domain deletion (*Anks3*$^{\Delta SAM}$) or a missense mutation in the SAM domain (*Anks3*^{KI}) which prevents ANKS3-SAM domain homopolymerisation but not ANKS3-ANKS6 binding. Furthermore, we crossed the *Anks3*^{KI} rat into the *Anks6*$^{p.R823W}$ PKD rat (TGR*Anks6*) to study the effect of defective ANKS3-SAM domain homopolymerisation in PKD (TGR*Anks6-Anks3*$^{KI/KI}$).

We provide the following crucial results: **1.** The spatial expression pattern of ANKS3 and ANKS6 in the kidney is tightly regulated during development and is disturbed by the *Anks6*$^{p.R823W}$ mutation in PKD rats. The *Anks6*$^{p.R823W}$ mutation decreases aquaporin 2 (*Aqp2*) expression and urinary concentration ability while the defective ANKS3 homopolymerisation in the *Anks3*$^{KI/KI}$ rats increases them, supporting a role of ANKS3 homopolymerisation in water regulation in the kidney. **2.** Defective ANKS3 polymerisation in TGR*Anks6-Anks3*$^{KI/KI}$ rats, retards cyst growth and reverses most pathways altered in TGR*Anks6* PKD rats, including the key signalling pathways Hippo, Wnt and cAMP as well as metabolic pathways. In addition, all DNA replication and repair pathways were upregulated in TGR*Anks6-Anks3*$^{KI/KI}$ rats vs. TGR*Anks6* and vs. wildtype rats. **3.** We provide evidence that the ANKS3-SAM domain, but not ANKS3-SAM domain homopolymerisation, is required for proper morphogenesis in embryos. Both, *Anks3* knockout and ANKS3-SAM domain deletion, results in an embryonically lethal, ciliopathic phenotype including disturbances in organ morphogenesis and laterality defects. Cilia formation did not appear to be disturbed. Expression profiling in *Anks3*$^{KO/KO}$ embryos revealed a significant downregulation of DNA replication and repair pathways vs. wildtype embryos, indicating a significant role of ANKS3 in DNA damage response and repair, which becomes crucial during periods of high proliferative stress, including embryogenesis and PKD. Unlike *Anks6*, the *Anks3* mutations did not cause a PKD phenotype.

Altogether, in the course of this thesis we provided three novel mutated *Anks3* rat models which, for the first time, allow the *in vivo* study of *Anks3* function in mammals and will contribute to further elucidate the molecular pathways of PKD and other ciliopathies, and their interactions.

ZUSAMMENFASSUNG

ANKS3 ist ein Ank und SAM Domänen enthaltenes Protein das sowohl mit Ziliopathien assoziierten NPHP Porteinen interagiert als auch mittels seiner SAM Domäne mit ANKS6 und dem RNA Bindungsprotein BICC1, deren Mutanten in Ratten bzw. Mäusen eine Polyzystische Nierenerkrankung (PKD) induzieren. Die ANKS3-SAM Domäne kann homopolymerisieren und mit BICC1 große Komplexe bilden. Die Bindung der ANKS6-ANKS3-SAM Domänen blockiert die ANKS3 Homopolymerisation. Diese ANKS6-ANKS3 Bindung wird durch die *Anks6*$^{p.R823W}$ Mutation verhindert, die in Ratten PKD verursacht und demzufolge eine ANKS3 Hyper-Homopolymerisation verursachen könnte. Die Funktion von ANKS3 in Säugetieren ist ungeklärt.

Das Ziel der Doktorarbeit bestand daher darin, die in vivo Funktion von *Anks3* und die pathophysiologische Relevanz der Homopolymerisation der ANKS3-SAM Domäne in der PKD zu untersuchen. Dazu generierten wir mittels CRISPR/Cas9 drei neue Rattenmodelle, die entweder einen *Anks3* knockout (*Anks3*^{KO}), eine ANKS3-SAM Domänendeletion (*Anks3*$^{\Delta SAM}$) oder eine Punktmutation in der SAM Domäne hatten (*Anks3*^{KI}), die die ANKS3-SAM Domänen-Homopolymerisation blockierte, die ANKS6 Bindung jedoch erlaubte. Diese *Anks3*^{KI} Ratten kreuzten wir homozygot in die zuvor generierte *Anks6*$^{p.R823W}$ PKD Ratten (TGR*Anks6*) zur Erzeuging der TGR*Anks6*) (TGR*Anks6-Anks3*$^{KI/KI}$).

Folgende wesentlich neue Ergebnisse konnten gewonnen werden: **1.** Das renale Expressionsmuster von Anks3 und Anks6 ist entwicklungsabhängig reguliert und durch die *Anks6*$^{p.R823W}$ Mutation in der TGR*Anks6* PKD Ratte gestört. Die *Anks6*$^{p.R823W}$ Mutation hemmt und die defektive ANKS3 Homopolymerisation infolge der *Anks3*^{KI} Mutation steigert die *Aqp2* expression und letztere auch die Fähigkeit zur Urinkonzentration, was auf eine Rolle der ANKS3-Homopolymerisation bei der renalen Flussigkeitsregulation deutet. **2.** Die defective ANKS3 SAM Domänen-Homopolymerisation in TGR*Anks6-Anks3*$^{KI/KI}$ Ratten reduziert das Zystenwachstum und normalisiert mehr als 100 in der TGR*Anks6* PKD Ratte veränderte Signalwege, darunter die Schlüsselsignalwege für Ziliopathien: Hippo, Wnt and cAMP wie auch zahlreiche metabolische Reaktionswege. Ausserdem sind im Vergleich zu TGR*Anks6* als auch zu Wildtyp-Ratten in der TGR*Anks6-Anks3*$^{KI/KI}$ Ratte alle DNA Damage Response und Reparatur Reaktionswege signifikant verstärkt exprimiert **3.** Sowohl ANKS3 als auch seine SAM Domäne, jedoch nicht die SAM Domänenhomopolymerisation sind essentiell für die korrekte Morphogenese während der Embryonalemtwicklung. Beide Mutanten *Anks3*^{KO} und *Anks3*$^{\Delta SAM}$ sind embryonal letal und zeigen für Ziliopathien typische Defekte einschliesslich Lateralisationsdefekte, wobei die Zilienformation nicht beeintrachtigt ist. Das Expressionsprofil der *Anks3*$^{KO/KO}$ Embryonen zeigte im Vergleich zu Wildtypembryonen eine starke Herunterregulation von Pathways, die zur DNA Damage Response und Reparatur gehören.

Zusammenfassend wurden im Rahmen dieser Arbeit neue *Anks3*-Rattenmutanten generiert, die erstmalig die Untersuchung der *Anks3* Funktionen in Säugern ermöglichte, und völlig neue Erkenntnisse zur Rolle und Funktion von *Anks3* gewonnen. .

ABBREVIATIONS

AC6- Adenylate cyclase 6

ADPKD- Autosomal dominant polycystic kidney disease

Ank- Ankyrin

ANKS3- Ankyrin repeat and SAM domain containing protein 3

Anks3^{KI}- *Anks3*-SAM$^{p.I35E}$

ANKS6- Ankyrin repeat and SAM domain containing protein 6

AQP2- Aquaporin 2

Ca^{2+}- Calcium

cAMP- Cyclic adenosine monophosphate

BBS- Bardet-Biedl syndrome

BICC1- Bicaudal C1

CHD- Congenital heart disease

CFTR- Cystic fibrosis transmembrane conductance regulator

CVH- Cerebellar vermis hypoplasia

EDTA- Ethylenedinitrilotetraacetic acid

ER- Endoplasmic reticulum

ESRD- End stage renal disease

FFPE- Formalin-fixed, paraffin-embedded

GFR- Glomerular filtration rate

GSEA- Gene set enrichment analysis

H&E- Haematoxylin and eosin

HNF1β- Hepatocyte nuclear factor 1β

IFT- Intraflagellar transport

IMCD- Inner medullary collecting duct

INSP3R- Inositol triphosphate receptor

JS- Joubert syndrome

JSRD- Joubert syndrome related disease

KH- K-homology

LCA- Leber congenital amaurosis

MKS- Meckel-Gruber syndrome

MTS- Molar tooth sign

NPHP- Nephronophthisis

OFD- Oral-facial-digital syndrome

P-bodies- RNA processing bodies

PBS- Phosphate buffered saline

PC1- Polycystin-1

PC2- Polycystin-2

PCD- Primary ciliary dyskinesia

PDE- Phosphodiesterase

PFA- Paraformaldehyde

PKD- Polycystic kidney disease

RYR2- Ryanodine receptor 2

SAM- Sterile alpha motif

SHH- Sonic hedgehog

SLS- Senior-Løken syndrome

TGR- Transgenic rat

TGR*Anks6*- TGRhCMV/*Anks6*$^{p.R823W}$

YAP- Yes-associated protein

1- INTRODUCTION

1.1- Cilia structure and function

Cilia are hair-like organelles found on nearly every cell type in vertebrates and have a number of physiological roles. The basic structure of a cilium is an extracellular extension of the cell, containing a microtubule core called the axoneme, generated by the interaction of a basal body with the plasma membrane. The axoneme contains nine peripheral microtubule doublets, each consisting of an A and B strand, and either no core (a 9+0 structure) or a central pair of microtubules (a 9+2 structure). Cilia can also be divided into those with dynein arms connecting the microtubule pairs called motile cilia and those without dynein arms called primary or non-motile cilia. Both motile and primary cilia can exist with or without a microtubule core depending on their function. Primary cilia act as antennae, regulating organ function and homeostasis, or as sensory organelles in the eyes, ears and nose. Motile cilia act as motors used in cell locomotion, including spermatozoa during sexual reproduction, or fluid propulsion. Both types are also involved in embryonic development (figure 1) (1).

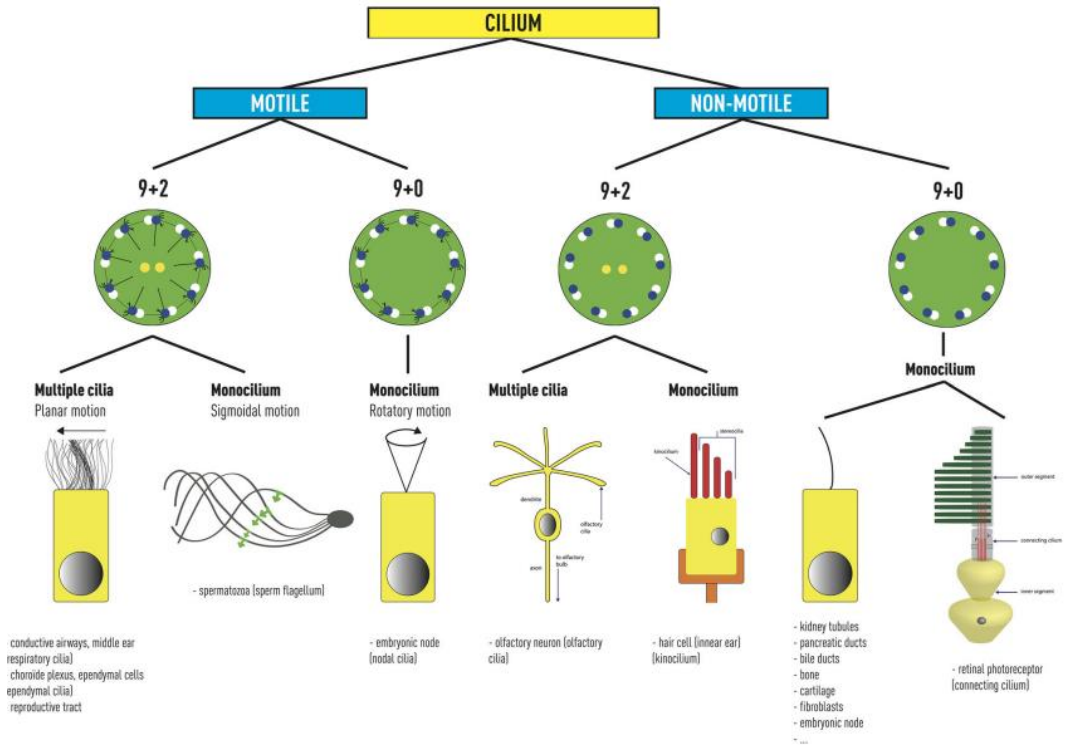

Figure 1- Functions of motile and primary cilia with 9+0 and 9+2 axonemes (1).

In addition to the microtubule doublets, a cilium contains the ciliary gate located around the base of the cilium which regulates the entry of proteins into the cilium and directs their

localisation within. The ciliary gate consists of the basal body outside the cilium and the transition zone, located within the cilium (2). The basal body derives from a mother centriole and organises primary cilia during cell quiescence. On cell cycle entry the basal body migrates to the nucleus and organises the centrosomes. Studies also indicate that

localisation of the basal body may be involved in relating changes from planar cell polarity to cell division. This illustrates the close link between cilia and the cell cycle. The basal body consists of the basal feet, which are anchored to cytoplasmic microtubules and are necessary for polarised alignment of the cilium, and transition fibers that originate from the appendages of the mother centriole. The transition fibres are important in importing parts of the intraflagellar transport (IFT) system (3). The basal body contains several key proteins including sodium channel and clathrin linker 1, CEP164, CEP89, CEP83, fas binding factor 1 and numerous other proteins which give rise to ciliopathic diseases when mutated. The transition zone is characterised by Y-shaped link fibers. One end of the link fiber attaches to a microtubule doublet of the axoneme and the other two bind to the ciliary necklace. The ciliary necklace consists of 3 strands of membrane particles which form rings around the cilium (4). The transition zone also contains two key protein complexes vital to its function; the nephronophthisis (NPHP) complex, consisting of NPHP1, NPHP4 and NPHP8, and the Meckel-Gruber syndrome (MKS) complex, consisting of Tctn proteins, B9 domain proteins, coiled-coil proteins and Tmem proteins (5). The transition zone works with the transition fibres in regulating the flow of proteins and other factors into the cilia and may play a role in loading cargo onto the IFT (6). There are two IFT protein complexes; IFT-B transports cargo from the ciliary gate towards the tip of the cilium, mediated by the kinesin-2 motor and the IFT-A protein complex is driven by the cytoplasmic dynein-2 motor and transports cargo from the tip of the cilium to the ciliary gate (figure 2) (2).

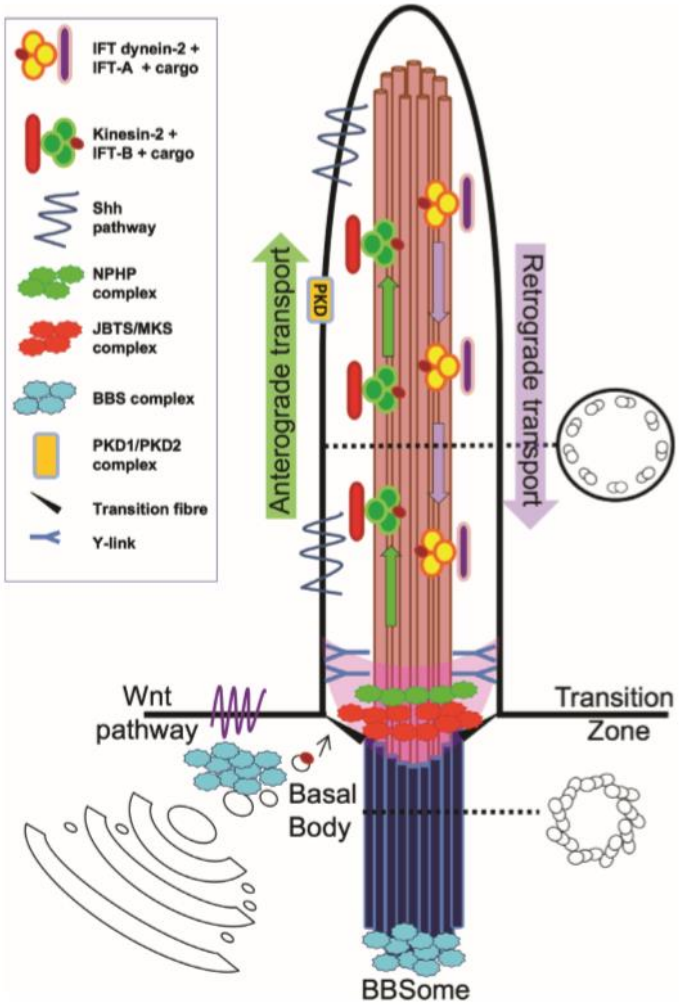

Figure 2- Structure of the primary cilium. Diagram shows the basal body, transition zone and IFT (2).

During early development, motile and primary cilia, both with 9+0 axoneme cores, work together to determine left-right asymmetry. At the embryonic node, centrally placed motile cilia generate a leftward flow of the surrounding fluid which is detected by peripheral primary cilia. This in turn activates Nodal signalling on the left side of the node via calcium (Ca^{2+}) signalling. Nodal signalling is the key determinant in correct left-right organ patterning (7). The primary cilia have a key role in ventral neural tube patterning during embryonic development. Neural tube patterning is controlled by a gradient of sonic hedgehog (SHH) protein, with low expression at the dorsal end to high expression at the ventral end. Shh signalling is the most important factor in regulating the fates of progenitor cells at the ventral end while Wnt and bone morphogenetic protein signalling are the key regulators at the dorsal end (6). The primary cilia are the focal points of the Shh signalling pathway as hedgehog signalling requires the IFT system to activate its targets via Gli transcription factors (8).

In addition to these specific roles in development, the primary cilia have general roles in cell division and migration that are also important in adults. During cell mitosis cilia must disassemble at the S/G2 phases to make the basal body centriole available for mitotic spindle assembly. Progression through the cell cycle is at least partially controlled by competition between proteins promoting either ciliogenesis or disassembly of the cilia. IFT27 and IFT88 promote and inhibit cell cycle progression respectively, (9, 10) while trichoplein inhibits primary cilium assembly and aurora A kinase promotes disassembly of the cilium (11). It is known that a link between cell migration and the primary cilia exists though the exact mechanisms have not been clarified yet. The RhoGTPases are known to be vital in a number of processes including migration and have been shown to localise to the basal body. The primary cilia are also thought to regulate Na^+/H^+ exchange protein 1 expression and its localisation within the plasma membrane in the direction of travel during migration. This is mediated via Pdgfrα signalling which in turn regulates AKT and MEK/ERK signalling (6).

1.2- Ciliopathies

Ciliopathies are a group of diseases which occur due to defects in either the motile or primary cilia. Due to the ubiquitous nature of cilia, ciliopathies can affect every major organ in a range of ways including developmental defects and cystic phenotypes.

Autosomal Dominant Polycystic Kidney Disease (ADPKD)

ADPKD is primarily characterised by the development of large, fluid filled cysts in both kidneys, typically developing into end stage renal disease (ESRD) between the sixth and eighth decade of life. The cysts arise along the length of the tubules and collecting ducts with the majority originating in the distal region in humans. The cysts arise as the epithelium has increased proliferation (leading to fusiform dilation of the tubule), aberrant fluid secretion (filling the cyst) and increased extracellular matrix formation. These fusiform dilations typically detach from the tubule, creating the cysts which continue to grow and be filled by transepithelial secretion, resulting in the compression of nearby structures. Cyst formation is also accompanied by a number of inflammatory events including increased cytokine production, increased formation of inflammatory cells (particularly macrophages) and the formation of interstitial fibrosis which becomes severe by the point of ESRD. Renal cysts can be accompanied by the formation of cysts in other organs, mostly in the liver (arising from the biliary epithelium) but also the pancreas, seminal vesicles and arachnoid membrane. Additionally, cardiovascular abnormalities are common in ADPKD patients,

including arterial hypertension with secondary left ventricular hypertrophy, cardiac valve defects, intracranial aneurysms in around 8 % of patients and other arterial dissections in some rare cases (12).

Estimates of ADPKD incidence are between 1:400 and 1:1,000 (13, 14) with the majority of cases due to mutations in two genes, *PKD1* and *PKD2*, which account for around 80 % and 15 % of cases respectively. *PKD1* encodes the polycystin-1 (PC1) protein which integrates with the plasma membrane at the primary cilia and cell junctions. It consists of a large extracellular domain at the N-terminus, eleven transmembrane domains and a small intracellular tail at the C-terminus. The extracellular domain has several predicted motifs thought to interact with extracellular proteins and carbohydrates. The transmembrane domains form a binding domain for an unknown ligand. Autoproteolytic cleavage of the extracellular N-terminus domain creates a large product which remains non-covalently bound to the transmembrane domains. The last 200 amino acids of the intracellular tail are also cleaved to create a product (PC1-P200) that localises to the nucleus and mitochondria. In the nucleus it interacts with transcriptional regulators of many signalling pathways. In the mitochondria the fragment is reported to have roles in the shape of the mitochondrial network and metabolic flux. The PC1 C-terminus tail also contains a G-protein activation domain specific to heteromeric G_i/G_O and a coiled-coil motif which binds to polycystin-2 (PC2). Furthermore, it interacts with Na^+/K^+-ATPase and increases its activity. At the cell junctions, PC1 provides a link between the extracellular matrix and the intracellular actin cytoskeleton by interacting with actin-binding proteins, focal adhesion proteins and cell adherent junction proteins. The loss of these interactions is thought to cause the formation of aneurysms in ADPKD patients (15).

The *PKD2* gene encodes PC2 which has six transmembrane domains and intracellular C- and N-terminus domains. PC2 also harbours an endoplasmic reticulum (ER) retention signal at its C-terminus and a ciliary localisation signal at the N-terminus. This results in PC2 mainly localising to the ER, but it is also found at the primary cilium and plasma membrane. PC2 assembles a homotetrameric Ca^{2+}-selective transient ion channel. The formation of this channel is mediated by an EF-hand motif and a coiled-coil domain on the C-terminus tail and an oligomerisation signal on the N-terminus tail. PC2 interacts with PC1 via the C-terminus coiled-coil domains on each protein. This interaction is important for the localisation of PC1 and PC2, PC2 Ca^{2+} channel function and for the activation of G_i/G_O proteins by PC1. Additionally, PC2 interacts with cytoskeleton proteins, including actin-

binding proteins and tropomyosin, and mDia1, a protein with roles in microtubule stabilisation and Ca^{2+} homeostasis (15). Patients with mutations in PC2 typically have a later onset of ESRD than those with mutations in PC1.

In addition to *PKD1* and *PKD2*, rare mutations in a few other genes are thought to cause ADPKD. The most common of these is hepatocyte nuclear factor 1β (*HNF1β*). HNF1β upregulates distinct polycystic kidney disease (PKD) associated proteins, including PC1 and PC2, neutral α-glucosidase AB (protein folding) and DNAJB11 (a chaperone protein). Mutations in a number of genes which are primarily involved in autosomal dominant polycystic liver disease can also lead to an ADPKD phenotype. This includes *SEC63* (required for protein transport across the ER membrane) and *PRKCSH* (a subunit of glycosidase 2 which has a role in protein folding) (12).

While the pathogenesis of ADPKD is not fully understood, several key cellular functions and pathways are known to be altered. One of the most important is intracellular and ciliary Ca^{2+} homeostasis which is disrupted by mutations in either *PKD1* or *PKD2*. This occurs due to loss of PC2 channel function or loss of its regulation by PC1, loss of regulation of the inositol triphosphate receptor (INSP3R), ryanodine receptor 2 (RYR2) and piezo1 channel, and changes in Ca^{2+} storage in the ER (15). Ciliary Ca^{2+} concentrations are maintained independently from the rest of the cell and are generally thought to be regulated by the ciliary PC2/PC1 mechanosensitive receptor complex allowing the entry of Ca^{2+} (16). However, at least one study has questioned this (17). PC1 and PC2 act on INSP3R induced Ca^{2+} release from the ER in a competitive manner; PC2 promotes and PC1 inhibits INSP3R. PC2 binds to RYR2 (found in cardiac tissue) when the channel is open, resulting in inhibition of its function, and to the Piezo1 channel (found in renal tubular epithelial cells) decreasing its ability to respond to stretching mechanical stimuli. In addition, PC2 can form channels with either TRPV4, creating a divalent cation channel responsive to thermal and mechanical stimulation of the cilia and epidermal growth factor signalling, or TRPC1, creating a Ca^{2+} permeable channel which localises to the cilia and plasma membrane. The final way that PC1 regulates Ca^{2+} homeostasis is through the large fragment cleaved at its C-terminus. This fragment interacts with the Ca^{2+}-sensor stromal interaction molecule 1 (STIM1), which detects a reduction in ER Ca^{2+} stores. The PC1 fragment inhibits the localisation of STIM1 to the plasma membrane where it would normally activate Orai1 Ca^{2+} channels to replenish lost Ca^{2+}. All of these factors mean that loss of PC1 or PC2 results in decreased Ca^{2+} signalling (15).

Perhaps the most important effect of decreased Ca^{2+} signalling in ADPKD is an increase in cyclic adenosine monophosphate (cAMP) levels. Synthesis of cAMP by adenylate cyclase 6 (AC6) is inhibited by Ca^{2+} and stimulated by vasopressin V2 receptor activity, while cAMP degradation by phosphodiesterases (PDEs) is Ca^{2+}/calmodulin-dependent. Thus, decreases in Ca^{2+} levels results in increased cAMP levels. Increased cAMP levels in turn leads to increased cell proliferation and changes in fluid secretion. cAMP regulates cell proliferation by phosphorylation of the B-Raf protein in the ERK pathway. Phosphorylation activates B-Raf, which also has reduced inhibition by AKT due to the lowered Ca^{2+} levels. cAMP regulates fluid secretion via protein kinase A which affects two main channels: aquaporin 2 (AQP2) and the cystic fibrosis transmembrane conductance regulator (CFTR). Increased cAMP levels activates AQP2 by phosphorylation which also causes its incorporation into the apical plasma membrane. The CFTR channel is hyper activated by cAMP, causing chlorine ions to flow into the lumen. This creates an electrical potential gradient across the membrane, leading to the outflow of sodium followed by water. cAMP activation of the potassium channels Kir6.2 and Kca3.1 in the apical membrane is also necessary for creating this electrical gradient (18).

In addition to ERK there are a number of other pathways dysregulated in ADPKD including Wnt, JAK/STAT, Hippo, JNK and mTOR. The Wnt pathway is essential for normal embryogenesis and is important in adult tissue homeostasis. PC1 and PC2 affect all three Wnt pathways; the canonical, which regulates gene transcription via nuclear accumulation of β-catenin, the non-canonical planar cell polarity and the non-canonical Wnt/Ca^{2+} pathway. The PC1-P200 fragment inhibits the β-catenin destruction complex (GSK3/APC/Axin) in the cytoplasm, resulting in β-catenin accumulation in the cytoplasm and nucleus where it activates, in complex with TCF/LEF, transcription of genes which stimulate proliferation. However, inhibitory effects of the PC1-P200 fragment on Wnt/β-catenin signalling have also been shown. By binding to β-catenin in the nucleus it inhibits TCF dependent gene transcription (15). In ADPKD patients, increased levels of PC1 C-terminal fragments are found in the nuclei, which leads to over-activation of the JAK-STAT pathway. These fragments directly activate STAT3 and STAT6 as well as increasing transcriptional activity of STAT1 and STAT3 via phosphorylation of JAK2. The Hippo pathway is dysregulated in ADPKD patients due to increased localisation of Yes-associated protein (YAP) to the nucleus and inactivation of cytoplasmic YAP by cAMP-induced phosphorylation. JNK signalling is thought to be a principal cause of apoptosis in cyst-lining cells due to dysregulation of the transcription factors c-Jun and AP-1. This is a result of either a loss of

PC1 regulation through Gα and Gβ subunits or loss of PC2 activation of JNK1 and p38 via PKCε. PC1 regulates the mTOR pathway by preventing tuberous sclerosis protein 2 from being degraded and retaining it at the membrane. This inhibits its phosphorylation by AKT, thus reducing mTOR activity. Consequently, in ADPKD patients, the mTOR pathway is overactive (15). Some altered pathways may contribute to the abnormal metabolic features of cells involved in ADPKD. In vitro studies showed that cells lacking PC1 exhibit a Warburg-like metabolic profile with a shift away from oxidative phosphorylation to aerobic glycolysis, as seen in cancer cells, primarily through changes in AMPK, mTOR and sirtuin 1 (19).

Treatment of ADPKD has typically been management of secondary effects including hypertension and pain due to enlarged kidneys. Management of ADPKD can include pharmacological agents or surgical reduction of cysts through fenestration or sclerosis, followed by renal transplant when the patient reaches ESRD. There are some pharmacological agents being developed to slow disease progression. The most heavily investigated class of agents so far has been the vasopressin V2 receptor antagonists. Of these, tolvaptan has been the most studied in ADPKD patients. Tolvaptan aims to lower intracellular cAMP levels in ADPKD patients by specifically inhibiting the vasopressin V2 receptors in the kidney collecting ducts. Patients in a phase IV clinical trial of tolvaptan showed only a 2.8 % increase in cyst volume per year if on tolvaptan, compared to 5.5 % in the placebo group, as well as a significantly slower decline in kidney function. In 2014 it was approved for use in ADPKD patients in Japan, Canada and the European Union. The US approved its use in 2018 after further trials studying its effectiveness in the late stages of the disease and its liver toxicity (20). The somatostatin analogs, octreotide and lanreotide, are also being trialled as possible means of reducing cyst growth by targeting cAMP levels. These act on five G_i proteins which subsequently reduce cAMP production (21).

In addition to pharmacological treatments, dietary interventions have been investigated for reducing cyst growth or glomerular filtration rate (GFR) decline. A small caloric restriction in ADPKD patients has been suggested as a way to target the Warburg-like metabolic phenotype of cystic cells, which should make them more sensitive to energy scarcities. However, while obesity is associated with increased total kidney volume and GFR decline in ADPKD (22) and caloric restriction in animal models of PKD reduces cyst growth (23), studies of caloric reduction in humans have not been conducted. A moderate reduction in sodium intake has been associated with improvements in both GFR decline and total kidney

volume increase (24). The relationship of ADPKD to potassium remains unclear, though studies have suggested a general reduction in chronic kidney disease with increased potassium intake. Increased water intake was theorised to reduce cyst growth via reduced vasopressin concentrations. While initial studies in a rat model of PKD were promising, concurrent studies showed no improvement in a mouse model of ADPKD. The largest study in humans, the CKD WIT trial, showed no significant differences between the groups after a year (25).

Autosomal Recessive Polycystic Kidney Disease (ARPKD)

ARPKD is primarily characterised by enlarged kidneys with fluid-filled cysts and interstitial fibrosis, and ductal plate malformation in the liver. These factors typically develop in utero leading the disease to be diagnosed at or shortly before birth. Between 30 % and 50 % of patients die shortly after birth due to pulmonary hypoplasia causing respiratory insufficiency. Of the survivors, 80 % develop high blood pressure which is resistant to treatment (26). ARPKD has an incidence of 1:20,000-1:40,000 (27) with mutations in the *PKHD1* gene accounting for 80 % of cases (28). This gene encodes fibrocystin, a transmembrane protein which is mostly expressed in the kidney, and to a lesser extent in the liver, in both foetuses and adults. The protein localises to the cilium and basal body (29) where its role is not yet defined though it may play a role in microtubule organisation or sensory functions. It is thought to regulate intercellular adhesion and proliferation by acting as a membrane-bound receptor (30). The severity of the disease correlates with the type of mutation. The disease is often perinatally lethal in patients with two truncating mutations in the gene and more mild in those with missense mutations (31). However, in some cases missense mutations can be as severe as truncating mutations and in around 20 % of families there is a high degree of variability between individuals (32). In addition to *PKHD1*, mutations in the *DZIP1L* gene have been proposed as a cause of ARPKD. The DZIP1L protein localises to the transition zone of the cilium and interacts with proteins involved in maintaining the periciliary diffusion barrier. Patients with mutations in this gene may have a milder phenotype than those with mutations in *PKHD1* as truncating mutations did not result in perinatal lethality (33).

NPHP

NPHP is an autosomal recessive disease with a reported incidence of between 1:50,000 in Finland and 1:1,000,000 in the USA (34). It is primarily characterised by cystic and fibrotic kidneys and is divided into three main subtypes based on the age of onset of ESRD: infantile,

juvenile and adolescent. Juvenile NPHP is the most common form of the disease with symptoms arising from the age of 6 and ESRD occurring at a median age of 13 (35). In juvenile NPHP the first changes seen in the kidney are interstitial fibrosis with very little inflammation, atrophic tubules with thickening of the tubular basement membrane, protrusions in the distal tubules and occasional periglomerular fibrosis. At the later stages of the disease the thickening and atrophy of the tubule basement membrane progresses, as does the glomerular fibrosis which can lead to glomerular collapse. This is accompanied by an increase in inflammation and the presence of small corticomedullary cysts which are associated with dedifferentiation of the tubules in this region. However, unlike ADPKD, these cysts do not cause enlargement of the kidneys (36). These factors manifest clinically as increased urine production (with proteinuria at the late stages), progressively severe anaemia and growth retardation secondary to ESRD (34). Adolescent NPHP, with a mean age of 19 for ESRD, has very similar clinical and pathological features to the juvenile form. Infantile NPHP results in ESRD before the age of 4 and is the rarest of the three subtypes (35). The progression of the disease is both faster and more severe with the kidneys enlarged due to large corticomedullary cysts. In some cases there is associated congenital heart disease (CHD) and situs inversus. In addition to the three widely accepted subtypes, a fourth subtype, adult onset, has been proposed to describe four families with onset of ESRD between 27 and 56 years of age. In around 20 % of NPHP cases there are additional extra-renal manifestations associated with other ciliopathic syndromes, including retinitis pigmentosa from Senior-Løken syndrome (SLS) and the molar tooth sign (MTS) from Joubert syndrome (JS) (36).

There are over 20 genes known to cause NPHP with mutations in *NPHP1* causing around 20 % of cases. The other genes account for a further 15 % of cases, leaving the cause of around two thirds of cases unresolved. *NPHP1* encodes nephrocystin-1 which acts as part of the NPHP1-4-8 complex in the ciliary transition zone. Nephrocystin-1 also interacts with proteins involved in cell-cell adhesion and cell signalling. Of note among the others are NPHP3, INVS (NPHP2), NEK8 (NPHP9) and CEP83 (NPHP18) which can cause the severe infantile form of the disease. NPHP3, INVS/NPHP2 and NEK8/NPHP9 act together as the NPHP2-3-9 complex in the inversin compartment of the cilium. There, the complex has roles in intercellular adhesion, planar cell polarity and switching between the canonical and non-canonical Wnt pathways (36). CEP83 is a centriolar distal-appendage protein involved in centriole to membrane docking which is required for cilia initiation (37). Other NPHP-causing genes are associated with specific extra-renal manifestations. Mutations in *IQCB1*

(*NPHP5*) are associated with NPHP with retinitis pigmentosa as the protein localises to the transition zone of the primary cilia in kidneys and calmodulin and a GTPase regulator in the retinal connecting cilia. *TMEM67* (*NPHP11*), which encodes a protein localised to the transition zone and is required for ciliogenesis, is commonly associated with liver fibrosis, the MTS and perinatal lethality. *CEP290* (*NPHP6*) encodes a centrosomal protein which interacts with TMEM67 and CC2D2A and has roles in ciliogenesis, cell signalling, DNA damage response and cyst formation. Mutations in the *CEP290* gene are linked to NPHP with the MTS and retinitis pigmentosa (36).

The pathogenesis of NPHP has not been fully elucidated however it is generally agreed that the primary cilium is the key player. Nearly all of the known causative genes encode proteins which localise to the cilia, basal body or centrosome. Many NPHP proteins localise to the same areas as other PKD causing proteins, including PC1 and PC2. These proteins may have similar functions even though NPHP and ADPKD have quite distinct pathologies. NPHP has less fluid secretion into the cysts but a much greater degree of fibrosis. Additionally, the pathways involved in the 2 diseases seem to have a high degree of overlap including cAMP, planar cell polarity, DNA damage and ciliary dysfunction. Loss of planar cell polarity in NPHP causes tubule dilation leading to the development of cysts. It is thought to be due to dysregulation of the canonical Wnt pathway which is regulated by INVS/NPHP2. As a result, mutations in this protein and its partners in the NPHP2-3-9 complex are implicated in cystogenesis. Additionally, loss of DCDC2 (NPHP19) leads to activation of Wnt signalling in vitro. CEP164 (NPHP15) interacts with disheveled protein 3, a key component of the Wnt pathway and regulates the switch between canonical and non-canonical Wnt signalling.

Loss of NPHP3, NPHP6 and RPGRIP1L (NPHP8) is linked to dysregulation of the cAMP pathway in vitro which results in increased proliferation. The primary cilium is thought to regulate mTOR signalling through its mechanosensing of flow, resulting in altered cell growth and proliferation. In addition to mTOR, the primary cilium regulates the Shh pathway via translocation of Smoothened protein. As such, dysregulation of the primary cilium may result in altered expression of these pathways. Shh signalling is thought to be particularly closely linked to the transition zone where many NPHP proteins localise, including NPHP1, RPGRIP1L/NPHP8, NPHP4 and CEP290, as well as Smoothened. Several NPHP proteins, including NEK8/NPHP9, CEP164, ZNF423 (NPHP14), SDCCAG8 (NPHP10) and CEP290, can localise to the nucleus and have been implicated in the DNA damage repair pathway. This is most important in times of high proliferation, such as embryonic

development, which is thought to be a reason that complete loss of certain NPHP proteins can result in additional extra-renal developmental manifestations and the severe infantile form of NPHP, while hypomorphic mutations in the same proteins can result in a milder phenotype (36).

Treatment of NPHP currently consists of managing the symptoms, particularly hypertension, followed by renal transplant, after which the disease does not reoccur. Several pharmacological compounds have been tested in animal models of renal cystic disease as possible treatments for NPHP. There is a large overlap of drugs tested for ADPKD and NPHP. These include tolvaptan (a vasopressin V2 receptor antagonist), rapamycin (mTOR antagonist), roscovitine (cyclin-dependent kinases antagonist), purmorphamine (Shh signalling pathway agonist) and FR167653 (p38 MAPK pathway antagonist). To date none of these have been approved for use in NPHP patients and none are curative but they could delay progression in order to allow time to find a suitable donor kidney (34).

Other Ciliopathies

JS is an autosomal recessive disease with an incidence of approximately 1:100,000 in the general population. The primary characteristic of the disease is a mid-hindbrain malformation called the MTS. This is a result of three defects- cerebellar vermis hypo-dysplasia, horizontalised, thickened and elongated superior cerebellar peduncles and deepening of the interpeduncular fossa in the isthmus and upper pons. The MTS causes a number of clinical manifestations including hypotonia, unusual eye movements, developmental delays and ataxia. JS is also associated with polydactyly, facial dysmorphism and defects in other organs including the retina (from Leber's congenital amaurosis (LCA) to progressive retinopathy), kidney (NPHP or cystic dysplastic kidneys) and liver (congenital fibrosis). The variability of phenotypes has resulted in several diseases with the MTS being described which are collectively termed JS related diseases (JSRD) (38). JS has been associated with mutations in at least 35 genes, many of which are also found to be mutated in other ciliopathies (figure 3) (2).

MKS is a lethal autosomal recessive disease with the primary clinical features of posterior fossa abnormailites, bilateral enlarged cystic kidneys and developmental defects of the liver. Secondary characteristics include polydactyly, bending of the long bones, CHD, craniofacial defects (including cleft palate) and microcephaly or anencephaly. The incidence has been estimated at 1:135,000 with 14 genes accounting for 50-60 % of cases. The remaining cases do not have a defined cause, though five further genes have been identified as possible

candidates in some families. There is a high degree of allelism with other ciliopathies including the *TMEM67*, *RPGRIP1L/NPHP8* and *CEP290* genes (figure 3) (39).

Bardet-Biedl Syndrome (BBS) is an autosomal recessive disease with an incidence of around 1:100,000 in North America and Europe (40). The primary clinical features are highly variable but include rod-cone dystrophy, postaxial polydactyly, obesity, mental retardation, hypogonadism and a variety of renal abnormalities. Secondary characteristics of the disease include anosmia, decreased peripheral sensation and mild facial dysmorphism (41-43). 80 % of cases can be linked to mutations in one of 21 genes, with *BBS1* and *BBS10* accounting for 51 % and 20 % of these cases respectively. There is an overlap of several of these genes with other ciliopathies including *MKK5*, *MKS1* and *CEP290*, though a large number are unique to BBS (figure 3) (40).

COACH syndrome is an autosomal recessive disorder with a combination of cerebellar vermis hypoplasia (CVH), oligophrenia, ataxia, colobomas, hepatic fibrosis and the MTS (44, 45). As COACH syndrome is a JSRD, with additional hepatic manifestations, patients exhibit many of the neurological features found in JS. Secondary features include renal cysts and dysmorphic facial features in some cases. As of 2010 around 40 cases had been reported, making it one of the rarest ciliopathies. Mutations in three genes have been identified in these cases: 82 % of families had *TMEM67* mutations (compared to 1 % of JSRD patients without hepatic manifestations), 9 % had mutations in *CC2D2A* and 4 % had mutations in *RPGRIP1L/NPHP8* (45).

Oral-facial-digital syndrome (OFD) is associated with 16 genes and has the primary clinical features of facial dysmorphism, oral defects and polydactyly. OFD has 13 subtypes with secondary features depending on the subtype (46). The most common form is OFDI which is a dominant X-linked disorder caused by a mutation in the *OFD1* gene and has an incidence of around 1:50,000. Its defining features are polycystic kidneys and complete or partial absence of the corpus callosum and is typically lethal in males before birth (47). The other subtypes are autosomal recessive disorders which exhibit a wide array of defects including retinopathy in OFDIX, absence of the tibia in OFDIV and the MTS in OFDVI (46).

SLS has the primary clinical characteristics of retinal lesions (ranging from LCA at the severe end to the milder retinitis pigmentosa) with NPHP (48). There have been reported cases of SLS associated with the MTS which could place it on the spectrum of JSRD (49).

It is one of the rarest ciliopathies with an incidence of around 1:1,000,000 and 7 associated genes (48).

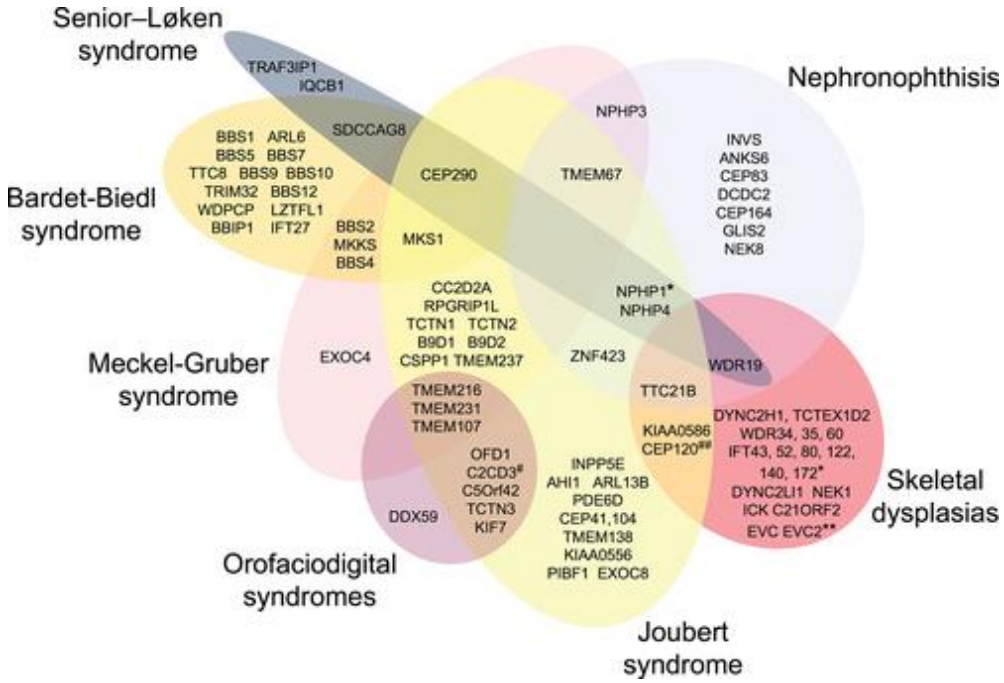

Figure 3– Overlap in genes associated with various ciliopathies (2).

Primary ciliary dyskinesia (PCD), also known as Kartagener's syndrome, occurs due to a defect in the motile cilia. This is unlike the other ciliopathies described here which occur due to defects in the primary cilia. The primary clinical manifestations of the disease are upper and lower respiratory symptoms, including neonatal respiratory distress, due to the inability of the motile cilia to clear mucus from the lungs. This is also accompanied by infertility in all males and asymmetry defects. This includes 6 % of patients with heterotaxy, which is strongly associated with CHD. It has an incidence of 1:10,000-1:20,000 and is associated with 33 genes, mainly genes involved in the dynein arms of the cilia (50).

1.3- Ankyrin repeat and SAM domain containing protein 6 (ANKS6)

1.3.1- ANKS6 structure

Also referred to as *PKDR1*, *NPHP16* and *SamCystin* in the literature, *ANKS6* is conserved in animals including mammals, birds, amphibians and fish (table 1). In both humans and rats, the protein contains 10 ankyrin (Ank) repeats at the N-terminus and a sterile alpha motif (SAM) at the C-terminus with a linking region in between (51). The Ank repeats and SAM domains of these species are highly homologous. SAM domains consist of approximately

70 amino acids formed into five alpha helices arranged in a globular confirmation, and are present in over 1000 proteins across eukaryotes and bacteria. These proteins have a diverse range of functions including protein scaffolding, kinases and regulation of transcription and translation. The range of functions is explained by the SAM domain's ability to form homo- and hetero-SAM domain interactions, which can result in either dimers or polymers, and the ability to bind RNA, with some SAM domains capable of both (52). Ank repeats are another commonly conserved motif consisting of 33 amino acids in 2 alpha helices folded together with a β-hairpin or long loop. They have been predicted in approximately 4000 proteins across all forms of life. Like the SAM domain, Ank repeats have been identified in proteins with a wide range of functions including transport, development, cell-cell signalling and transcriptional regulation. Ank domains function by facilitating protein-protein interactions (53).

Table 1- ANKS6 mRNA transcripts and proteins across animal species.

(there are two validated isoforms of Anks6 in the house mouse, data is shown for isoform 1).

Organism	mRNA transcript length (bp)	Exons	Protein length (aa)	Amino Acid Homology (compared to human)
Homo sapiens (Human)**	7190	15	871	100 % identical
Rattus norvegicus (Norway Rat)*	4367	16	885	85.7 %- identical 89.4 %- positive
Mus musculus (House Mouse)***	3798	15	883	85.6 %- identical 89.5 %- positive
Xenopus tropicalis (Tropical Clawed Frog)*	4214	16	903	63.2 %- identical 75.5 %- positive
Gallus gallus (Chicken)	4031	17	932	66.5 %- identical 76.7 %- positive
Nothobranchius furzeri (Turquoise Killifish)	3495	18	918	60.7 %- identical 73.4 %- positive

*data is provisional, ** data reviewed, *** data validated, other data is predicted

1.3.2- Mutant ANKS6 animal models

In 1989 a spontaneous ADPKD-like phenotype developed in an outbred rat line, named Han:SPRD(cy/+). The line was first established when some ill six month old male rats were dissected and found to have bilateral polycystic kidneys (figure 4). It was also established through further breeding that the phenotype was inherited in an autosomal dominant manner (54). The line was then inbred to allow linkage studies to be performed. This inbred line was called the PKD/Mhm(cy/+) line and was used for further characterisation of the phenotype. In heterozygous animals, cysts develop within four weeks of birth, and 50 % of males die of

uremia between the ages of 12 and 21 months (55). No heterozygous females have been observed to die due to uremia, though some old ones did develop azotemia (55, 56). Homozygous animals died of uremia within three to four weeks after birth (55).

In the two month old heterozygous animals, cysts mainly develop in the inner cortex where 75 % of cysts originate from the proximal tubules. Additional cysts can be found in the outer cortex and some tubule dilation occurs in the outer medulla. At the later stages of the disease when the rats are 12 months old, all tubular segments are dilated or cystic. Initial cyst formation is associated with increased proliferation of the epithelial cells and the formation of patches of dedifferentiated epithelial cells. Dedifferentiation is seen by a loss of the brush border and basolateral interdigitations, and a reduction in lysosomes and reabsorptive vesicles. This progresses to reduced differentiation of the entire epithelium in the latter stages of the disease. These patches of dedifferentiated cells are associated with accumulation of collagen IV and laminin in the extracellular matrix resulting in its thickening (figure 5). Interstitial fibrosis and increased inflammatory cells in the pericystic interstitium are also observed in the heterozygotes (55).

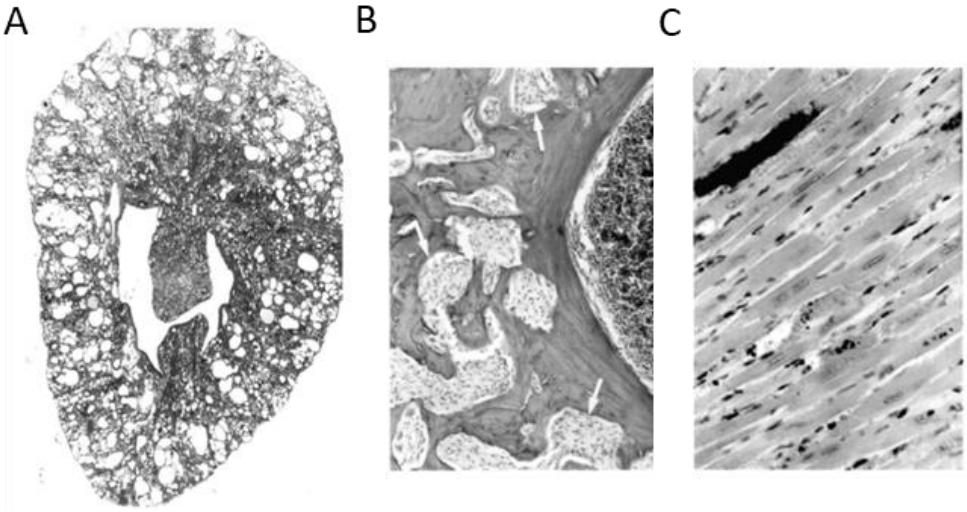

Figure 4- Phenotype observed in the Han:SPRD(cy/+) rat. A- polycystic kidneys, B- osteodystrophia and C- calcification of heart muscle fibres (54).

Extrarenal manifestations observed in the six month heterozygous males include renal secondary hyperparathyroidism, osteodystrophia fibrosa of the skull and femur, and calcification of the kidney, heart, stomach and large arteries (figure 4) (54). Liver and pancreatic cysts were observed in the very old, 21 months of age, female rats at rates of 42 % and 69 % respectively. The liver cysts were similar to those found in human ADPKD patients in the age of occurrence and in their origin in the biliary epithelium. The extra renal cysts also had similar extracellular matrix changes to the renal cysts in the rats (56).

Several differences have been observed between the phenotype in PKD/Mhm(cy/+) rats and human ADPKD. The two key differences are earlier manifestation of the disease in the rats and the origin of the cysts being in the proximal tubules in rats and distal tubules in humans (54). In addition, the rat model does not develop hypertension, has no change in the spatial expression of the Na^+/K^+-ATPase and has a decrease in renin levels, however in human patients renin is increased (55).

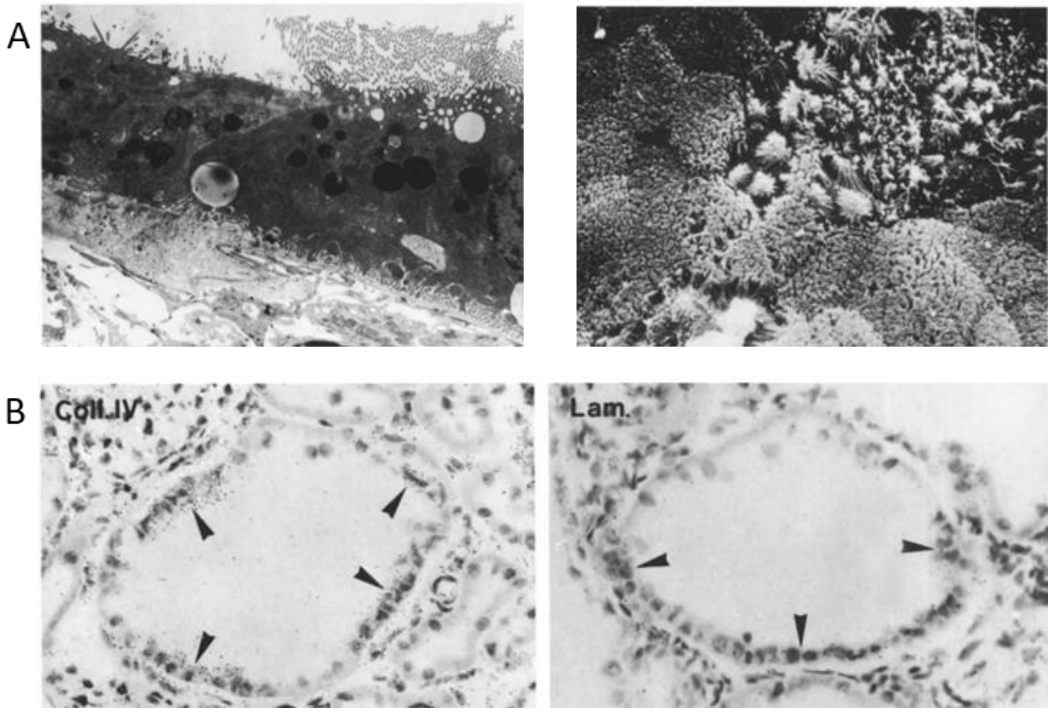

Figure 5– Changes in the tubular epithelium of the PKD/Mhm(cy/+) rat. A- Patches of dedifferentiated cells in the epithelium of Han:SPRD(cy/+) rats showing loss of the brush border, increased basement membrane thickness and loss of basolateral interdigitations (left) and the patches of dedifferentiated cells under a scanning electron micrograph (right). B- Focal accumulation of collagen IV and laminin in the tubules (55).

The PKD/Mhm(cy/+) rat was the only available rat model for human ADPKD. Although the genotype was extensively investigated, the disease causing gene mutation was unresolved for 16 years. Using linkage studies, the gene was determined to be on the rat chromosome 5 and was thus neither *Pkd1* or *Pkd2*, so was originally termed *Pkdr1* (56). This was then further refined by sequencing, to an arginine to tryptophan missense mutation in the SAM domain at the 823rd position of the ANKS6 protein, termed SamCystin at the time. Its low homology to known proteins meant that its physiological role could not be predicted. However, the presence of both Ank and SAM domains indicated a possible role in scaffolding (57). After the *Anks6* gene and p.R823W mutation were identified, the causal link between the mutation and disease was established by the creation of a transgenic rat (TGR) strain which overexpressed the mutant ANKS6$^{p.R823W}$ protein in the tubular

epithelium. It has been shown that this overexpressed mutant protein acts in a dominant negative and dose dependent fashion. The rats carrying the transgene develop similar polycystic kidneys to the PKD/Mhm(cy/+) rat. The first cysts arise in the proximal tubules of the inner cortex, as in the PKD/Mhm(cy/+) rat, at the age of 10 days. Cyst growth was associated with dedifferentiation of the epithelium as well as increased proliferation and apoptosis. These increases were linked to changes in *c-Myc* and *p21* expression which, after kidney development is complete, should decrease and increase expression respectively. This developmental shift did not occur in the *Anks6*$^{p.R823W}$ overexpressing rats (58).

Further studies of ANKS6 in different animal models have been performed, the first being a knockdown of *anks6* mRNA in zebrafish and Xenopus. In the zebrafish this resulted in pronephric cysts and laterality defects. In Xenopus, knockdown resulted in simplification of the pronephros convolute and gross body oedema, typical for defects in renal excretion and seen in *nphp3* and *invs/nphp2* depletion (59).

Furthermore, two mouse models derived from N-ethyl-N-nitrosourea libraries with missense mutations in *Anks6* develop phenotypes associated with ciliopathies. The first of these carries an isoleucine to asparagine mutation in the SAM domain at the 747th position (*Anks6*$^{p.I747N}$). This is only six residues away from the amino acid homologous to the *Anks6*$^{p.R823W}$ mutation in rats, however the phenotypes of the two mutants are significantly different. In the *Anks6*$^{p.I747N}$ mice, renal cysts were only observed in homozygous mutant animals and the disease progression was slower than in the heterozygous PKD/Mhm(cy/+) rats, with an average life expectancy of around 18 months (figure 6). Both tubular and glomerular cysts were observed and the cysts were found to originate predominantly in the collecting ducts and thick ascending limb segment of Henle's loop. Cysts never originated in the proximal tubules, unlike the PKD/Mhm(cy/+) rats where the proximal tubule is the principal origin of cysts (60).

The second mouse model, called *Anks6*^{Streaker}, carries a methionine to lysine mutation at amino acid 187, a highly conserved position within the Ank repeats. The phenotype is recessive and has three primary features: left-right asymmetry (with around 50 % of homozygotes exhibiting heterotaxy and 25 % situs inversus totalis), complex CHD and cystic kidneys. CHD was strongly linked to heterotaxy, with all homozygotes with heterotaxy dying perinatally due to heart defects. Those animals with situs solitus or situs inversus totalis had long term survival without cardiovascular issues in most cases. The CHD found in the heterotaxy animals mostly consisted of atrioventricular septal defects and

transposition of the aorta and pulmonary artery, in several cases both great arteries were attached to the right ventricle. In a few cases right atrial isomerism, muscular or perimembranous ventricular septal defects and inversion or duplication of the inferior vena cava were also observed. In new born animals, renal cysts were extensive in the glomeruli and were accompanied by cystic dilation of the tubules in the juxtamedullary region. This progressed to large corticomedullary cysts and occupation of most of the renal parenchyma with glomerular cysts in 9-10 month old mice (figure 6). The cysts were also accompanied by secondary interstitial consolidation changes and inflammation. Outside the heart and kidney, heterotaxy mutants often showed three or four lung lobes bilaterally and in 50 % of cases aberrant abdominal left-right patterning of the liver, spleen and stomach (61).

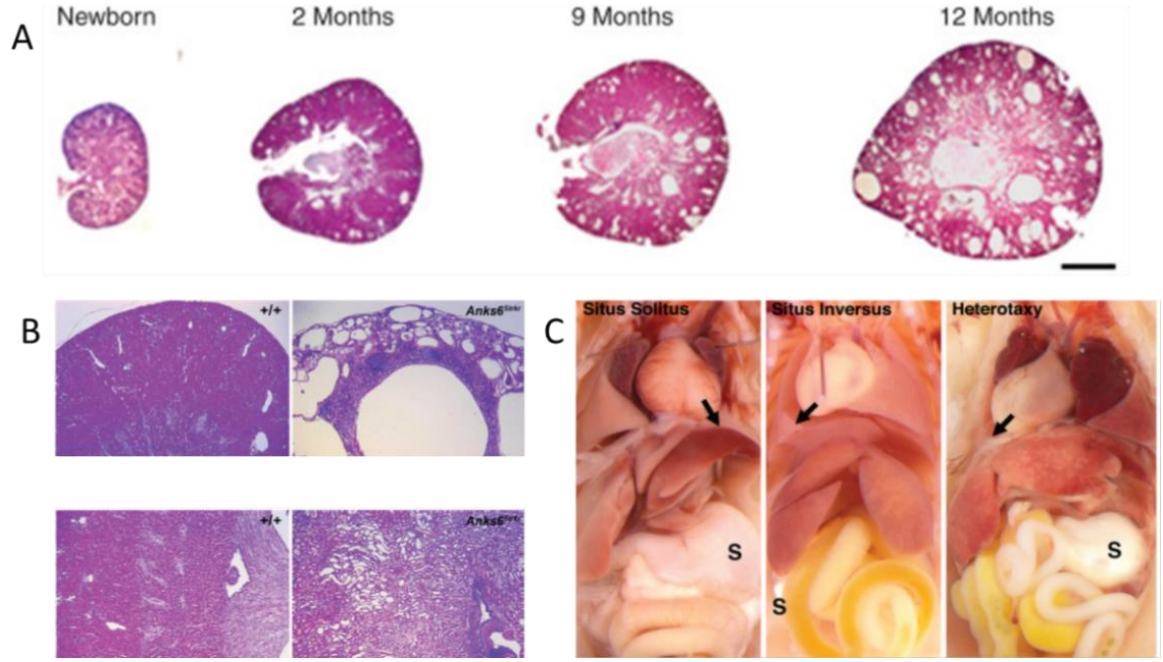

Figure 6- Phenotype of homozygous Anks6$^{p.I747N}$ and Anks6^{Streaker} mice. A- Progression of cyst development in homozygous Anks6$^{p.I747N}$ mice between birth and 1 year of age (60). B- Glomerluar cysts (Top) and tubule dilation in the corticomedullary region (bottom) in Anks6^{Streaker}mice. C- Situs inversus and heterotaxy in Anks6^{Streaker} mice (61).

The human ortholog of *Anks6* was identified on chromosome 9 (57) and subsequent studies in human patients have found mutations in *ANKS6* associated with NPHP-like phenotypes. In some cases the phenotype is similar to the *Anks6*^{Streaker} mice and the Xenopus and zebrafish knockdowns. Cystic kidney and congenital heart defects have been identified in eight patients from six families (59), six members of a consanguineous Turkish family (62) and a Chinese boy (63). Due to the very limited sample sizes the molecular mechanisms have not been investigated in detail.

1.3.3- Interaction partners of ANKS6

The interaction partners of ANKS6 can be broadly divided into those which interact with its SAM domain and those which interact with the Ank repeats. There are currently two known SAM domain interacting partners: Bicaudal C1 (BICC1) and Ank repeat and SAM domain containing protein 3 (ANKS3), which will be discussed later. The BICC1 protein, mutated in the *bpk* and *jcpk* mouse models of PKD, contains three K-homology (KH) domains, which are RNA-binding motifs, at the N-terminus and a SAM domain at the C-terminus. The *jcpk* mouse model was created in a chlorambucil mutagenesis screen and carries a truncating mutation in the first KH domain. In this model, homozygous mutants die at age 7 to 10 days after developing massive cystic kidneys. These cysts first arise in the corticomedullary region but by the time of death are in all parts of the kidney. The cysts are accompanied by tubule dilation in the bile and pancreatic ducts. Heterozygous animals over a year old developed some renal cysts in around 25 % of cases (64).

The co-localisation and binding capabilities of BICC1 with ANKS6 were initially discovered in inner medullary collecting duct (IMCD) cells transfected with recombinant, tagged versions of the proteins. These were observed to co-immunoprecipitate each other and co-localise in the cytoplasm of these cells, though not in the cilia. Using truncated versions of each protein it was determined that the SAM domain of ANKS6 was necessary for the interaction but removal of the ankryin repeats or the *Anks6*$^{p.R823W}$ mutation did not affect it. For BICC1, the SAM domain was necessary for the interaction but it became significantly weaker if the KH domains or the RNA in solution were removed (51). The *Anks6*$^{p.I747N}$ mice provided evidence for the ANKS6-BICC1 interaction playing a significant role in cystic disease as BICC1 precipitated six times more ANKS6 in homozygous mutant animals than wildtype controls. This was associated with increased expression of DVL2 and decreased PC2 expression, both known to be regulated by BICC1 and indicative of defective BICC1 signalling. The data suggests that increased ANKS6 binding can sequester and inactivate BICC1 in these mice. Similarities in the cyst patterning of *Anks6*$^{p.I747N}$ and *Bicc1*^{jcpk} mice also supports this (60). Additionally, in the *Nphp3*$^{p.G2A}$ mouse model, where ANKS6 is no longer phosphorylated, it was shown that BICC1 and ANKS6 binding significantly increased. These mice developed severely cystic kidneys by the age of three weeks, with glomerular cysts and tubule dilation in the early stages. It is unknown if this is related to the ANKS6-BICC1 interaction or the interaction of ANKS6 with proteins at the cilia (65). Further modelling of the interaction of ANKS6 with BICC1 and ANKS3 has been done which will be discussed later.

The interacting partners of the ANKS6 Ank repeats are cilia-related proteins. The first ciliary interaction partner of ANKS6 to be identified was NEK8/NPHP9. The interaction was discovered in a co-immunoprecipitation using NEK8/NPHP9 from HEK293T cells as bait with follow-up mass spectroscopy. ANKS6 was then found to localise to the proximal segment of the cilium, similar to INVS/NPHP2, NPHP3 and NEK8/NPHP9. Additionally, depletion of *anks6* in Xenopus and zebrafish produced a similar phenotype to depletion of *nek8/nphp9* or *nphp3*. These details, combined with similarities in NPHP patients with mutations in *ANKS6*, *NEK8/NPHP9*, *INVS/NPHP2* and *NPHP3*, suggested that ANKS6 was recruited to the cilium as part of the NPHP2-3-9 complex. It was then established that ANKS6 links NPHP3 and INVS/NPHP2 to NEK8/NPHP9, with INVS/NPHP2 localising the complex to the cilium. The linking is strengthened by hydroxylation of ANKS6 by HIF1α (59). It was then demonstrated in IMCD cells that the ANKS6-NEK8/NPHP9 interaction requires the ANKS6-SAM domain and the NEK8/NPHP9 kinase domain and results in phosphorylation of both proteins. Transfection of the cells with a kinase dead form of NEK8/NPHP9 showed that the interaction is not dependant on phosphorylation (61).

1.4- ANKS3

1.4.1- ANKS3 structure

The *ANKS3* gene consists of 15 exons coding a 656 amino acid protein in humans. Similar to ANKS6, ANKS3 contains an Ank repeat domain (with six repeats in humans, rats and mice) at the N-terminus and a SAM domain at the C-terminus (figure 7 and table 2). In addition to the canonical sequence, four isoforms of *ANKS3* have been validated in humans. These isoforms result in the partial or complete removal of the Ank domains. The other domains are preserved across all of the isoforms.

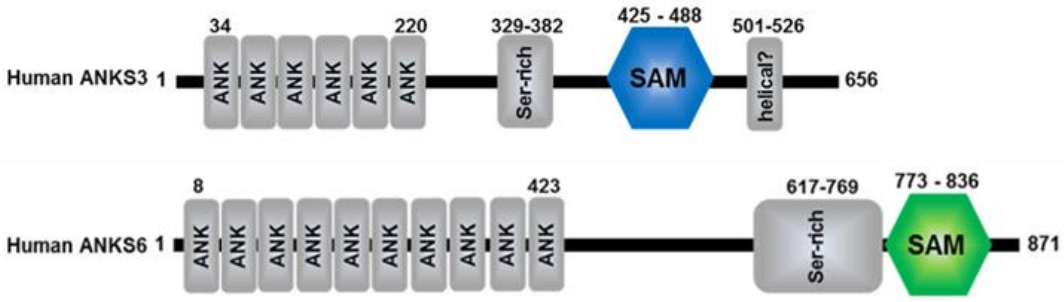

Figure 7- Comparison of human ANKS3 and ANKS6 structures and amino acid numbers of the domains (66)

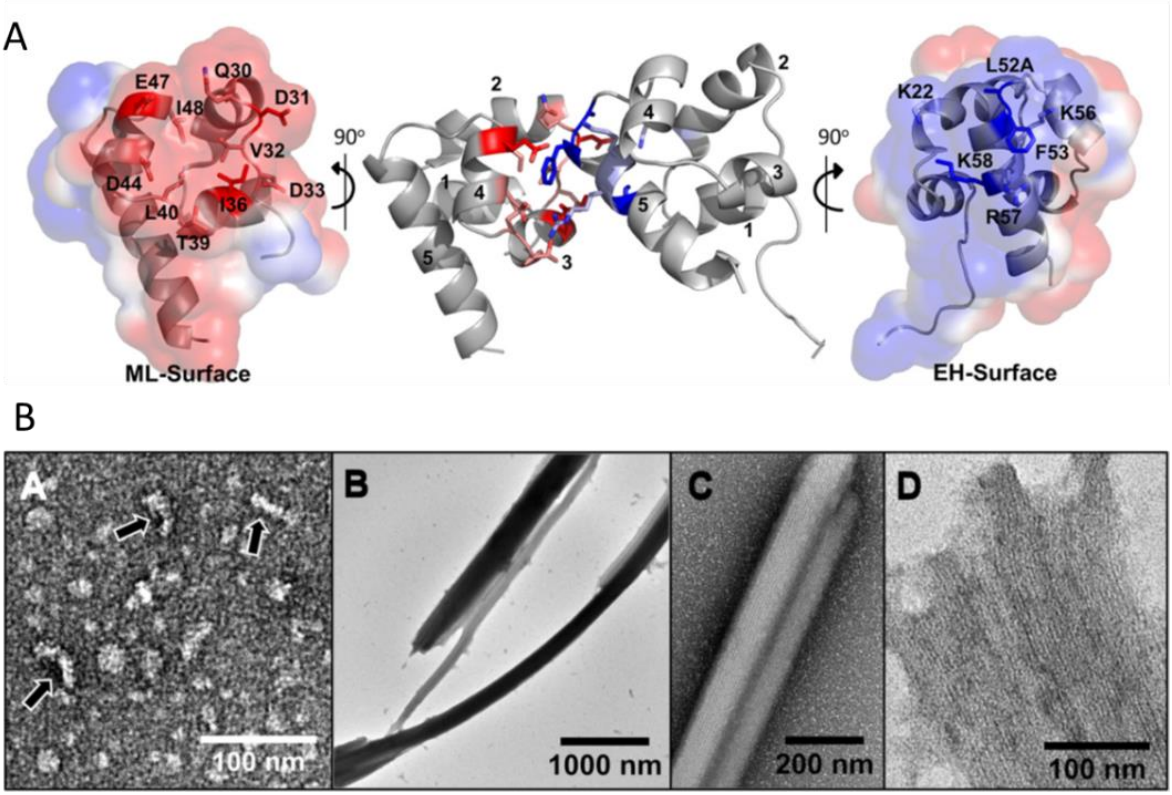

Figure 8- Formation of ANKS3 homopolymeric strands by SAM-SAM interactions. A- Interacting surfaces of the ANKS3-SAM domain (L52A mutation is to allow for crystallisation of the polymer). B- negGFP tagged ANKS3 forms short polymers (leftmost image) and larger polymer sheets when the negGFP is removed (remaining images) (66).

ANKS3 was first identified as having the potential ability to form homopolymers by the mid loop of one ANKS3-SAM domain binding to the end helix of the next SAM domain (67). This is mediated by a four residue hydrophobic patch beside four negatively charged residues on the mid loop interacting with four positively charged residues and a phenylalanine on the end helix. The four charged residues form ionic bonds and the phenylalanine packs the hydrophobic patch. By removing the neg-GFP tag used in the original experiment, it was observed that ANKS3 could form large fibrous sheets in solution which then precipitated (figure 8) (66).

Table 2- ANKS3 mRNA transcripts and proteins across animal species. (There are five validated isoforms of ANKS3 in humans, data is shown for isoform 1).

Organism	mRNA transcript length (bp)	Exons	Protein length (aa)	Amino Acid Homology (compared to human)
Homo sapiens (Human)***	2664	15	656	100 %- identical
Rattus norvegicus (Norway Rat)*	2419	15	663	83.8 %- identical 87.9 %- positive
Mus musculus (House Mouse)***	2483	15	655	81.8 %- identical 87.4 %- positive
Xenopus tropicalis (Tropical Clawed Frog)	2480	17	635	58.9 %- identical 73.7 %- positive
Gallus gallus (Chicken)	4088	18	656	68.1 %- identical 79.5 %- positive
Nothobranchius furzeri (Turquoise Killifish)	2906	16	633	55.5 %- identical 67.9 %- positive

(*data is provisional, ** data reviewed, *** data validated, other data is predicted).

1.4.2- Mutated ANKS3 animal models

Knockdown of *anks3* was first studied in zebrafish embryos using antisense morpholino oligonucleotides. These fish developed pronephric cysts, curvature defects, hydrocephalus and an increased rate of situs inversus, all consistent with an NPHP-like phenotype. It was observed that in these embryos, cilia were present but had reduced or no motility in most cases and beat in the wrong direction a few cases (68). This study was followed up with depletion of *Anks3* mRNA in four day old mice for two weeks using injections of antisense constructs. These mice did not develop any pathological features associated with NPHP. However there was increased expression of *Aqp1, Aqp2* and *Aqp3* (indicating a possible role of ANKS3 in water excretion involving vasopressin), increased proliferation and apoptosis, and changes in the expression of mRNAs for proteins associated with the ciliary axoneme (downregulation of *Gli2* and upregulation of *Nek8/NPHP9*) (69).

In humans, a recessive mutation in *ANKS3* has been reported in two children of a consanguineous Saudi Arabian family, who developed a severe disease associated with situs inversus totalis. The first child died when very young from complex CHD. The second child also had complex CHD: dextrocardia, a single unified atrium, mild narrowing of the aorta, several ventricular septum defects and an interruption of the inferior vena cava between the hepatic and renal veins. In addition, the second child also had mild hypoplasia of the corpus callosum and mild atrophy of the entire brain, resulting in global developmental delay. The mutation was identified as the exchange of a highly conserved histidine at position 147, within the Ank repeats, with an asparagine (*ANKS3*^{H147N}). mRNA of the *ANKS3*^{H147N} variant

did not rescue the *anks3* knockdown phenotype in zebrafish, whereas wildtype *ANKS3* mRNA did (70).

1.4.3- Interaction partners of ANKS3

As with ANKS6, ANKS3 has different interacting partners for its Ank repeats and SAM domain. The first interacting partner described was ANKS6. Inactivating missense mutations in the mid loop and end helix of each protein's SAM domain demonstrated that the interaction occurred through binding of the ANKS6 mid loop to the ANKS3 end helix. The ANKS6 mid loop contains a four residue hydrophobic region with five adjacent negatively charged residues which mediate binding to the ANKS3 end helix, in a similar manner to the ANKS3 mid loop (figure 9). As the extension of ANKS3 polymers requires the availability of both the end helix and mid loop, ANKS3-ANKS6 binding was hypothesised to disrupt formation of these polymers. This was demonstrated by the incubation of Anks6 with the insoluble ANKS3 polymers, which were resolubilised in a dose-dependent manner (figure 9). This effect was completely abolished by the ANKS6$^{p.R823W}$ mutation. This mutation is not in the end helix or mid loop but was found to cause a loss of SAM domain stability and increased unfolding (66, 71). Further research showed that ANKS3 and ANKS6 can recruit the other protein's Ank repeats in pulldown assays, indicating that the Ank repeats may also play a role in this interaction (72).

The other ANKS3-SAM domain interacting partner is BICC1, which can also form homopolymers through its SAM domain. These BICC1 homopolymers have been shown to aggregate in vivo into cytoplasmic puncta. This stabilises the protein and is necessary for translational silencing of mRNA recruited by the KH domains (73). Studies using mutated BICC1- and ANKS3-SAM domains showed that the mid loop of either protein could bind to the end helix of the other, and vice versa, allowing the formation of co-polymers of the two proteins. The truncated BICC1-KH domains and ANKS3 Ank repeats were also shown to bind to full length ANKS3 and BICC1 proteins, though the truncated versions did not interact with each other. These studies also showed that the direct interaction between BICC1 and ANKS6 is extremely weak.

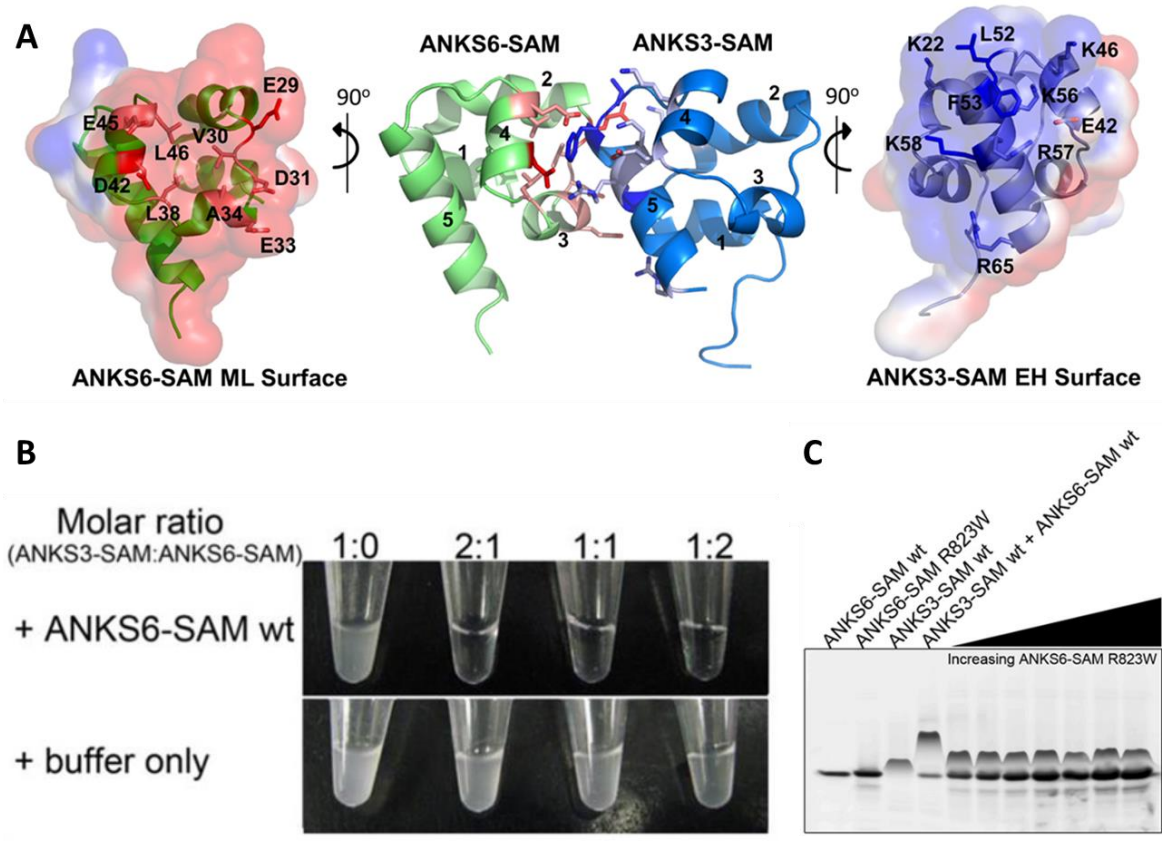

Figure 9- ANKS3-ANKS6-SAM domain interaction blocks ANKS3 homopolymer formation. A- Interacting surfaces of the ANKS6- and ANKS3-SAM domains. B- Resolubilisation of ANKS3-SAM domain polymers by the presence of the ANKS6-SAM domain. C- ANKS6-SAM domain with the p.R823W cystic mutation does not bind the ANKS3-SAM domain(66).

Co-expression of ANKS3, ANKS6 and BICC1 in HeLa cells in different combinations showed that the three proteins can affect each other's intracellular localisation. When expressed alone ANKS3 is diffusely expressed in the cytoplasm, BICC1 forms large cytoplasmic foci and ANKS6 is concentrated at cell protrusions and the cortex below the cell membrane. When ANKS3 was co-expressed with BICC1 or ANKS6 it co-localised with the other protein in cytoplasmic foci with the two proteins evenly distributed in the aggregate. The ANKS6-ANKS3 foci were large while the BICC1-ANKS3 foci were much smaller than those seen when BICC1 was expressed alone. When ANKS6 and BICC1 were co-expressed they did not co-localise. When all three proteins were co-expressed they formed cytoplasmic bodies, larger than any of the previously seen foci, with evenly distributed ANKS6 and BICC1, and ANKS3 concentrated at the periphery (figure 10). BICC1 without the SAM domain was unable to form foci when expressed alone but was partially able to do so when co-expressed with ANKS3 and ANKS6. This further indicates that the interaction is not purely SAM domain to SAM domain. Additionally, co-expression

of *Ac6* mRNA rescued the formation of large BICC1 foci in the presence of ANKS3, with ANKS3 concentrated at the periphery of these foci.

These experiments strongly support an interaction network of BICC1-ANKS3-ANKS6 where BICC1 and ANKS6 bind directly to ANKS3 mainly via the SAM domains. The balance of ANKS3-ANKS6 binding then regulates the formation of BICC1 cytoplasmic foci. mRNA bound to the BICC1-KH domains and the Ank repeats of ANKS3 and ANKS6 also modulate the interaction. It is not initially clear as to what role the formation of these foci have. Initial experiments showed that BICC1 could downregulate AC6 expression with or without ANKS3 or ANKS6. There are indications that these foci are biologically important as though the BICC1^{bpk} mutant protein still binds to ANKS3, it is only partially recruited to the ANKS3-ANKS6 foci with the rest remaining diffused in the cytoplasm (72). These results may be related to the previously observed relationship between BICC1 and RNA processing bodies (P-bodies). It was shown that BICC1 co-localises with P-bodies and the associated stress granules (74). Cytoplasmic clustering of BICC1 has been related to its ability to recruit and silence mRNA but not to its inhibition of DVL2 protein activity. Silencing of mRNA by binding to BICC1 is thought to occur through locally concentrating the mRNA, improving the thermodynamics for silencing factors to bind, or creating secondary RNA structures which present binding sites for miRNAs or proteins (73).

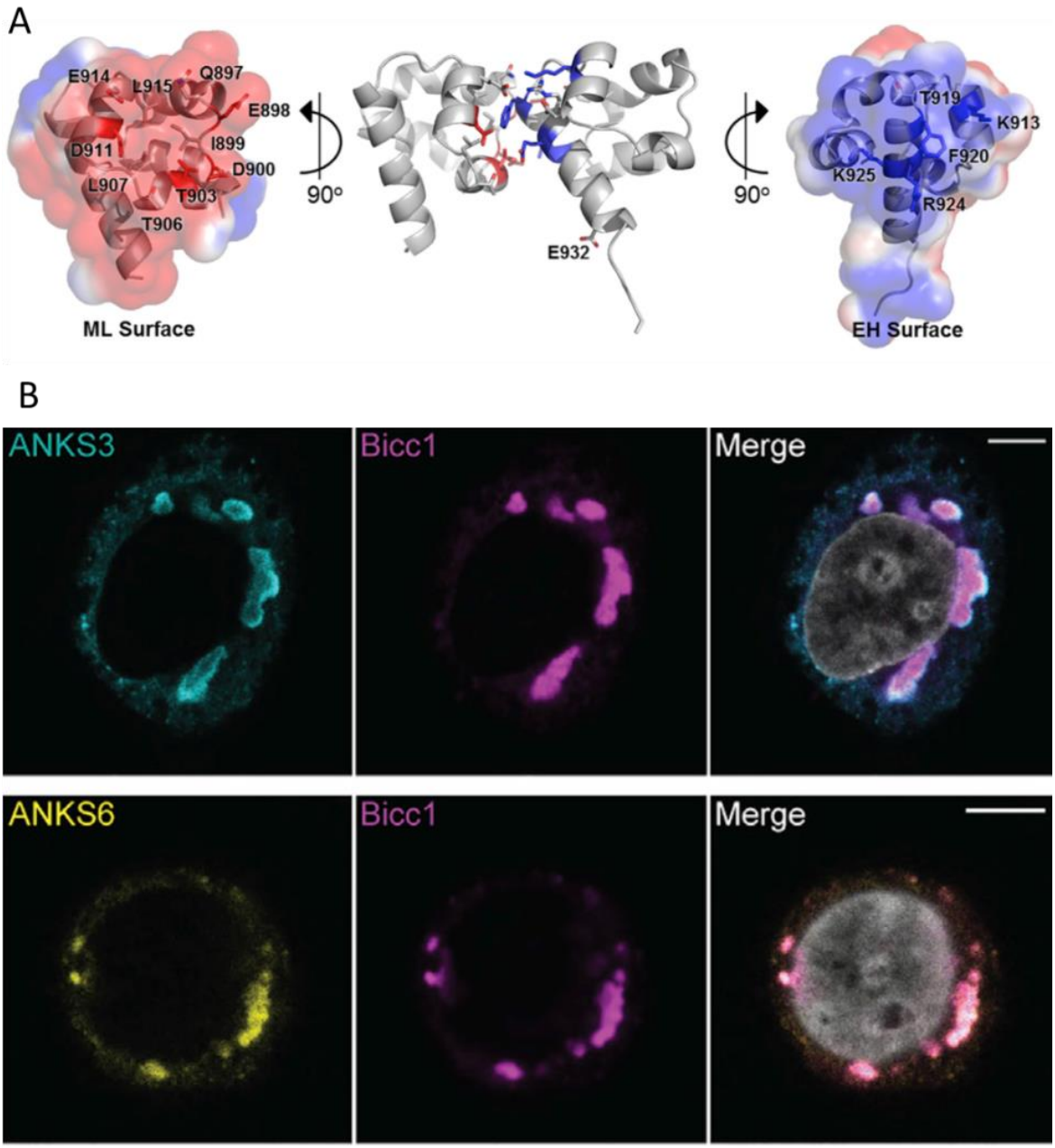

Figure 10– Formation of ANKS3-ANKS6-BICC1 cytoplasmic foci. A- Interacting surfaces of the BICC1 SAM forming homopolymers. B- Formation of large cytoplasmic foci with the co-expression of ANKS3, ANKS6 and BICC1, showing even distribution of BICC1 and ANKS6 and the concentration of ANKS3 in the periphery (72).

In addition to ANKS6 and BICC1, ANKS3 interacts with the NPHP1-4-8 complex. The direct interaction appears to occur between NPHP1 and ANKS3 with the two proteins most strongly co-precipitating each other. Transfection of Xenopus embryos with GFP-tagged ANKS3 showed NPHP1 co-localising with ANKS3 in the basal body of the cilia with some small clusters of ANKS3 in the cytoplasm. However, when NPHP1 was depleted, localisation of ANKS3 to the basal body was partially lost and the cytoplasmic clusters, potentially the BICC1 foci, were significantly increased in size. NEK8/NPHP9, a partner of

ANKS6 in the NPHP2-3-9 complex, was also shown to be capable of associating with ANKS3, though the ANKS3-NPHP1 interaction is stronger. Whether the ANKS3-NEK8/NPHP9 interaction is a direct connection or occurs via ANKS6 has not been established (68).

ANKS3 also interacts with NEK7 via its Ank repeats. This interaction results in a significant increase in the molecular weight of ANKS3. The modification occurs even when bound to a kinase-dead NEK7 and after incubation with a phosphatase. This indicates that NEK7 is not directly responsible for the modification and may instead recruit other proteins. When NEK7 was overexpressed alone it localised to the cytoplasm and nuclei, however when co-expressed with Anks3 it was no longer found in the nuclei. Therefore this ANKS3-NEK7 interaction may be related to the role of NEK7 in mitotic progression (75).

HIF1AN has been shown to hydroxylate ANKS3 at residues in the Ank domain. The physiological role of this has not been investigated but may be similar to ANKS6 where the hydroxlation strengthens its interaction with the ciliary complex (68).

2- AIMS

ANKS3 is still a poorly characterised protein. It interacts with ANKS6, which causes an ADPKD-like phenotype in rats through a missense mutation in its SAM domain, but also interacts and operates with NPHP protein complexes. The ANKS6-ANKS3 interaction via the SAM domain is disrupted in *Anks6*$^{p.R823W}$ PKD rats. Thus, we conclude that the ANKS3-SAM domain and its interaction with ANKS6 might be involved in PKD disease. Additionally, previous experiments showed that ANKS6 prevents ANKS3 homopolymer formation. The *Anks6*$^{p.R823W}$ mutation blocks ANKS6 binding to ANKS3 and, consequently, should increase the ability of ANKS3 to form homopolymers. The in vivo role of ANKS3 in mammals remains completely unknown. Thus, the present work aimed to investigate the following points:

1. Spatio-temporal expression pattern of ANKS3 and ANKS6 in the kidneys of wildtype and PKD/Mhm cystic rats; an ANKS3-ANKS6 interaction can only have relevance in cells where they are co-expressed.
2. The role of ANKS3-SAM domain polymerisation in the TGR*Anks6* model of ADPKD.
3. The effect of *Anks3* knockout and *Anks3*-SAM domain deletion in vivo.

We approached these aims by creating several new rat lines with mutations in the endogenous *Anks3* gene. This included a total knockout of *Anks3*, deletion of the ANKS3-SAM domain and a point mutation in the ANKS3-SAM domain to block ANKS3-SAM domain homopolymerisation.

3- MATERIALS AND METHODS

3.1- Materials

3.1.1- Reagents

Table 3- List of reagents used.

Reagent	Company	Order Number
16 % Paraformaldehyde (PFA) Solution	Thermo Fischer	15710
2,2'-Azobis[2-(2-imidazolin-2-yl) propane] Dihydrochloride (VA-044)	FUJIFILM Wako Chemicals	925-41020 - VA-044
2 % Bisacrylamide Solution	Bio-Rad	1610142
40 % Acrylamide Solution	Bio-Rad	1610140
Acetic Acid (Glacial) 100 %	Merck	1.00063.2511
Aniline Blue Diammonium Salt	Sigma Aldrich	415049-25G
Aniline Oil ≥99.5 %	Sigma Aldrich	3535395-100ML
Agarose	Biozym	Art# 840004
Bromophenol Blue	Sigma Aldrich	B0126-25G
Bovine Serum Albumin (Heat Shock Fraction) ≥98 %	Sigma Aldrich	A9647-50G
Chloroform	Merck	1.02445.1000
Ethylenedinitrilotetraacetic Acid (EDTA)	Sigma Aldrich	1233508 USP
UltraPure Ethidium Bromide, 10 mg/mL	Invitrogen	15585011
Ethanol ≥99.8 %	Roth	K928.4
37 % Formaldehyde	Merck	K25344503
Eosin Y	Sigma Aldrich	E4009-25G
25 % Glutaraldehyde	Roth	3778.1
Hematoxylin Solution	Merck	1051741000
37 % Hydrochloric Acid	J.T. Baker	6011
Hydrogen Peroxide	J.T. Baker	7047
Isopropanol	Roth	6752.1
Mayer’s Haemalum	Merck	HX071163
Methanol	Roth	8388.6
Orange G	Sigma Aldrich	O7252-25G
PFA	Sigma Aldrich	P6148-1KG
Phosphotungstic Acid Hydrate	Merck	100582.01
KH_2PO_4	J.T. Baker	0240
Potassium Chloride	Sigma Aldrich	60129-2504
Protease Inhibitor Tablets	Roth	12037300
Na_2HPO_4	Merck	F1099059 534
Sodium Acetate	Sigma Aldrich	S2889
Sodium Acrylate (97 %)	Sigma Aldrich	408220-100G
Sodium Chloride	Sigma Aldrich	S3014-1KG
Sodium Dodecyl Sulphate	Sigma Aldrich	L4509-500G
Sodium Hydroxide	J.T. Baker	0288
Sucrose	Sigma Aldrich	S0389-1KG
Sytox Green	Invitrogen	10768273
Trisodiumcitrate-Dihydrate	Merck	A967048 905
Triton X-100	J.T. Baker	2840
Trizma Base	Sigma Aldrich	T6066-1KG
Tween-20	J.T. Baker	7374
Xylene	J.T. Baker	3410

Table 4- List of antibodies used.

Antibody	Company	Order Number
GAPDH (FL-335)	Santa Cruz	Sc-25778
ANKS3 (S-13)	Santa Cruz	Sc-138124
ANKS6 (G-15)	Santa Cruz	Sc-162531
AQP2 (C-17)	Santa Cruz	Sc-9882
Acetylated Tubulin	Sigma Aldrich	T7451-200UL
KI-67	Dako	M7248
goat anti-rabbit IgG-HRP	Pierce	1858415
donkey anti-goat IgG-HRP	Santa Cruz	Sc-2020
goat anti-mouse IgG-HRP	Santa Cruz	Sc-2061
AlexaFluor 647 chicken anti-mouse IgG	Life Technologies	A21463

Table 5- List of enzymes and buffers used.

Enyzme/Buffer	Company	Order Number
RNase A	Sigma Aldrich	10109142001
Proteinase K	Thermo Fisher	AM2542
SuperHotTaq DNA Polymerase	Bioron	119010
EcoRI	Invitrogen	15202039
10X Buffer H	Invitrogen	A4001A
Superscript III	Invitrogen	P/N56575
5x First Strand Buffer	Invitrogen	Y02321

Table 6- List of kits used.

Kit	Company	Order Number
QIAquick Gel Extraction Kit	Qiagen	28706
RNeasy Mini Kit	Qiagen	74106
Platinum PCR Kit	Invitrogen	13000013
Peroxidase Substrate Kit DAB	Vector	SK-4100
Vectastain ABC Kit	Vector	PK-6100
Quantitect SYBR Green PCR Kit	Qiagen	204143

Table 7- List of consumables used.

Item	Company	Order Number
4-12 % Bis-Tris Acrylamide Gel	Invitrogen	NP0321BOX
Immobilon-P Transfer (PDVF) Membrane	Merck	IPV1-100010
Clariom^{TM} D Array, Rat	Thermo Fisher	902632
GeneChip RaGene2.0 ST Array	Thermo Fisher	902124
Precision Plus Protein Dual Color Standards	Bio-rad	#161-0374
100bp DNA Ladder	Bioron	304005
Random Primers	Promega	C118B
RNasin	Promega	N211B
0.1M DTT	Invitrogen	Y00147

3.1.2- Solutions

Table 8- List of pre-prepared solutions used.

Solution	Company	Order Number
Pierce Protein-Free T20 Blocking Buffer	Thermo Fischer	37573
Bradford Reagent	Bio-Rad	500-0006
MES SDS Running Buffer	Novex	NP0002
20X Transfer Buffer	Novex	NP0006-1
Restore Western Blot Stripping Buffer	Thermo Fisher	21059
Western Blot Luminol Reagent	Santa Cruz	sc-2048
NuPAGE Sample Reducing Agent	Invitrogen	NP0009
NuPAGE 4x LDS Sample Buffer	Invitrogen	NP0007
TRIzol	Ambion	15596018
RIPA Lysis and Extraction Buffer	Thermo Fisher	89901

Acetic Alcohol

- 10 ml acetic acid
- Make up to 1 L with 96 % ethanol

Acrylamide Hydrogel Solution

- Make on ice and protect from light
- 25 ml 40 % acrylamide solution
- 1.25 ml 2 % bisacrylamide solution
- 12.5 ml 16 % PFA solution
- 5 g sodium acrylate
- 0.5 ml 10 % VA-044 in 1 x phosphate buffered saline (PBS)
- 5 ml 10 x PBS
- Make up to 50 ml with ddH_2O
- Centrifuge for 3 min at 1000 g
- Take upper transparent solution

Aniline Alcohol

- 1 ml aniline oil
- Make up to 1 L with 96 % ethanol

Aniline Blue-Orange G Solution

- 5 g aniline blue
- 20 g orange G
- 800 ml ddH_2O
- 80 ml acetic acid
- Make up to 1 L with ddH_2O

0.1 % Azocarmine G

- 1 g azocarmine G
- 800 ml ddH_2O
- Heat for 1 hour then cool to room temperature
- 6 ml glacial acetic acid
- Make up to 1 L with ddH_2O, filter

10mM Citrate Buffer

- 2.94 g trisodiumcitrate-dihydrate
- 1 L of ddH_2O
- pH to 6.0-6.2

Denaturing Solution (Expansion microscopy)

- 25 ml 10 % SDS solution
- 1.25 ml 5 M NaCl
- 12.5 ml 1 M Tris (pH 9.0)
- 5 ml 10 x PBS
- Make up to 50ml with ddH_2O

10x DNA Loading Buffer

- 4 g sucrose
- 2.5 mg bromophenol blue
- 10 ml TE buffer

0.5M EDTA (pH 8.0)

- 186.1 g EDTA
- 800 ml ddH_2O
- pH to 8.0 with NaOH
- Make up to 1 L with ddH_2O, autoclave

Eosin Y Stock

- 1 g eosin Y
- 20 ml ddH_2O
- Mix until dissolved
- 80 ml 95 % ethanol
- For working solution add 300 ml of 80 % ethanol and 2 ml of glacial acetic acid per 100 ml of stock solution

Immunohistochemistry Blocking Solution

- 1 g BSA
- 5 0µl Triton X-100
- Make up to 50 ml with PBS

4 % PFA

- 40 g PFA
- 100 ml 10x PBS
- 700 ml ddH_2O
- Add 3-4 drops of concentrated NaOH
- Heat with stirring until dissolved
- pH to 7.4 with NaOH
- Make up to 1 L with ddH_2O, filter and store at -20°C

10x PBS

- 80 g NaCl
- 2 g KCl
- 2.4 g KH_2PO_4
- 14.4 g Na_2HPO_4
- Add 800 ml ddH_2O
- pH to 7.4 with HCl
- Make up to 1 L with ddH_2O, autoclave

Phosphotungstic Acid

- 50 g phosphotungstic acid hydrate
- Make up to 1 L with ddH_2O

Proteinase K

- 100 mg proteinase K
- 10 ml ddH_2O, aliquot and store at -20°C

RNase A

- 100 mg RNase A
- 10 ml 10mM sodium acetate
- Heat to 100°C for 15 minutes, cool to room temperature
- Adjust the pH to 7.4 with 1 M Tris-HCl
- Aliquot and store at -20°C

18 % Sucrose

- 90 g sucrose
- 50 ml 10 x PBS
- Make up to 450 ml with ddH_2O

50 x TAE Buffer

- 242 g trizma base
- 57.5 ml acetic acid
- 100 ml 0.5 M EDTA (pH 8.0)
- Make up to 800 ml with ddH_2O
- pH to 8.5 with concentrated NaOH, make up to 1 L with ddH_2O, autoclave

Tail Buffer

- 50 ml 1 M Tris-HCl (ph 8.0)
- 200 ml 0.5 M EDTA
- 20 ml 5 M NaCl
- 100 ml 10 % SDS
- Make up to 1 L with ddH_2O, autoclave

TBST Buffer

- 30 ml 5 M NaCl
- 10 ml 1 M Tris-HCl (pH 8.0)
- 1 ml Tween-20
- Make up to 1 L with ddH_2O

TE Buffer

- 2 ml 0.5 M EDTA (pH 8.0)
- 10 ml 1 M Tris-HCl (pH 7.4)
- Make up to 1 L with ddH_2O, autoclave

1 M Tris-HCl

- 121 g trizma base
- 800 ml ddH_2O
- Use concentrated HCl to get to desired pH
- Make up to 1 L with ddH_2O, autoclave

3.1.3- Apparatus

Table 9- List of apparatus used.

Item	Company	Order Number
Axio Scan.Z1 Slide Scanner	Zeiss	Axio Scan.Z1
Sp8 Confocal Microscope	Leica	Leica TCS SP8
Dyad Peltier Thermal Cycler	Bio-Rad	PTC-220
HistoCore MULTICUT - Semi-Automated Rotary Microtome	Leica	149MULTI0C1
Multi-Functional Precision Balances	A&D Medical	APOLLO GF-A
Semi-enclosed Benchtop Tissue Processor	Leica	TP1020
Vibrating Blade Microtome	Leica	VT1200 S
HistoCore Arcadia H- Heated Paraffin Embedding Station	Leica	14039357258
Cobas c 311 Analyzer	Roche Diagnostics International Ltd.	RS-232C
Gel Electrophoresis System	Thermo Scientific	OW-D2BP
GEL iX20 Imager Windows Version	Intas	13414434
Infinite® 200 PRO Plate Reader	Tecan Trading AG	Infinite M200
XCell SureLock Mini-Cell Gel Running Tank	Thermo Fisher	EI0002
XCell II™ Blot Module	Thermo Fisher	EI0002
Centrifuge 5415R	Eppendorf	0075 425 112-01/GB3/7T/0604/FEEL
Fusion Solo 4M	Vilber Lourmat	289109
DFC 450 Camera	Leica	0694944413
Leica DMRE Microscope	Leica	020-525-025
LightCycler® 480	Roche	04729692001
Nanodrop 2000c	Thermo Fischer	E112352

3.2- Methods

3.2.1- Animal methods

All experiments were performed in genetically modified rats, either previously generated in our group/institute (TGRhCMV/*Anks6*$^{p.R823W}$ and PKD/Mhm rats) or which we received from the INSERM (France) and their wildtype littermates. We generated the new *Anks3* knockout rat line in our group. Rats were kept under controlled conditions at 22°C ± 1°C temperature, 60 % ± 10 % relative humidity and 12 hour alternate light and dark cycle with 100 % fresh air exchange and standard rat diet (containing 19 % protein) and tap water ad libitum. All experiments were conducted in accordance with the German Animal Protection

Law and were approved by the local authority (Regierungspräsidium Karlsruhe, Germany) (No. G-213/16, G-19/18, I11/07, I19/08, I-15/10, I-17/21).

Generation of Anks3 knockout rats

Anks3 was knocked out using the CRISPR/Cas9 system. gRNAs directed against the second exon at aa5-12 : AGCGATGAAGCCAGCGAGCCGG of *Anks3* were provided and tested by Sigma. We injected a mixture of gRNA coding plasmid and *Cas9* mRNA into the pronucleus and cytoplasm of one-cell, fertilised oocytes of Sprague-Dawley rats as previously described (76). Among six progenies, two carried either a 5 bp or 8 bp deletion at the targetted region.

Metabolic parameters

24 hour metabolic cage: Metabolic cages were set up with unrestricted food and water and with the food, water, urine container and faeces container all pre-weighed. The rat was weighed and placed in the cage for 24 hours after which it was removed and reweighed. The food, water, urine container and faeces container were all reweighed. The urine was collected, centrifuged at 600 g for 5 minutes at 4°C before being aliquoted and stored at -20°C. Urine parameters were then determined in the central facility with most parameters measured with a Hitachi Automatic Analyzer except the albumin (determined using a competitive ELISA with a HRP-conjugated rabbit anti-rat albumin antibody) and the osmolarity (determined using an osmometer).

Retrobulbar blood sampling: Rats were anesthetised with isoflurane after which a capillary was used to puncture the retrobulbar venous plexus and the blood collected in a tube containing lithium-heparin. This was centrifuged at 3000 g for 5 minutes at 4°C then the clear upper phase was transferred to a fresh tube and stored at -20°C. Plasma parameters were then determined in the central facility using a Hitachi Automatic Analyzer.

Section of animals

Animals to be perfused were sedated by an intraperitoneal injection of 87.5 mg/kg of ketamine and 12.5 mg/kg xylazine. Once sedation was confirmed the animals were fixed in position and opened. The blood vessels serving the left kidney were clamped and the left kidney was removed and snap frozen for protein or RNA isolation. Perfusion was then carried out using 2 % PFA with 0.05 % glutaraldehyde for 3 minutes at 220 mbar of pressure. Histology samples were incubated in 2 % PFA with 0.05 % glutaraldehyde for 2 hours at 4°C. Animals not to be perfused were sacrificed by CO_2 or cervical dislocation if adult or

decapitation if newborn. Samples for histology were incubated in 2 % PFA with 0.05 % glutaraldehyde for 24 hours at 4°C.

Histology samples to be formalin fixed and paraffin embedded (FFPE) were placed in an autotechnican which moved through the following solutions with 90 minute incubations at each step- twice in 4 % formalin, 70 % ethanol, 80 % ethanol, 96 % ethanol, twice in 99 % ethanol, twice in xylene and 3 times in paraffin. Afterwards they were embedded in paraffin and stored at room temperature.

3.2.2- Genotyping

Isopropanol DNA extraction

0.5cm of rat tail was lysed overnight in 700 µl tail buffer and 35 µl of proteinase K at 55°C with shaking. The lysate was cooled for 10 minutes on ice then 300 µl of 5 M NaCl was added and mixed then incubated on ice for a further 5 minutes. The mixture was centrifuged at 16,000 g, 4°C for 10 minutes. The supernatant was moved to a fresh tube and 2µl of 10mg/ml RNase A was added and incubated at 37°C for 15 minutes. 1 ml of isopropanol was added and mixed until the DNA precipitated. This was centrifuged at 16,000 g, 4°C for 30 minutes. The supernatant was discarded and the pellet was resuspended in 1ml of 75 % ethanol. This was centrifuged at 16,000 g, 4°C for 10 minutes. The supernatant was discarded and the pellet air dried for 30 minutes at room temperature after which it was dissolved in 100-200 µl of ddH_2O, measured in a nanodrop and an aliquot of the stock was diluted to 20 ng/µl.

NaOH DNA extraction

2 mm of rat tail, or an ear clipping from the rat, was mixed with 75 µl of 25 mM NaOH/0.2 mM EDTA and incubated at 98°C for 1 hour then cooled to room temperature. 75 µl of 40 mM Tris-HCl (pH 5.5) was added and the mixture centrifuged at 4,000 g for 3 minutes.

PCR

Table 10- List of primers used for genotyping the Anks3 rat lines.

Line	Forward Primer		Reverse Primer		Processing
	Name	Sequence	Name	Sequence	
Anks3^{KO}	597fw	ctccataggtgtttctgtcc	597rv	accacctcatactggccaat	Sequencing
Anks3$^{\Delta SAM}$	A84	ggcagaaatggaaactggaa	A97	ttctccccagcctgttgtag	Image on gel
Anks3^{KI}	A84	ggcagaaatggaaactggaa	A85	caaaggtccagcatacagca	EcoRI digest

With the Bioran HotStart Taq kit, a master mix was made containing 5 µl of 10 x PCR buffer, 1 µl of 10 mM dNTPs, 2.5 µl of each primer (100 µM), 0.1 µl of HotStart Taq and either 36.9 µl of ddH_2O for NaOH extracted DNA or 33.9 µl of ddH_2O for isopropanol extracted DNA per sample. With the Platinum PCR kit, a master mix was made containing 25 µl 2 x platinum PCR master mix, 1 µl of each primer and either 21 µl of ddH_2O for NaOH extracted DNA or 18 µl of ddH_2O for isopropanol extracted DNA per sample. 2 µl of NaOH extracted DNA or 5 µl of 20 ng/µl isopropanol extracted DNA was then made up to 50 µl with the master mix. The specific primers used for each line are noted in table 10. The mix was then placed in a thermocycler and the appropriate program run (table 11).

Table 11- PCR cycle parameters for genotyping the Anks3 rat lines.

Line		*Anks3*^{KO}	*Anks3*$^{\Delta SAM}$	*Anks3*^{KI}
Preincubation	Temperature (°C)	94	94	94
	Time (s)	300	300	300
Denaturation	Temperature (°C)	94	94	94
	Time (s)	45	45	45
Annealing	Temperature (°C)	56	60	60
	Time (s)	45	45	45
Extension	Temperature (°C)	72	72	72
	Time (s)	60	60	60
Number of cycles		40	40	40
Final Extension	Temperature (°C)	72	72	72
	Time (s)	300	300	300

Depending on the line, the PCR products were visualised on a 1.5 % TAE-agarose gel, digested as described below then visualised on a 1.5 % TAE-agarose gel or seperated on a 0.8 % TAE-agarose gel and the gel fragment containing the PCR product excised for sequencing as described below (table 10).

PCR product digestion

Anks3^{KI} mutation- 25 µl of PCR product was mixed with 2.5 µl of REact 3 buffer, 1 µl EcoRI and 21.5 µl ddH_2O then incubated at 37°C for 1 hour and visualised on a 1.5 % TAE-agarose gel.

Sequencing

PCR products in excised gel fragments were cleaned up using the Qiagen Gel Extraction kit according to the protocol including the optional QG buffer wash, the 5 minute incubation with the PE buffer on the column and the 5 minute incubation with the EB buffer (pre-heated to 50°C) on the column. The elution was diluted to 5ng/µl with ddH_2O in a total volume of 15 µl after which 2 µl of the forward primer was added. Sequencing was then carried out by Eurofins Genomics.

3.2.3- Histological methods

Haematoxylin and eosin (H&E) stain

3µm sections were cut from FFPE tissue and placed on silanised slides after which they were dried at 60°C for 1 hour then cooled for 10 minutes at room temperature. The sections were deparaffinised and rehydrated by incubating 3 times in xylene for 5 minutes and then in the following series of ethanol concentrations- 100 %, 96 %, 80 %, 70 % and ddH_2O for 2 minutes each. They were then stained by incubating for 4 minutes in haematoxylin, washing for 10 minutes in running tap water and incubating for 2 minutes in eosin. Finally the sections were dehydrated and cleared by incubating in ddH_2O for 1 minute then in the following series of ethanol concentrations- 70 %, 80 %, 96 % and 3 times in 100 % ethanol for 2 minutes each followed by three times in xylene for 5 minutes each.

Azan stain

3µm sections were cut from FFPE tissue and placed on silanised slides after which they were dried at 60°C for 1 hour then cooled for 10 minutes at room temperature. The sections were deparaffinised and rehydrated by incubating three times in xylene for 5 minutes and then in the following series of ethanol concentrations- 100 %, 96 %, 80 %, 70 % and ddH_2O for 2 minutes each. Staining was then carried out by incubating the sections in 0.1 % azocarmine G for 20 minutes at 56°C followed by washing in running tap water. The intensity of stain was controlled with three brief (5 seconds - 1 minute) incubations in aniline alcohol until the nucleus and cytoplasm were differentially stained after which the reaction was stopped by acetic alcohol. The collagen was then counter-stained by incubation in 5 % phosphotungstic

acid for 20 minutes, washing in running water and finally incubation in aniline blue-orange G solution. The sections were then dehydrated and cleared by washing once in ddH_2O and twice in 96 % ethanol and then incubated twice in 100 % ethanol for 2 minutes and twice in xylene for 5 minutes.

Fibrosis was quantified by digitally scanning the azan stained sections with Aperio CS2 (Leica Biosystems). The pictures were then analysed with ilastik which distinguished the red stained non-fibrotic tissue from blue stained fibrotic tissue. Follow-up computations were done with Matlab.

MRI imaging

MRI images were performed in collaboration with Marc Pretze, Department Molecular Imaging and Radiochemistry, Department of Clinical Radiology and Nuclear Medicine, Medical Faculty Mannheim of Heidelberg University, Mannheim, Germany. Embryos from developmental day 17.5 were immobilised in a 2 % agarose in ddH_2O gel within a 15 ml falcon. The MRI scan was then performed in a 20 min, ICON™ (Avance III MRI) 1 Tesla cryogen-free, coil type: RF RES head coil; 45 mm, 30 mm outer and inner diameter (Bruker, Ettlingen, Germany) machine with the parameters described below (table 12).

Table 12- Parameters used during MRI imaging.

Measurement	T2 RAREnav highres 3D
Repetition time (ms)	4000
Echo time (ms)	84.0
Acquisition time	2h 50min 40sec
Flip angle	90
Slice	13.696
Field of view (mm)	19.95x16.07x13.70
Matrix	160x160x64
Averages	2
Repetitions	1
Echo spacing (ms)	28
Rare factor	8
Resolution (mm)	0.125x0.1x0.214

3.2.4- Protein analysis

Immunohistochemistry

3 µM sections were cut from FFPE tissue and placed on silanised slides (2 sections per slide) after which they were dried at 60°C for 1 hour then cooled for 10 minutes at room temperature. The sections were deparaffinised and rehydrated by incubating 3 times in xylene for 10 minutes and then in the following series of ethanol concentrations- 3 times in

100 %, 2 times in 96 %, 2 times in 80 % for 3 minutes each and once in 70 % for 5 minutes. Endogenous peroxidase activity was reduced by incubating the sections in 0.3 % hydrogen peroxide in methanol, after which sections were then washed 3 times in PBS. Antigen retrieval was carried out by incubating in 10 mM citrate buffer and heating in a steamer for 20 minutes then leaving the sections to cool at room temperature for 30 minutes. The slides were then washed twice in PBS for 10 minutes after which they were dried and the sections drawn around with a PAP grease pen. 100 µl of blocking solution was added to each section which were then incubated in a humid chamber for 30 minutes-2 hours.

Before dilution, the primary antibody stock solution was centrifuged at 13,500 g for 2 minutes at 4°C after which it was diluted to the appropriate concentration in 2 % BSA in PBS. The blocking solution was then removed from each section and 60µl of either the diluted antibody or 2 % BSA in PBS (for the negative controls) was added and incubated for a minimum of 1 hour at room temperature, up to 2 hours at room temperature and overnight at 4°C in a humid chamber. The primary antibody solution was then removed and the sections washed 3 times with PBS for 5 minutes. The biotinylated secondary antibody was diluted in 2 % BSA in PBS and then centrifuged at 13,500 g for 2 minutes at 4°C. The PBS wash was then removed and the diluted secondary antibody added to each section and incubated for 1 hour at room temperature in a humid chamber. The ABC reagent was then prepared by mixing 1 drop of reagent A with 1 drop of reagent B in 2.5 ml of PBS and left to stand at room temperature for 30 minutes. The secondary antibody was then removed and the sections washed 3 times for 5 minutes in PBS. The PBS wash was then removed and 50 µl of the ABC reagent was added to each section and incubated for 30 minutes in a humid chamber at room temperature. The ABC reagent was then removed and the sections washed 3 times for 5 minutes in PBS. The DAB-substrate solution was prepared by mixing 1 drop of buffer stock solution, 2 drops of DAB solution and 1 drop of hydrogen peroxide in 2.5 ml ddH_2O (1 drop of NiCl solution can be added to create a darker stain). The PBS wash was then removed and 50 µl of DAB-substrate solution added to each section. The incubation time was determined by monitoring the colour formation under a microscope (typically in the range of 2-5 minutes). The slides were then quickly washed in ddH_2O and then washed for 5 minutes in PBS 3 times. 40 µl of 40 % glycerol in PBS was added per section and a coverslip placed on.

Expansion microscopy

Embryos were fixed for 24 hours in 4 % PFA at 4°C. Embryos were then placed in acrylamide hydrogel solution for 3 days at 4°C with shaking. The hydrogel was then polymerised for 2-3 hours at 37°C in a humid chamber. The gel was trimmed as much as possible without damaging the sample and then washed in PBS for 2 hours. The samples were cut into 500 µm thick sagittal sections using a vibratome. The sections were placed in denaturing solution in a humid chamber at 70°C for 24 hours and then 95°C for 24 hours. The sections were washed for 4 hours in 1 x PBS with 0.1 % Triton X-100, with repeated changes of the wash solution after which the sections were blocked in 1 x PBS with 1 % Triton X-100 for 24 hours at 37°C. The primary antibody was diluted in 1 x PBS with 1 % Triton X-100 and incubated with the sections for 16-24 hours at 37°C. The sections were then washed 3 times for 2 hours in 1xPBS with 1 % Triton X-100. The secondary antibody was diluted in 1 x PBS with 1 % Triton X-100 and 50 nM sytox green and incubated with the sections for 16-24 hours at 37°C. The sections were then washed for 2 hours, 3 times in 1 x PBS with 1 % Triton X-100. Sections could then be imaged using the confocal microscope or expanded further by incubating in ddH_2O for 24 hours before imaging.

Protein extraction

100 mg of tissue was excised from snap frozen organs, finely minced and placed in 1 ml of RIPA buffer (1 tablet of proteinase inhibitor was dissolved in 50 ml RIPA buffer prior to this) in a hand homogeniser. The tissue was then homogenised and the homogenate centrifuged at 4°C, 13,500 g for 6 minutes. To quantify protein concentration in the samples, a standard curve was made with Bradford reagent (diluted 1 in 5 in ddH_2O) and a stock BSA solution, after which the unknown samples were measured in triplicate.

Western blot

Samples were prepared for loading as follows- 40 µg of protein, 5 µl 4 x LDS sample buffer, 2 µl reduction agent, made up to 20 µl with ddH_2O and heated to 50°C for 10 minutes. The samples were then loaded on a 4-12 % bis-tris acrylamide gel along with a protein ladder and were run at 170-190 V until the dye reached the bottom of the gel. Prior to transfer, the PDVF membrane was activated in methanol for 30 seconds and washed in transfer buffer. The transfer chamber was assembled (all components of the assembly were soaked in transfer buffer) with the membrane between the gel and the positive plate, and filled with transfer buffer. The transfer was run at 30 V for 90 minutes. The membrane was washed twice in TBST for 10 minutes then incubated for 2 hours in blocking medium. The primary

antibody was diluted in blocking solution and incubated on the membrane for a minimum of 1 hour at room temperature, up to 2 hours at room temperature and overnight at 4°C. The primary antibody was removed and the membrane washed 3 times for 5 minutes in TBST. The HRP-conjugated secondary antibody was diluted in blocking solution and incubated on the membrane for 1 hour at room temperature. The secondary antibody was removed and the membrane washed 5 times in TBST for 5 minutes. The imaging solution was prepared and incubated on the membrane for 1 minute then removed and the membrane imaged (using the Fusion Solo apparatus). If the membrane was to be reused it was incubated in stripping solution for 20 minutes, then washed 2 times in TBST for 10 minutes and incubated in blocking medium for 1 hour.

3.2.5- RNA analysis

Total RNA extraction

50 mg of fresh, frozen tissue was removed from the stock and minced for no more than 10 seconds then placed into 1 ml of Trizol on ice. A mechanical homogeniser was used in 20 second bursts, with 40 second rests in between, until the sample was fully homogenised. The homogenate was then incubated at room temperature for 5 minutes and 200 µl of chloroform was added before the mixture was vortexed for 15 seconds and incubated at room temperature for 3 minutes. This was centrifuged at 12,000 g for 15 minutes at 4°C and the clear upper phase was transferred to a fresh tube. 1.5 volumes of 100 % ethanol was added to the upper phase and mixed by pipetting. 700 µl of this mixture was transferred to a RNeasy Mini Spin Column which was centrifuged at 8,000 g for 15 seconds at room temperature. The flow through was discarded and the previous step was repeated until all of the mixture was passed through the column. 700µl of Buffer RWT was added to the column then centrifuged at 8,000 g for 15 seconds at room temperature and the flow through discarded. 500µl of Buffer RPE was added to the column and centrifuged at 8,000 g for 15 seconds at room temperature and the flow through discarded. 500µl of Buffer RPE was added to the column then centrifuged at 8,000 g for 2 minutes at room temperature. The column was moved to a new 2ml tube and centrifuged at 16,000g for 1 minute at room temperature. The column was then moved to a fresh 1.5 ml tube and 30 µl of RNase-free water was added to the centre of the column and centrifuged at 8,000g for 1 minute at room temperature. The column was moved to a fresh 1.5 ml tube and the flow through from the previous step was collected after which the previous step was repeated. The collected flow through was then measured on a nanodrop and the 28S and 18S rRNA bands analysed on a gel to check for degradation.

RT-qPCR

A cDNA library was synthesised by mixing 2 µg of isolated RNA, diluted in a total volume of 12 µl with RNase free water, 1 µl of 50 ng/µl random primers and 1 µl of dNTP-mix. This was incubated at 65°C for 5 minutes then chilled on ice for 5 minutes. 4 µl 5 x first strand buffer, 2 µl 0.1 M DTT and 1 µl 40 U/µl RNasin were added and the mixture incubated for 2 minutes at room temperature. 1 µl of 200 U/µl superscript reverse transcriptase was added to each experimental sample and 1 µl of RNase free water to each negative control. The mixture was incubated at the following conditions- 25°C for 10 minutes, 42°C for 50 minutes and 70°C for 15 minutes. The synthesised cDNA was diluted 1 in 10 in ddH_2O, with 5 µl used per reaction. In addition to the experimental samples, 200 ng of Sprague-Dawley rat genomic DNA, reverse transcription negative and water controls were included. The reaction master mix was created with 10 µl QuantiTect SYBR Green PCR Master Mix, 1 µl 10 mM forward primer, 1 µl 10 mM reverse primer and 3 µl of ddH_2O per sample, with 15 µl of the master mix added to each reaction well (primer sequences used are listed in table 13). The reaction was carried out in a Lightcycler 480, using the conditions specified in table 14, which also processed the data.

Table 13- List of primers used in qPCR and RT-PCR.

Gene	Direction	Sequence
Aqp2	Forward	gctgtcaatgctctccacaa
	Reverse	ggagcaaccggtgaaataga
Anks3	Exon 11	cactgttggaacagatcggc
	Exon 12	ctagggcatcactaggtggg
	Exon 13	ggatgtcctttcgggcacta
Gapdh	Forward	tgcaccaccaactgctta
	Reverse	ggatgcagggatgatgttc

Table 14- PCR cycle parameters for RT-PCR and qPCR of Anks3, Aqp2 and Gapdh from cDNA.

Line		*Anks3*	*Aqp2*	*Gapdh*
Preincubation	Temperature (°C)	95	95	95
	Time (s)	600	600	600
Denaturation	Temperature (°C)	95	95	95
	Time (s)	15	15	15
Annealing	Temperature (°C)	54	55	55
	Time (s)	30	25	25
Extension	Temperature (°C)	72	72	72
	Time (s)	30	25	25
Number of cycles		40	40	40
High Resolution Melting	Temperature (°C)	95	95	95
	Time (s)	60	60	60
	Temperature (°C)	40	40	40
	Time (s)	60	60	60
	Temperature (°C)	65	65	65
	Time (s)	1	1	1
	Temperature (°C)	97	97	97
	Time (s)	1	1	1

Microarrays

Gene expression profiling was performed using arrays of rat RaGene-2.0-st-type from Affymetrix and the Clariom D array from Thermo Fischer. Biotinylated antisense cDNA was then prepared according to the Affymetrix standard labelling protocol with the GeneChip® WT Plus Reagent. Both microarrays were hybridized using GeneChip® Hybridization, Wash and Stain Kit (both from Affymetrix, Santa Clara, USA) and chips remained overnight on a GeneChip Hybridization oven 640. The following day, they were dyed in the GeneChip Fluidics Station 450 and thereafter scanned with a GeneChip Scanner 3000. All of the equipment used was from the Affymetrix-Company (Affymetrix, High Wycombe, UK).A Custom CDF Version 21 with ENTREZ based gene definitions was used to annotate the arrays. The raw fluorescence intensity values were normalised applying quantile normalisation and RMA background correction. OneWay-ANOVA was performed to identify differentially expressed genes using a commercial software package SAS JMP10 Genomics, version 6, from SAS (SAS Institute, Cary, NC, USA). A false positive rate of a=0.05 with FDR correction was taken as the level of significance.Gene Set Enrichment Analysis (GSEA) was used to determine whether defined lists (or sets) of genes exhibit a statistically significant bias in their distribution within a ranked gene list using the software GSEA (77). Pathways belonging to various cell functions such as cell cycle or apoptosis were obtained from public external databases (KEGG, http://www.genome.jp/kegg).

4- RESULTS

4.1- Renal spatial expression of ANKS3 and ANKS6 is tightly regulated and disturbed by the *Anks6*$^{p.R823W}$ mutation

It has previously been shown that ANKS3 forms homopolymer complexes and binding of ANKS3 to ANKS6, via the SAM domain, prevents this polymerisation. The *Anks6*$^{p.R823W}$ mutation, which causes an ADPKD-like phenotype, disrupts the binding of ANKS6 to the ANKS3-SAM domain. Thus, we hypothesise that the loss of this interaction may play a role in the development of the ADPKD phenotype, possibly due to increased formation of Anks3 homopolymers. As this interaction could only occur if the two proteins are concurrently expressed in the same cell, we investigated their spatial expression in PKD/Mhm and wildtype rats. As shown in figure 11, in adult wildtype rats ANKS3 and ANKS6 strongly co-localise in the distal tubules of the outer cortex. However, they do not co-localise in the juxtamedullary region. Here, ANKS6 expression is restricted to the S3 segment of the proximal tubule and ANKS3 expression to the distal tubules. In adult heterozygous PKD/Mhm(cy/+) rats, ANKS3 and ANKS6 are strongly co-expressed in the cortex in non-cystic tubules, but not in cystic tubules (figure 12). Next, we studied ANKS3 and ANKS6 expression in the cortex and medulla of the developing (10 day old) and mature kidney (three to four weeks old) in both wildtype and PKD/Mhm(cy/cy) rats, in which ANKS6 is unable to bind to the ANKS3-SAM domain. Kidney development in the rat is completed around three weeks after birth. Homozygous PKD/Mhm(cy/cy) rats die around two to three weeks after birth and thus were sacrificed shortly before their life expectancy ended. AQP2 was used as a collecting duct marker. Figure 13 shows that in the immature kidneys of 10 day old wildtype rats, ANKS3 and ANKS6 expression is restricted to the renal cortex and they do not co-localise with each other or with AQP2. However, a completely different spatial expression pattern was found in the developing cystic kidneys of 10 day old PKD/Mhm(cy/cy) rats (figure 14). ANKS3 and ANKS6 were strongly expressed in both the cortex and medulla and co-localise with each other and AQP2. Of note, in the mature wildtype kidney we observed a switch in the spatial expression pattern of ANKS3 and ANKS6 (figure 15). Both ANKS3 and ANKS6 are now strongly expressed and co-localised with each other and with AQP2 in the epithelial cells of the medullary collecting ducts but not in the upper cortical parts of the collecting ducts. Furthermore, we found a strong co-localisation of ANKS3 and ANKS6 in the convoluted distal tubular epithelium in the renal cortex, which is particularly involved in the concentration of urine. However, the two

proteins do not co-localise in the corticomedullary renal border. ANKS6 is expressed in the S3 segment of proximal tubules and ANKS3 in the distal tubules, as previously shown in eight week old wildtype rats (figure 11). In the adult homozygous PKD/Mhm(cy/cy) rats, ANKS6 and ANKS3 were co-expressed with AQP2 in the medullary collecting duct cells located between the cysts, similar to the pattern observed in the 10 day old homozygous PKD/Mhm(cy/cy) rats (figure 16). Thus, in wildtype rats a developmental switch in the spatial expression of the ANKS6 and ANKS3 proteins occurred. In contrast, homozygous PKD/Mhm(cy/cy) rats displayed a dysregulated spatial expression pattern of ANKS6 and ANKS3 during renal development.

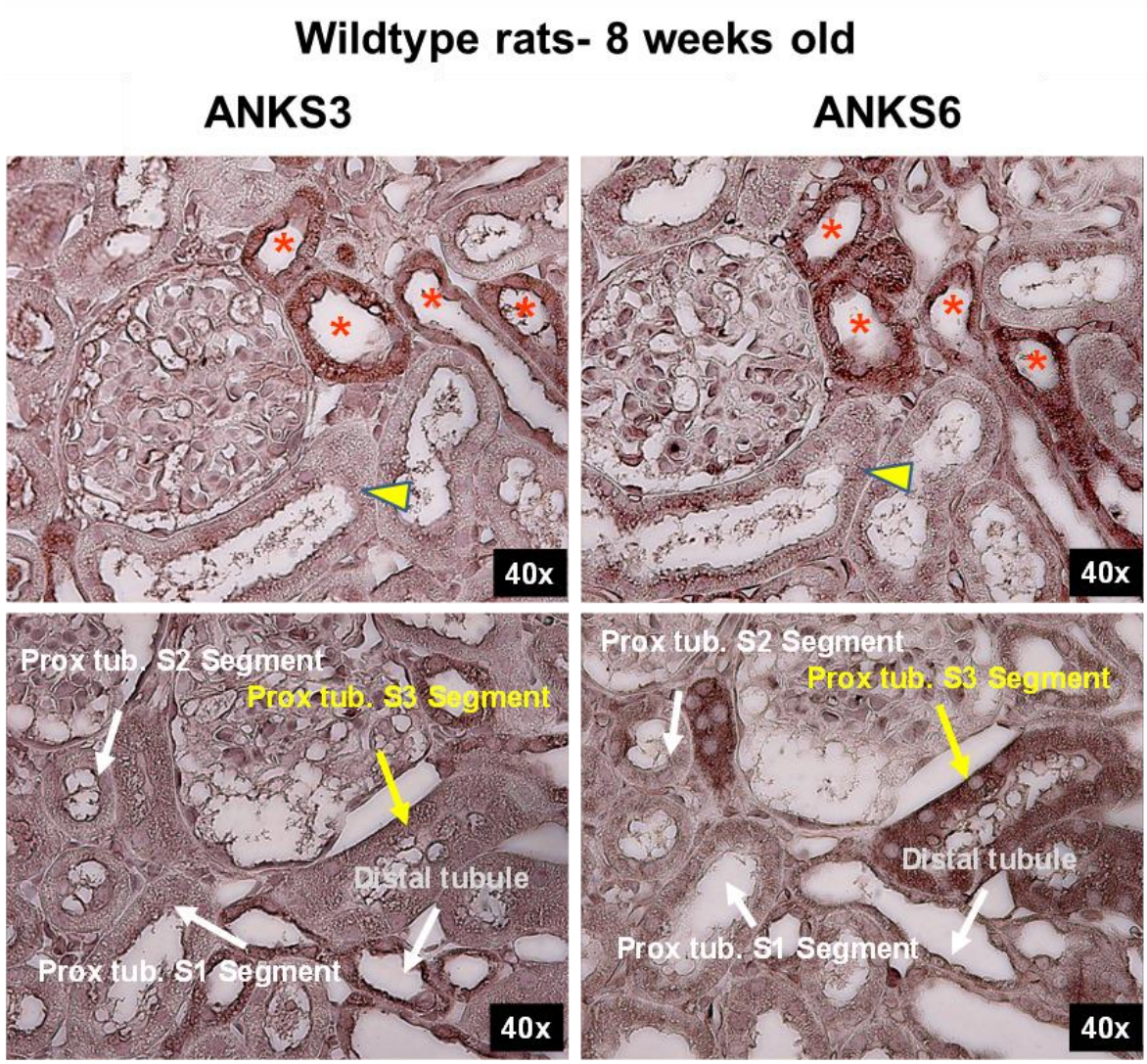

Figure 11- Immunohistochemistry of ANKS3 and ANKS6 in 8 week old wildtype rat kidneys. Co-localisation of ANKS3 and ANKS6 is seen in the distal tubules of the outer cortex (star); arrow tip - S1 segment of proximal tubules (top). No co-localisation is seen in the juxtamedullary region, where ANKS6 is expressed in the S3 segment of the proximal tubules and ANKS3 in the distal tubules (bottom).

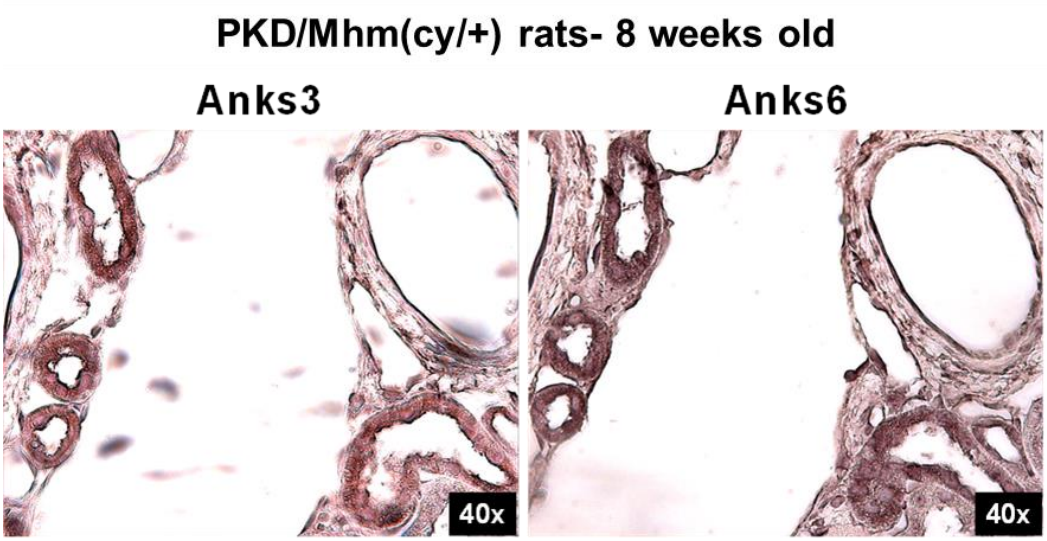

Figure 12- Immunohistochemistry of ANKS3 and ANKS6 in 8 week old heterozygous PKD/Mhm(cy/+) rat kidneys. ANKS3 and ANKS6 co-localise in the non-cystic cortical tubules between large cysts.

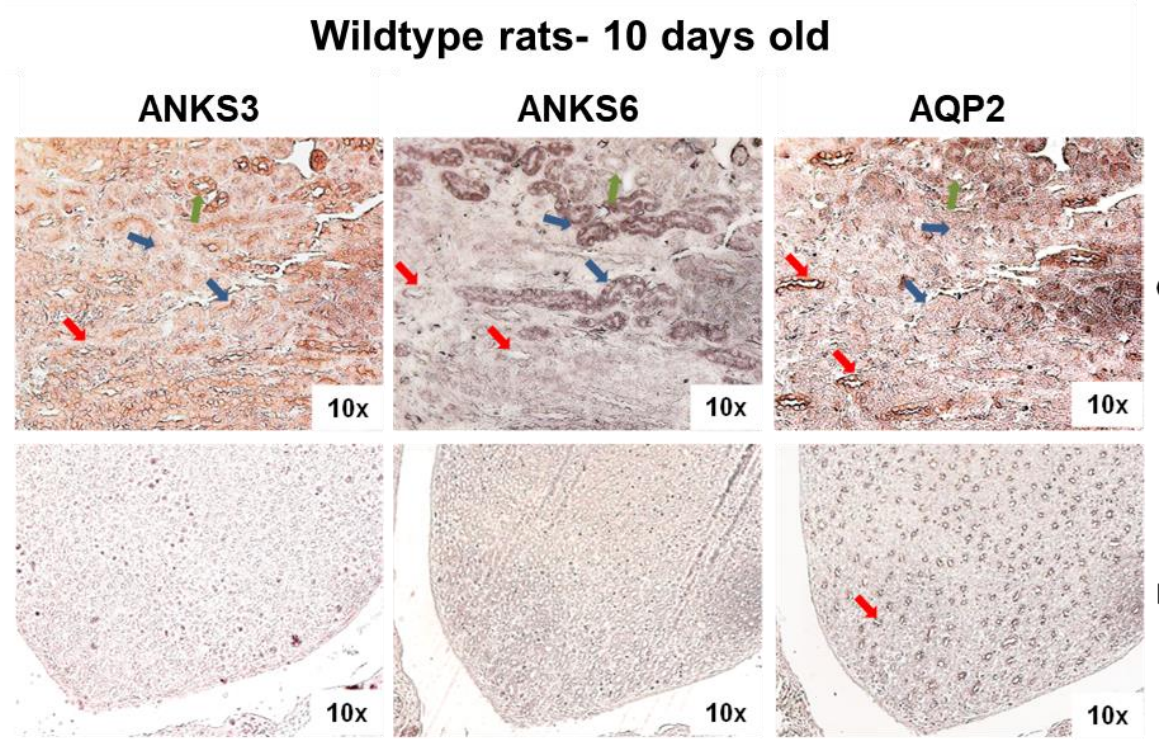

Figure 13- Immunohistochemistry of ANKS3, ANKS6 and AQP2 in 10 day old wildtype rat kidneys. ANKS6 and ANKS3 are expressed only in the cortex (top) not in the medulla (bottom). In the cortex they do not co-localise with each other or with AQP2. Arrows: green- ANKS3 position, blue- ANKS6 position, red- AQP2 position.

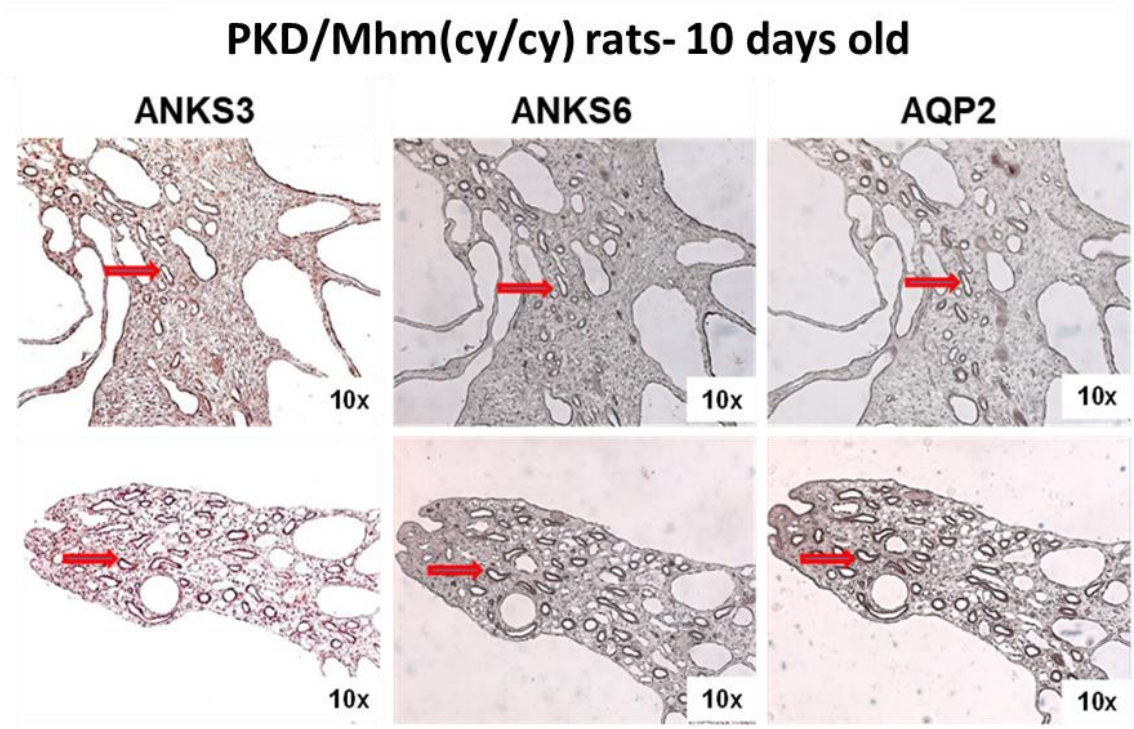

Figure 14- Immunohistochemistry of ANKS3, ANKS6 and AQP2 in 10 day old PKD/Mhm(cy/cy) rat kidneys. ANKS6 and ANKS3 are expressed in both the cortex (top) and medulla (bottom) and in both regions they co-localise with each other and with AQP2 (arrows).

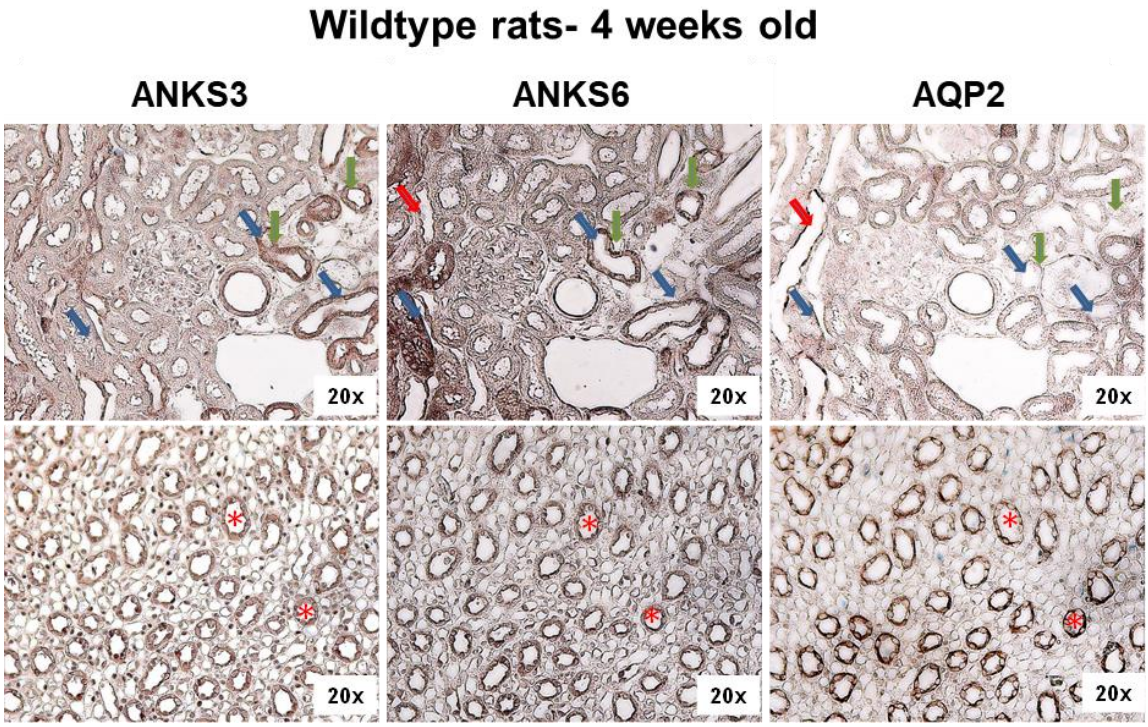

Figure 15- Immunohistochemistry of ANKS3, ANKS6 and AQP2 in mature wildtype rat kidneys. ANKS6 and ANKS3 are expressed and co-localise in the cortical distal tubules (top) and with AQP2 only in the medulla (bottom, stars). Arrows: green- ANKS3 position, blue- ANKS6 position, red- AQP2 position.

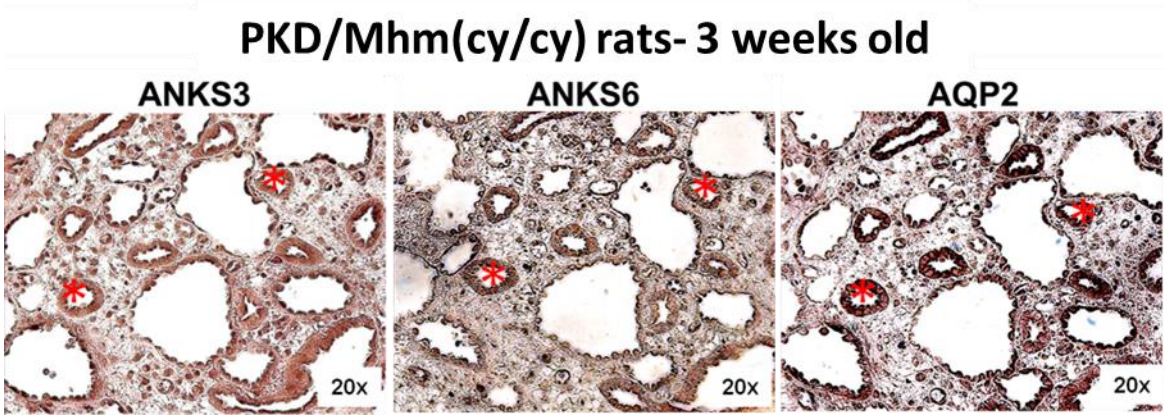

Figure 16- Immunohistochemistry of ANKS3, ANKS6 and AQP2 in mature homozygous PKD/Mhm(cy/cy) rat kidneys. all 3 proteins are co-expressed in the medullary collecting ducts (stars)- a comparable pattern to the developing PKD/Mhm(cy/cy) rat kidneys.

4.1.1- Aqp2 expression is downregulated in TGRAnks6$^{p.R823W}$ PKD rats

AQP2 is a key therapeutic target currently being investigated for the treatment of ADPKD. We show that AQP2 co-localises with ANKS3 and ANKS6 in the mature, but not in the developing, wildtype kidney. By contrast, in the PKD/Mhm(cy/cy) rat kidneys all three components already co-localise in the 10 day old developing kidney, when cysts are beginning to develop. Since ANKS3 and ANKS6 work in complexes with BICC1, an RNA binding protein, we investigated whether *Aqp2* expression levels are changed in the mutants. For this experiment 10 day old and eight week old TGR-hCMV/*Anks6*$^{p.R823W}$ rats (hereafter referred to as TGR*Anks6*), which were previously generated in our group (58), were used with wildtype comparisons. The qPCR data showed decreased expression of *Aqp2* mRNA. Thus, in TGR*Anks6* rat kidneys increased ANKS3-SAM polymerisation due to the loss of ANKS6-ANKS3-SAM domain binding may act in an inhibitory manner on *Aqp2* mRNA levels (figure 17), which may in turn result in reduced water reabsorption in the kidney tubules.

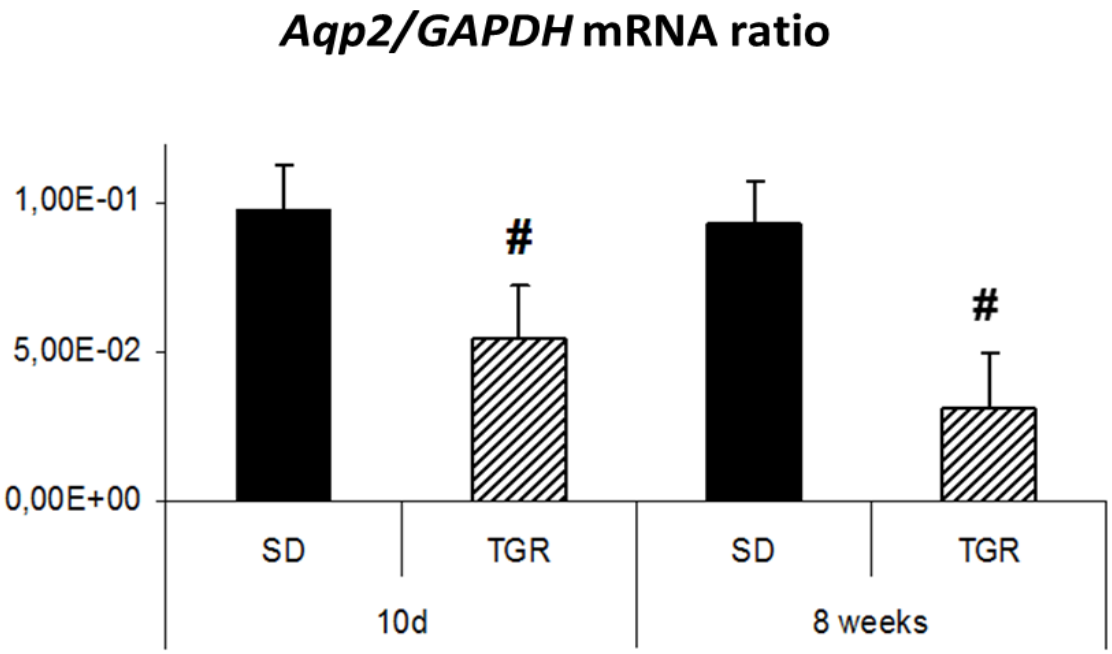

Figure 17- Aqp2 expression in TGRAnks6 rat kidneys. qPCR data shows decreased expression of Aqp2 mRNA in both the developing and mature kidneys of TGRAnks6 rats (TGR) compared to wildtype controls (SD) (unpaired t-test- # $p<0.05$).

4.2- Generation of new mutant *Anks3* rat lines

In order to identify: a) the in vivo function of ANKS3, b) the role of ANKS3-SAM domain polymerisation and c) the role of the ANKS3-SAM domain, we generated three novel rat models with either a total ANKS3 knockout or different mutations in the ANKS3-SAM domain:

a. *Anks3* knockout rat (*Anks3*^{KO})
b. *Anks3*-SAM$^{p.I35E}$ knockin rat (*Anks3*^{KI})
c. *Anks3*$^{\Delta SAM}$ rat (deletion between position I35 and F52 of the SAM domain)

The positions of the mutations are indicated in figure 18.

Since the function of *Anks3* is not yet known in mammals we created the *Anks3* knockout rat using CRISPR/Cas9 injected into fertilised one-cell rat eggs. The gRNA was targeted to exon 2 at aa5-12: AGCGATGAAGCCAGCGAGCCGG.

Among 6 progenies, two founders were obtained with either a 5 or 8 bp deletion at the targetted position.

Rat lines carrying the ANKS3-SAM mutations were generated at the INSERM (France) using the CRISPR/Cas9 system and suitable targets (78). The p.I35E mutation was introduced into the SAM domain in exon 11. This mutation has previously been shown to prevent the polymerisation of ANKS3, but has no effect on ANKS6 binding (66). In a third rat line, important parts of the SAM domain between positions I35 and F52 were deleted by simultaneous targeting of I35 and F52 using specific gRNAs. Thus, we would theoretically expect a loss of all ANKS3 function in the *Anks3*^{KO} line, a loss of ANKS3 polymerisation while SAM domain binding to ANKS6 and Ank domain function would remain intact in the *Anks3*^{KI} line and, in the *Anks3*$^{\Delta SAM}$ rats, a total loss of SAM domain function with Ank domain function and the C-terminal end preserved.

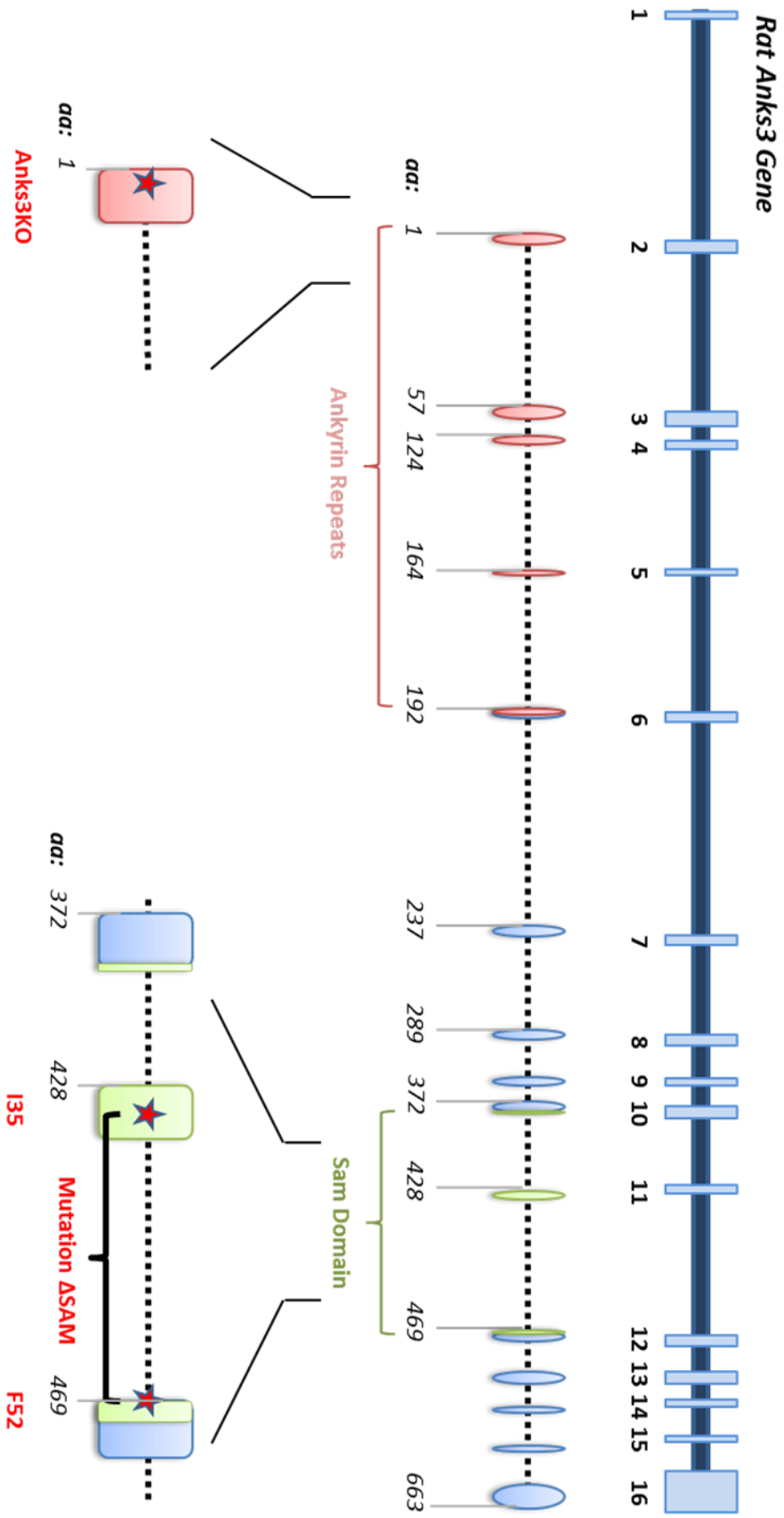

Figure 18- The rat Anks3 gene and the location of the CRISPR gRNA targeting sites.

4.2.1- Genotyping

Rats were genotyped at 3 weeks of age by sequencing and those carrying mutations of interest were then further bred to create the lines used.

4.2.1.1- *Anks3*^{KO} rat

Both, the 5bp and 8bp deletion in the founders created a frameshift after aa10 or aa8 and a premature stop after aa 46 or aa 45, repectively (figure 19).

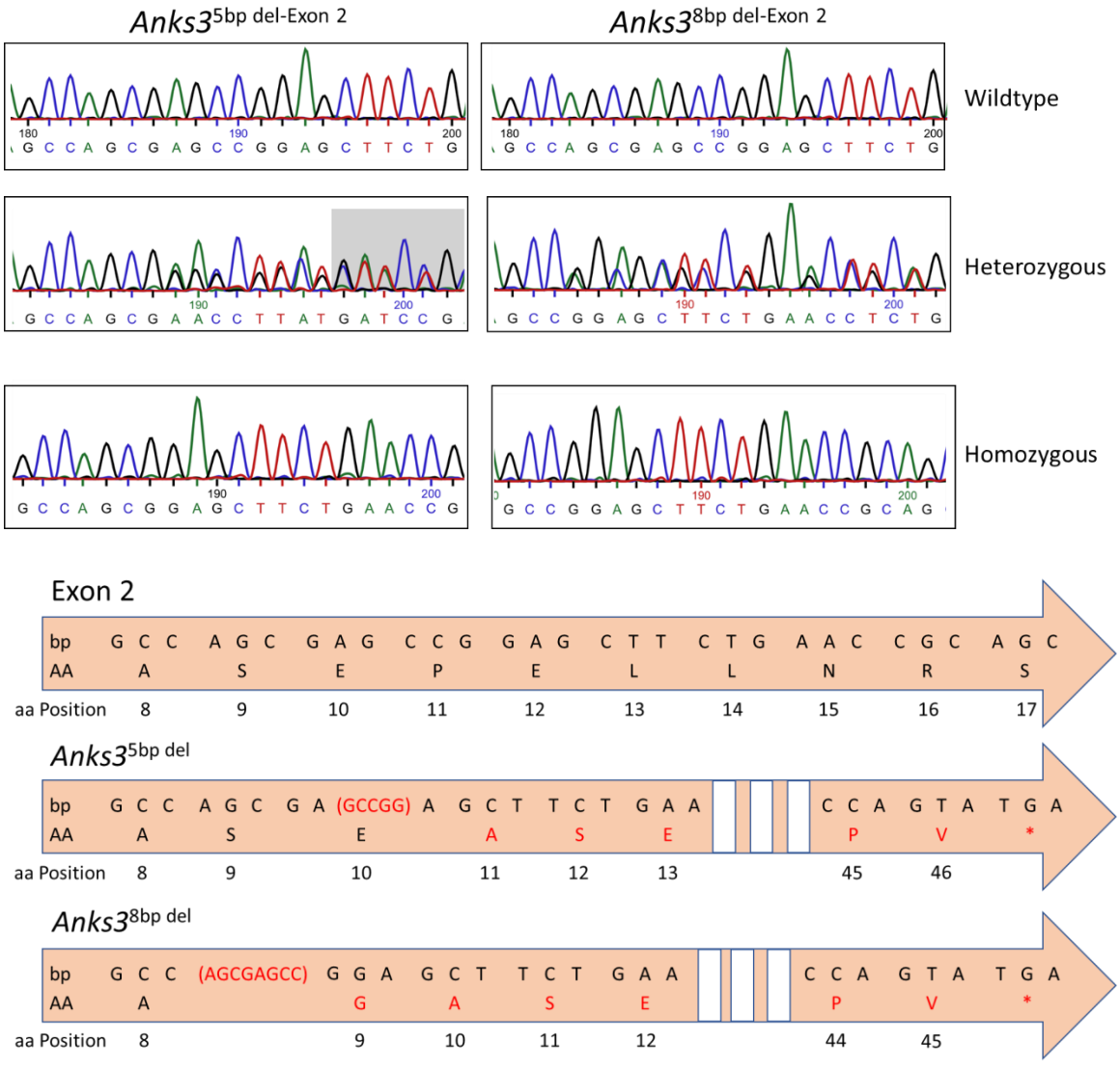

Figure 19- Genotyping of in Anks3^{KO} *rats. Top: Sequencing results of the targeted position in 2*nd *exon from amino acid 5 to 12 in heterozygous and homozygous rats of two different Anks3*^{KO} *lines with either 5 bp or 8 bp deletion. Bottom: base pair and amino acid changes due to mutations in Anks3*^{KO} *rats are shown. (base pair and amino acid changes noted in red). Both mutations result in a frame shift and truncation after 46 amino acids (5 bp deletion) or 45 amino acids (8 bp deletion).*

4.2.1.2- *Anks3*-SAM$^{p.I35E}$ rat

The *Anks3*^{KI} rats were generated at the INSERM (France) by using a gRNA targetting the position I35 of the SAM domain, found in exon 11, and a suitable template DNA carrying the mutation and additional silent changes at the I35 site to create an EcoRI restriction site in the mutants. The EcoRI site simplified genotyping since only a PCR followed by an EcoRI digestion was required (78). We investigated the genotype of the *Anks3*^{KI} rats in more detail and three additional mutations within intron 11, close to the splice site, among progeny carrying the *Anks3*^{KI} mutation (figure 20 and 21).

Inheritance of these intron 11 mutations revealed that the *Anks3*^{KI} mutation was linked to one of the three intron 11 mutations in each case. Consequently we had to check the *Anks3*^{KI} progenies for changes in splicing around exon 12. This was first investigated by RT-PCR using primer pairs between exon 11 and exon 12 to check for inclusion of exon 12 in the mature *Anks3* mRNA, and exon 11 and exon 13, to check for exon skipping (p. 46, Mat. Meth). Figure 22 shows that no changes in splicing were seen. In addition to this, a whole exon screen of *Anks3* was performed on homozygous adult *Anks3*$^{KI/KI}$ and wildtype rats and compared with embryonic day 17.5 *Anks3*$^{KO/KO}$ and wildtype rats as part of microarray experiments. No differences were observed between the mutants and their wildtype counterparts or between the adults and embryos, indicating that there were no differences in *Anks3* splicing amoung these groups (figure 23).

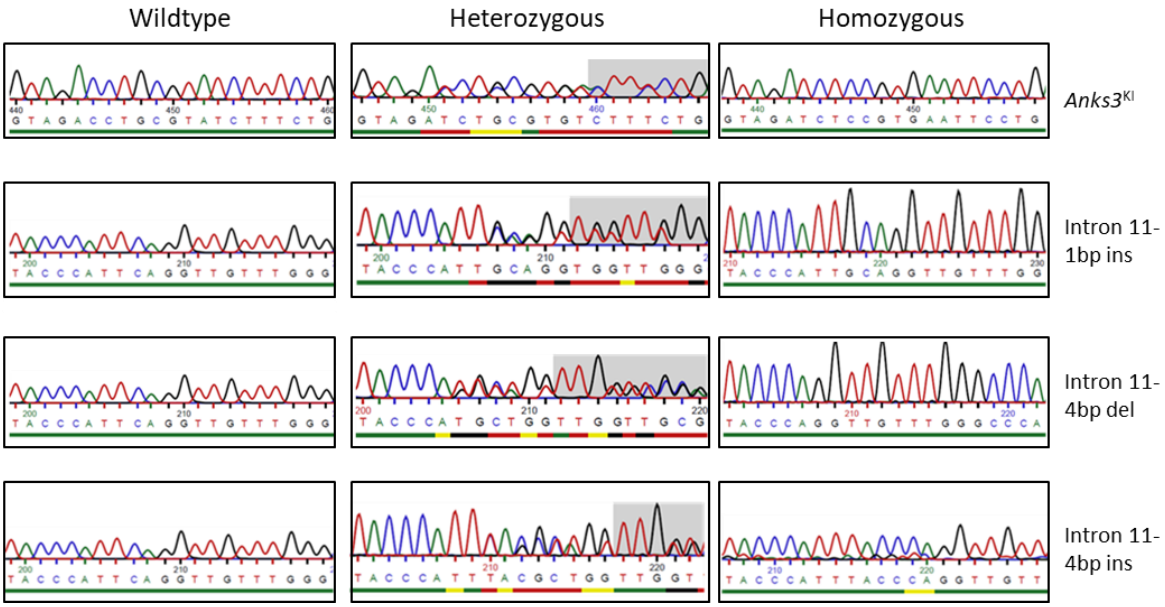

Figure 20- Genotyping in Anks3^{KI} rats. Sequencing of the Anks3^{KI} mutation and the three mutations in intron 11: The Anks3-SAM$^{p.I35E}$ was correctly inserted along with the EcoRI restriction site. This was coupled in each case with a 1 bp insertion, 4 bp insertion or 4 bp deletion within intron 11 immediately before the splice site with intron11/exon12.

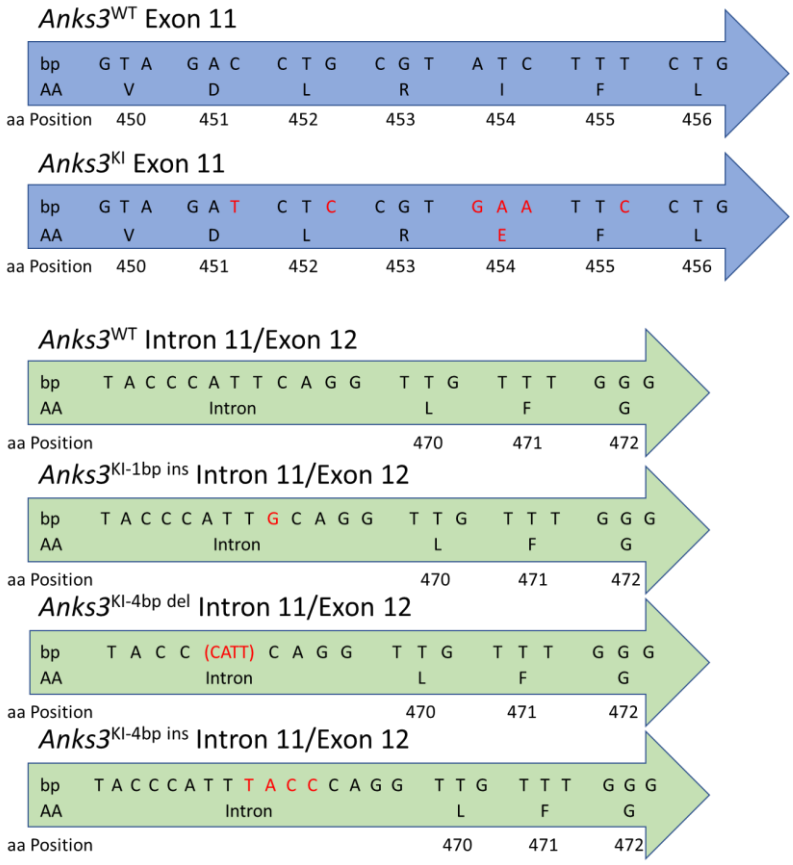

Figure 21- Nucleotide and amino acid sequences for the Anks3^{KI} mutation and the three mutations in intron 11 (base pair and amino acid changes noted in red).

Table 15- Expected changes in the length of RT-PCR transcripts in the different mutant lines.

Mutation	Expected Base Pair Change	Exon 11-Exon 12 transcript size	Exon11-Exon 13 transcript size
Wildtype	No Change	195bp	366bp
Anks3^{KI}	No Change	195bp	366bp
Anks3$^{\Delta SAM}$	45bp decrease	150bp	321bp

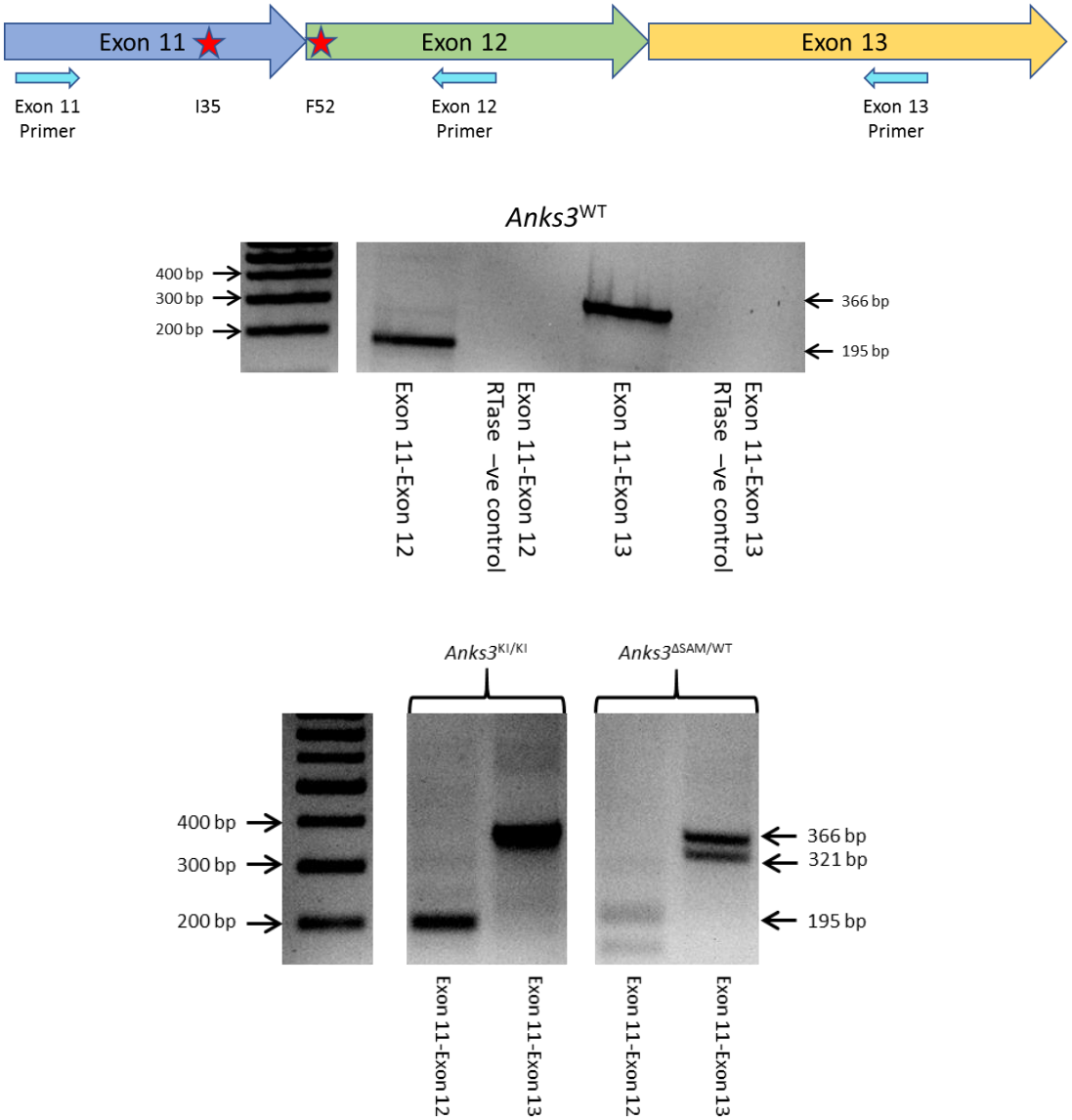

Figure 22- RT-PCR of the Anks3^{KI} *and Anks3*$^{\Delta SAM}$ *rats to check splicing of exon 12. RT-PCR of Anks3*$^{KI/KI}$ *rats showed no changes in the splicing of exon 12. Heterozygous Anks3*$^{\Delta SAM/WT}$ *rats also showed no changes in splicing but had an additional lower band from the mutant allele as expected.*

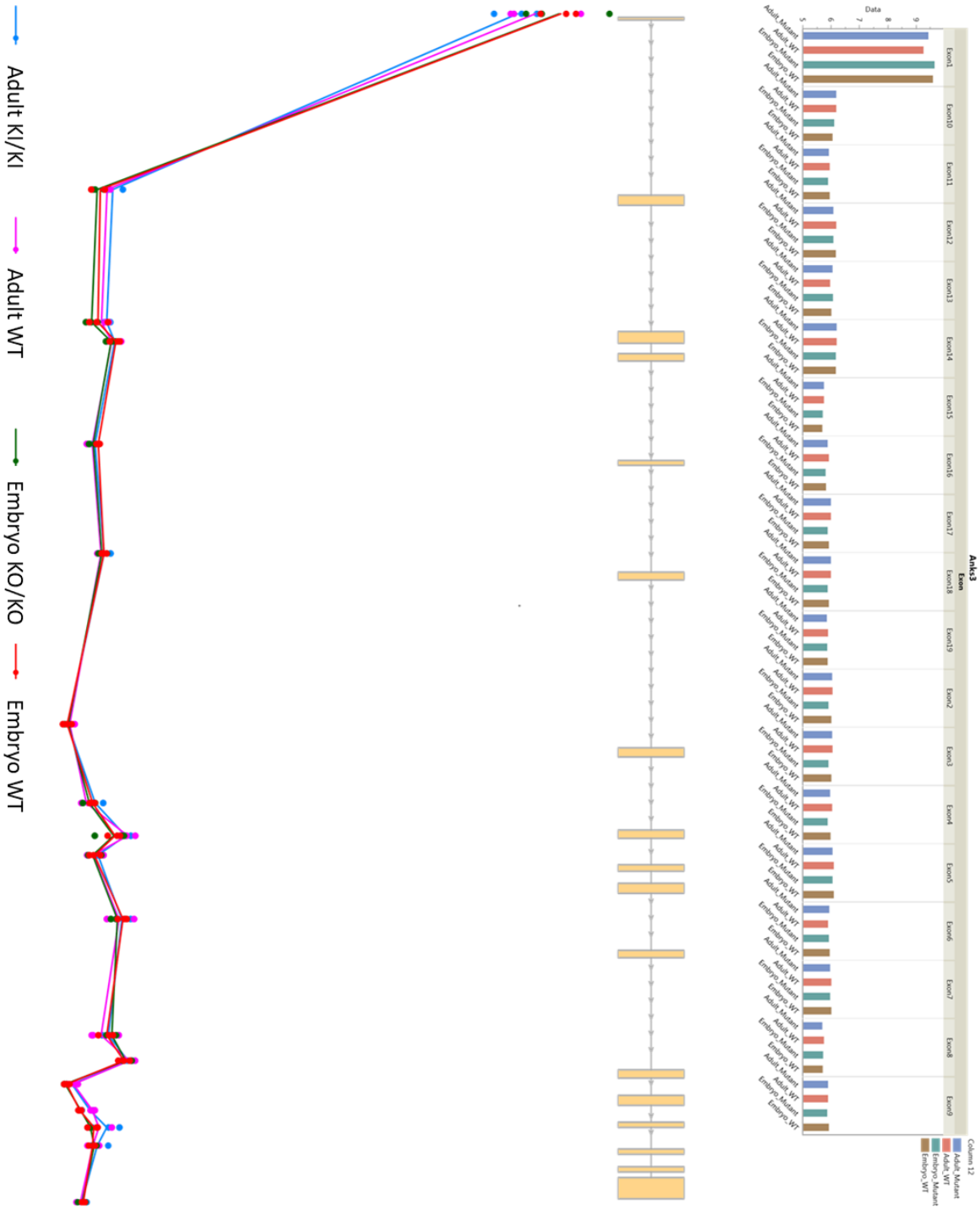

Figure 23- Anks3 exon intensity from RNA expression profiling (ClariomD array). There is no difference in the intensity of exons between adult Anks3$^{KI/KI}$ rats (Adult KI/KI), adult wildtype rats (Adult WT), Anks3$^{KO/KO}$ (Embryo KO/KO) and wildtype rat embryos (Embryo WT) indicating no changes in splicing.

4.2.1.3- *Anks3*$^{\Delta SAM}$ rat

The *Anks3*$^{\Delta SAM}$ rats were generated by using two different gRNAs simultaneously targeting the position I35 in exon 11 and F52 in exon 12 to delete important parts of the SAM domain. We found 17 amino acids were deleted and two amino acids were inserted, partially from intron 11, so that the changes occurred in-frame (figure 24 and 25). As in the case of the *Anks3*^{KI} lines, the exact effect of the *Anks3*$^{\Delta SAM}$ mutation on splicing was unknown. Correct splicing was proven by RT-PCR of heterozygous animals. Figure 22 shows the expected bands for the two alleles in the heterozygous *Anks3*$^{\Delta SAM/WT}$ rats (table 13).

The *Anks3*$^{\Delta SAM}$ mutation should destroy all functionality of the ANKS3-SAM domain as the deletion removed key amino acids from both the mid loop and end helix regions and would severely affect folding of the region. However, the functionality of the Ank domains and C-terminal end should be conserved.

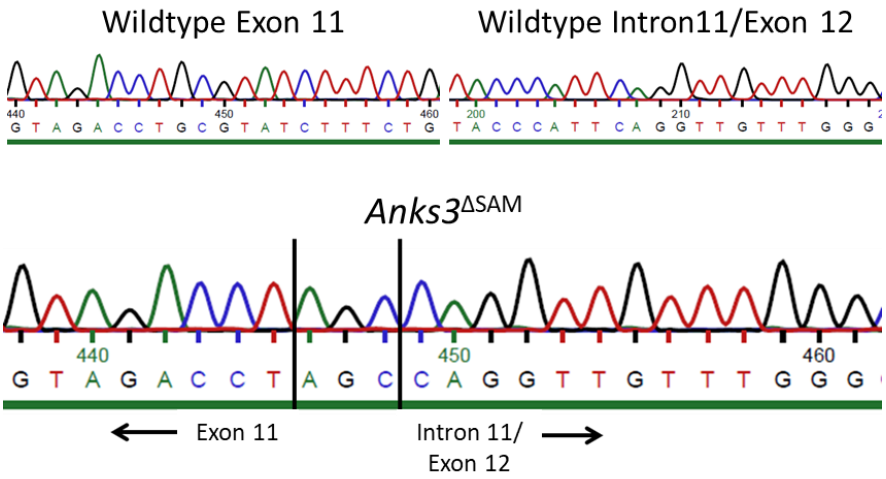

Figure 24- Genotyping of Anks3$^{\Delta SAM}$ *rats indicating the in frame deletion. Sequencing results of the Anks3*$^{\Delta SAM}$ *mutation with wildtype comparisons: part of exon 11 and almost all of intron 11 were removed and three new base pairs were randomly inserted.*

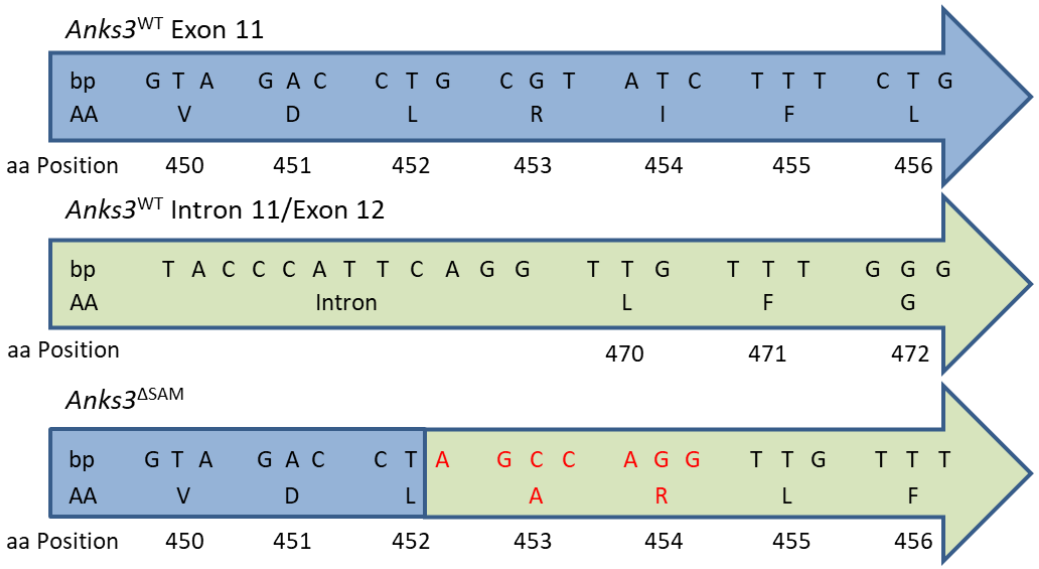

Figure 25- Nucleotide and amino acid sequences for the in-frame Anks3$^{\Delta SAM}$ mutation (base pair and amino acid changes noted in red). The deletion and insertions resulted in an in-frame mutation with seventeen amino acids deleted and two new amino acids inserted in the SAM domain.

4.2.2- Phenotype of the Anks3^{KO} and Anks3$^{\Delta SAM}$ rats

4.2.2.1- The *Anks3*^{KO} and *Anks3*$^{\Delta SAM}$ mutations are prenatally lethal in homozygotes

Among the *Anks3* lines only the *Anks3*^{KI} rats were capable of producing homozygous offspring. The *Anks3*^{KO} and *Anks3*$^{\Delta SAM}$ lines only produced wildtype and heterozygous offspring when both parents were heterozygous. The frequency of wildtype and heterozygous genotypes in the offspring of these lines coincides with the expected frequencies if the homozygous genotype is prenatally lethal. Hence, the majority of further studies were done in the embryos of these lines with some heterozygous animals being aged up to check for any longer-term health problems (table 14).

Table 16- Numbers and percentages of genotypes among the offspring in the new Anks3 rat lines and the expected rates with and without homozygous lethality.

	Total Number of Pups	Wildtype		Heterozygous		Homozygous	
		Number	%	Number	%	Number	%
Anks3^{KI}	109	33	30.2	49	45.0	27	24.8
Anks3^{KO}	101	34	33.7	67	66.3	0	0.0
Anks3$^{\Delta SAM}$	78	24	30.8	54	69.2	0	0.0
Expected			25.0		50.0		25.0
Expected if homozgous die			33.3		66.7		0.0

4.2.2.2- Homozygous *Anks3*^{KO} and *Anks3*$^{\Delta SAM}$ rat embryos display situs inversus and major disturbances in organ patterning

Homozygous rats of the *Anks3*^{KO} and *Anks3*$^{\Delta SAM}$ lines died prenatally showing considerable phenotypic variability similar to other ciliopathic diseases. Though the homozygous embryos were smaller in size and weight than their wildtype or heterozygous littermates many had a normal outer appearance. Localised haemorrhages were the most common defect observed externally followed by obvious malformations of the craniofacial structure and oedema in some animals (figure 26 and 27). The internal anatomy of the homozygous embryos had several noticeable abnormalities including enlarged hearts, smaller kidneys and, in some cases, several pale organs (heart, lungs and intestines). These defects were seen in both lines, usually becoming visible between embryonic days 14.5 and 17.5 (figure 26). MRI imaging of *Anks3*^{KO} embryos also revealed occasional instances of situs inversus of the liver and bladder as well as showing defects in the heart chambers (figure 28). MRI imaging was performed by Marc Pretze (Molecular Imaging and Radiochemistry, Department of Clinical Radiology and Nuclear Medicine, Medical Faculty Mannheim of Heidelberg University, Mannheim, Germany).

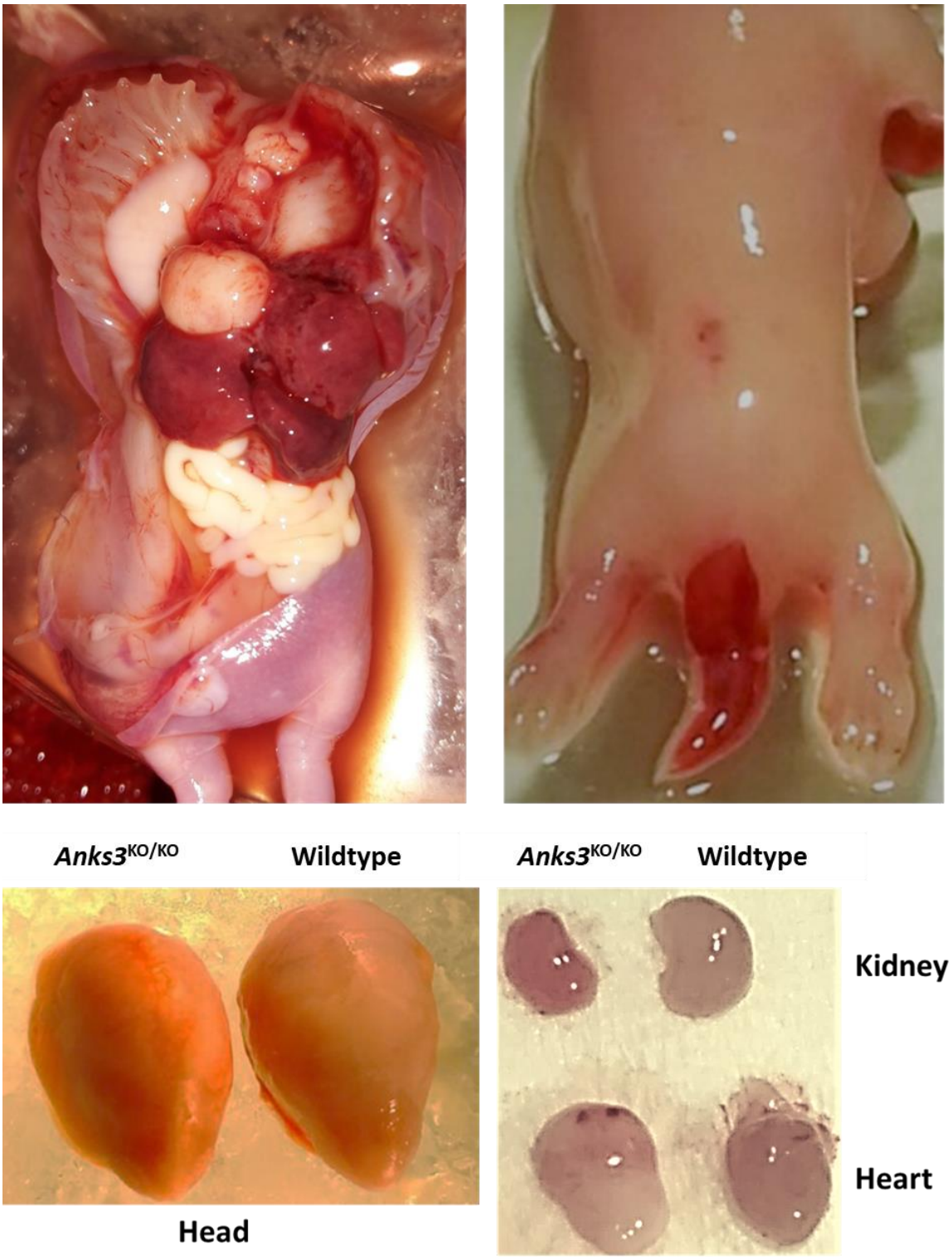

Figure 26- Gross anatomical images of homozygous E17.5 Anks3$^{KO/KO}$ embryos: showing pale organs (top left), focal haemorrhage of the tail (top right), reduced kidney size, enlarged heart and smaller and malformed skull (bottom).

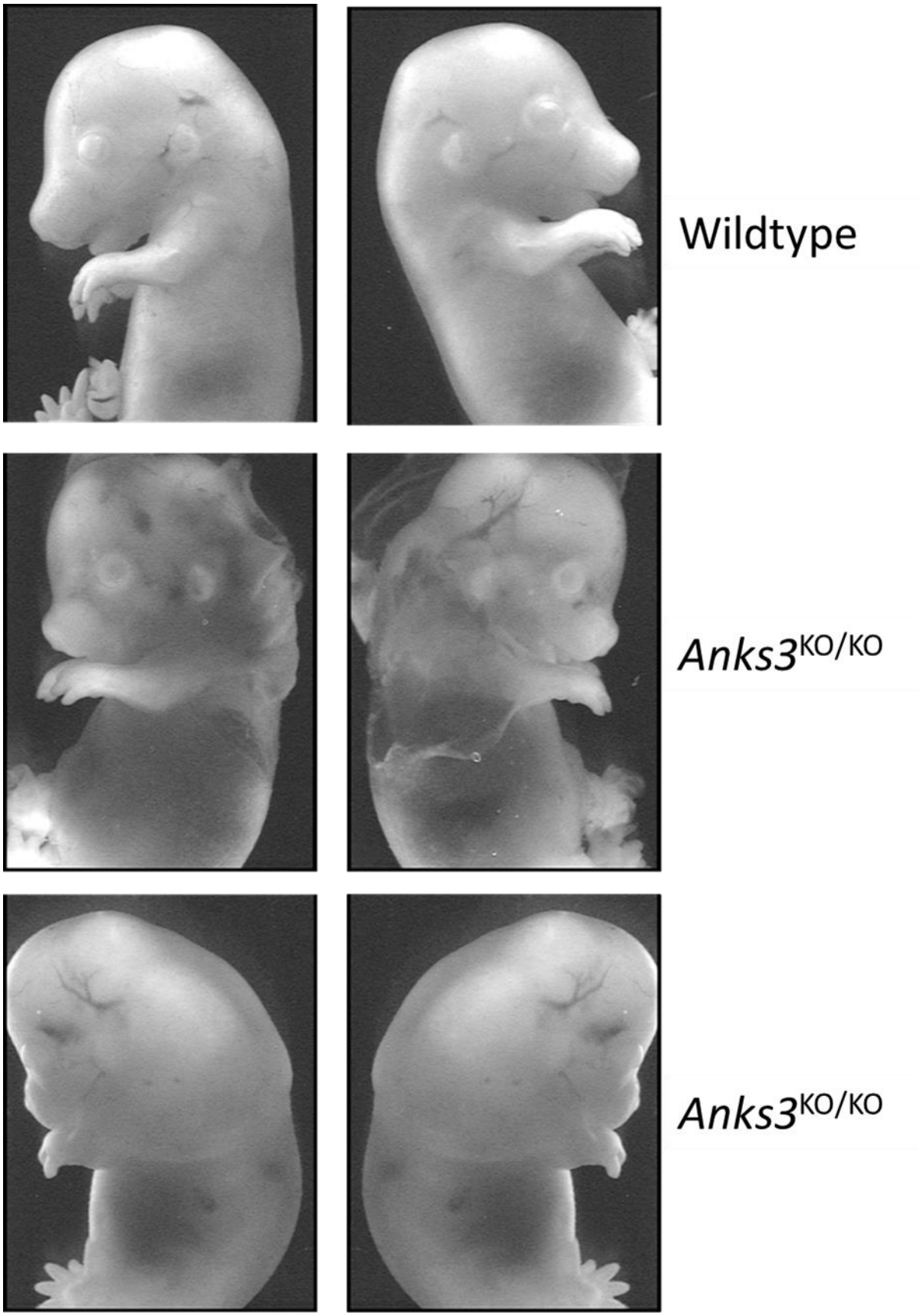

Figure 27- External manifestations in E17.5 homozygous Anks3$^{KO/KO}$ embryos: underdeveloped jaw and poorly formed skull (middle), and significantly retarded growth with oedema (bottom).

The *Anks3*^{KI} mutation reversed important pathways which were upregulated in the TGR*Anks6* rats such as Wnt, Hippo, HIF1 and cAMP signalling and cancer-associated pathways, which are known to be involved in cyst growth, returning them to normal. In the TGR*Anks6* kidneys metabolic pathways related to mitochondrial function (TCA cycle, fatty acid degradation, carbohydrate, lipid and amino acid metabolism) were downregulated which was reversed by the *Anks3*^{KI} mutation in the TGR*Anks6-Anks3*$^{KI/KI}$ rats (figure 43). However, 10 pathways were altered similarly in both the TGR*Anks6* and TGR*Anks6-Anks3*$^{KI/KI}$ kidneys indicating that the inability of the ANKS3-SAM domain to form homopolymers due to the *Anks3*^{KI} mutation has no influence on these, in the context of PKD (figure 44). These pathways included ‘fatty acid metabolism’, ‘oxidative phosphorylation’ and ‘collecting duct acid secretion’, which were downregulated and ‘DNA replication’, ‘PI3K-Akt signalling’ and ‘cell cycle’, which were upregulated in both genotypes.

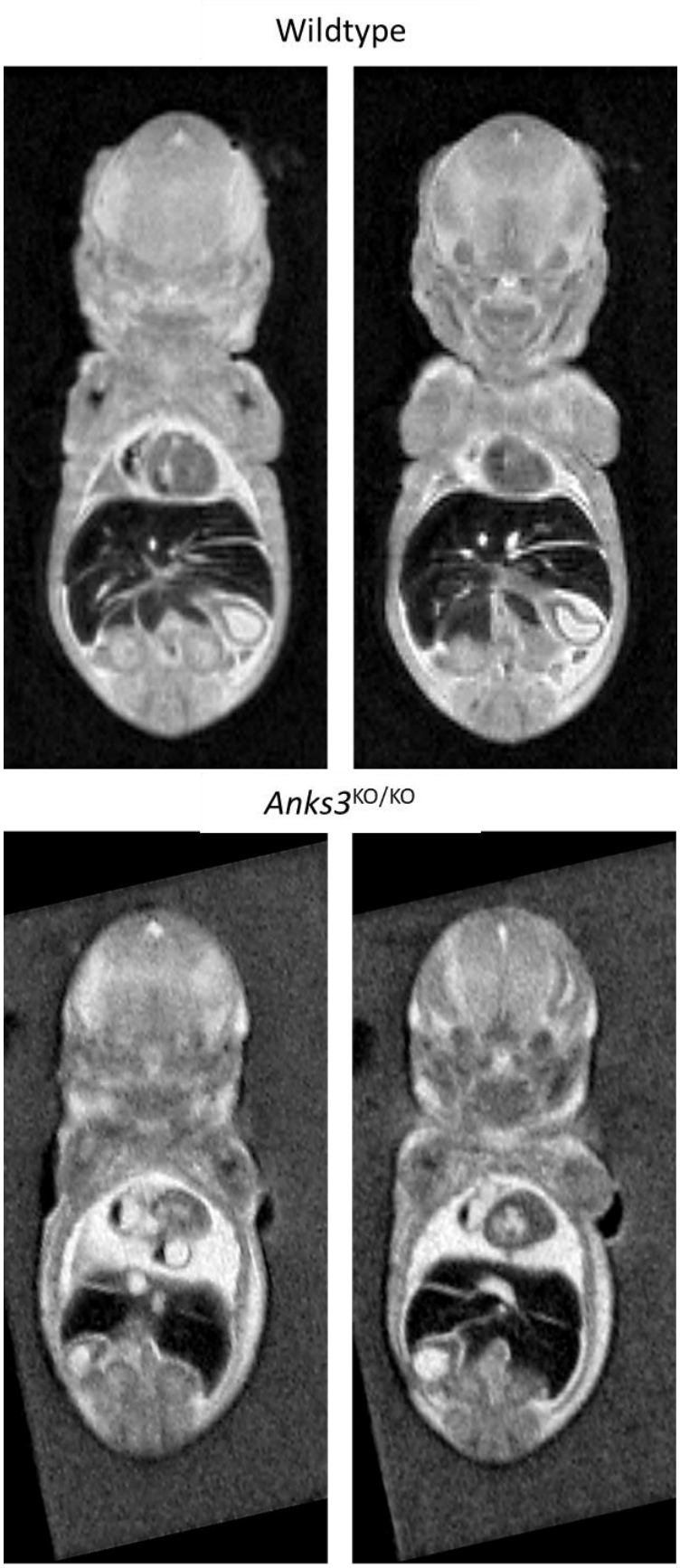

Figure 28- MRI images of E17.5 Anks3$^{KO/KO}$ embryos showing instances of situs inversus of the liver and bladder, as well as abnormal cardiac structures.

Histological examination of the homozygous embryos revealed the defects in the heart, kidney and craniofacial structure in greater detail. In the heart, the atria were greatly dilated while the ventricle walls were thin (figure 29). Additionally, septum defects were often observed resulting in a single ventricle or atrium. In the craniofacial region there were defects in the development of the cortex and midbrain, cleft palates and underdeveloped mandibles. Additional defects were seen in skeletal and neuronal patterning and neural tube closure (figure 30). These defects were seen in both lines however the severity of each defect varied among individual homozygous offspring.

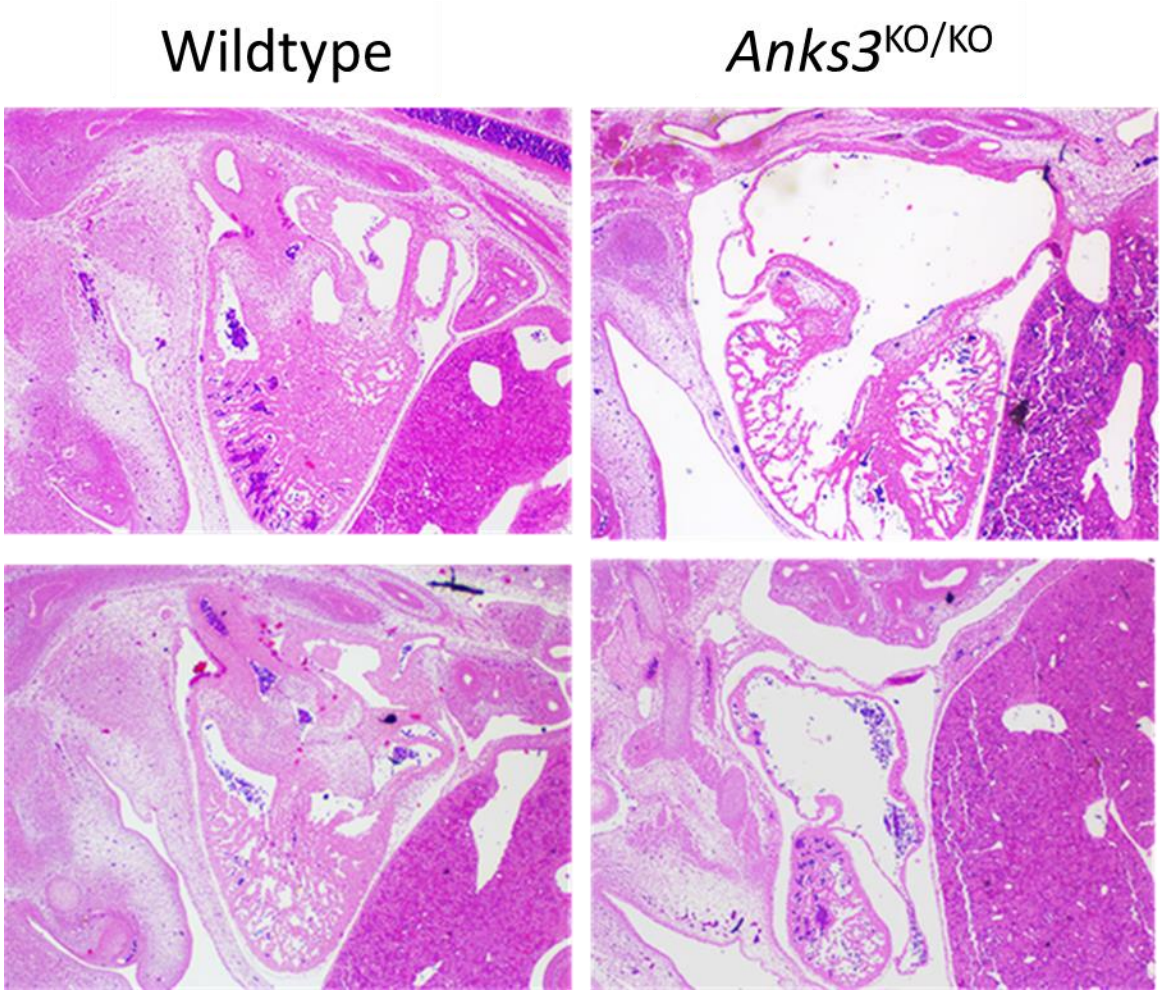

Figure 29- Histology of hearts from E17.5 homozygous Anks3$^{KO/KO}$ embryos with dilated atria and thin, poorly formed ventricle walls.

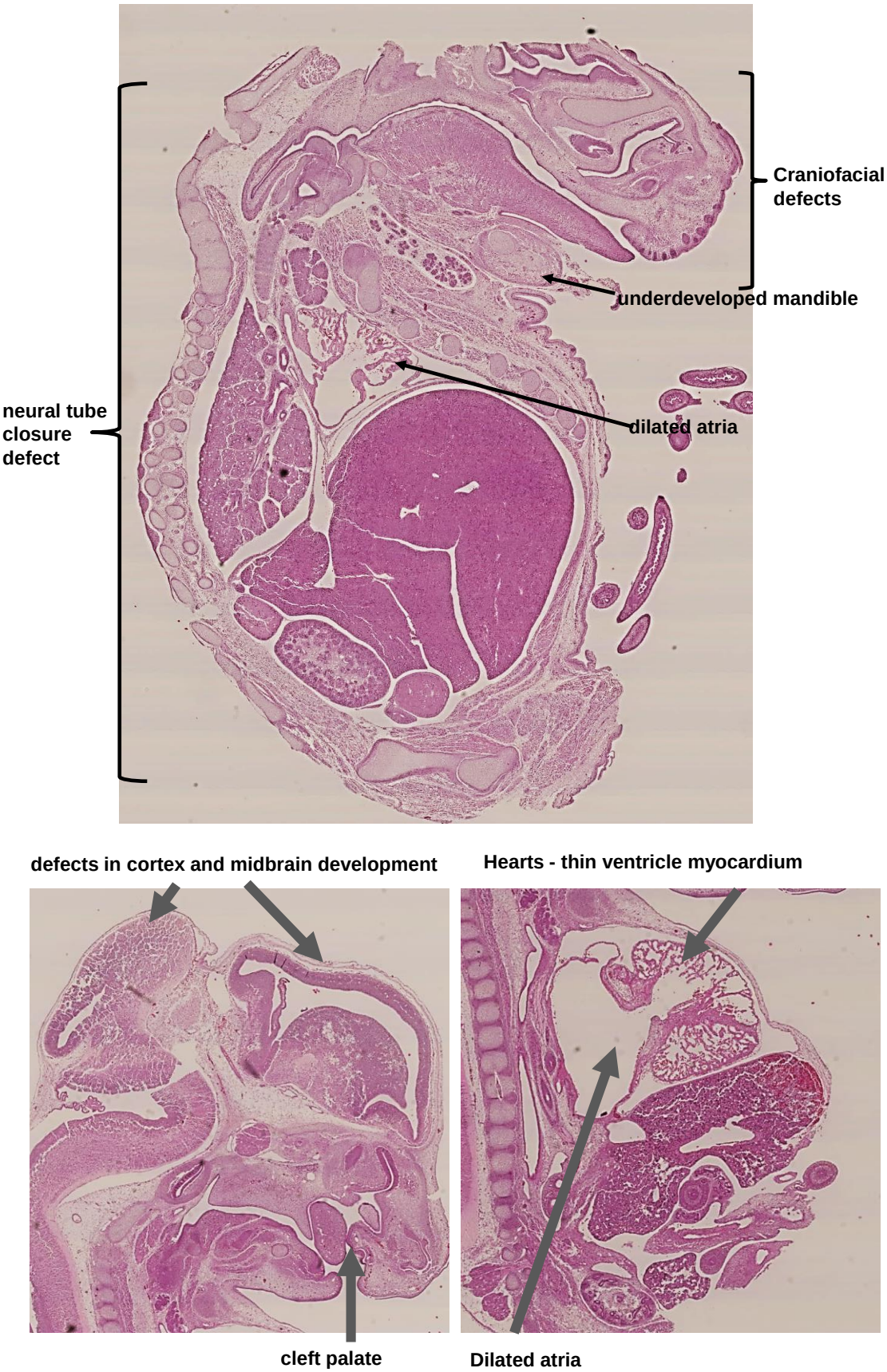

Figure 30- Histology of E18.5 homozygous Anks3$^{KO/KO}$ embryos with the developmental defects indicated.

Histological evaluation of homozygous *Anks3*$^{KO/KO}$ embryos revealed poorly organised muscle tissue in the heart. The kidneys were often smaller and showed severe disturbances of renal glomerulogenesis and tubulogenesis and a reduced number of tubules (figure 31). Cystic kidneys, like those seen in *Anks6* mutant rat embryos, were never observed. The histopathological evaluation was supported by Prof. Gröne (DKFZ, University Heidelberg) and Prof. Dobreva (Medical Faculty Mannheim, University Heidelberg)

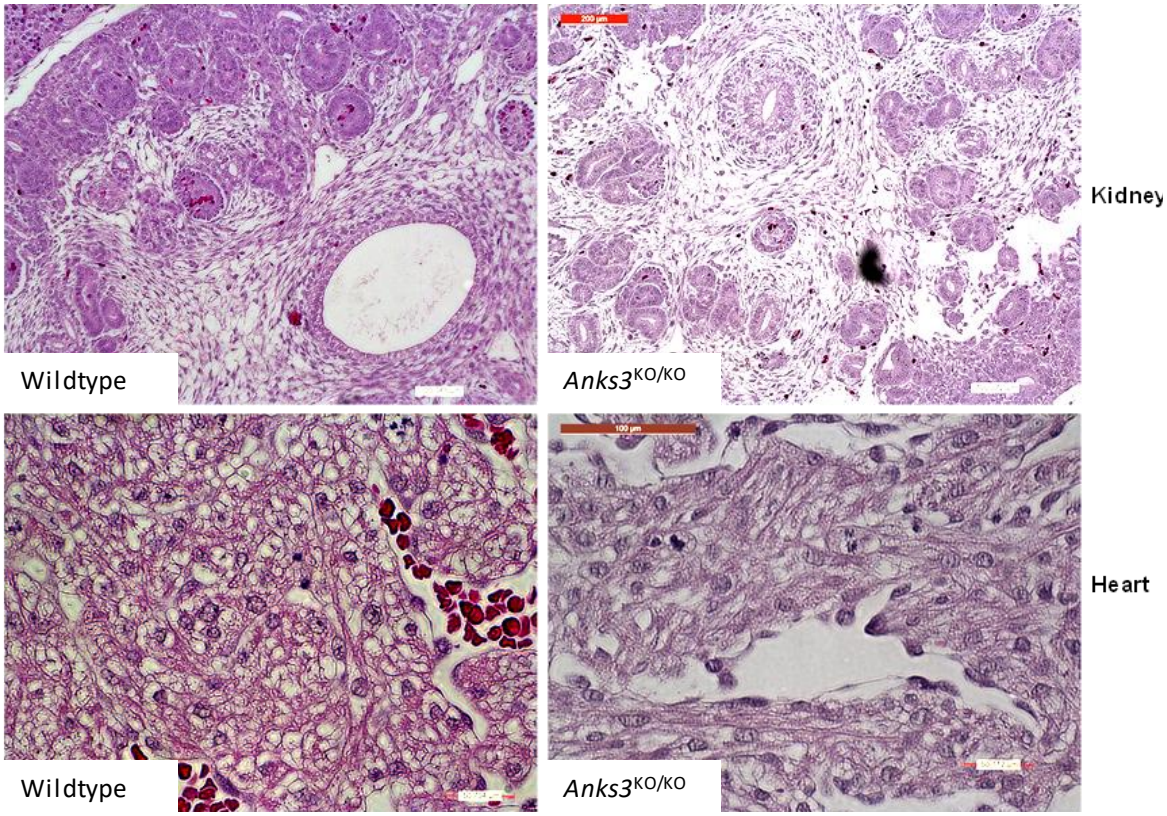

Figure 31 Histology of heart and kidneys from E17.5 homozygous Anks3$^{KO/KO}$ *embryos. Haematoxylin/eosin staining showes disturbances in glomerulogenesis and tubulogenesis (top) and poorly organised heart muscle tissue (bottom).*

The phenotype we observed in the homozygous *Anks3*$^{KO/KO}$ and *Anks3*$^{\Delta SAM}$ rats had the typical features of a ciliopathic disorder. As such, we performed immunohistochemistry for acetylated tubulin to stain the cilia. Figure 32 shows that cilia formation is not disturbed although they seem to be longer in *Anks3*$^{KO/KO}$ compared to wildtype embryos. However, we did not investigate whether cilia function is altered.

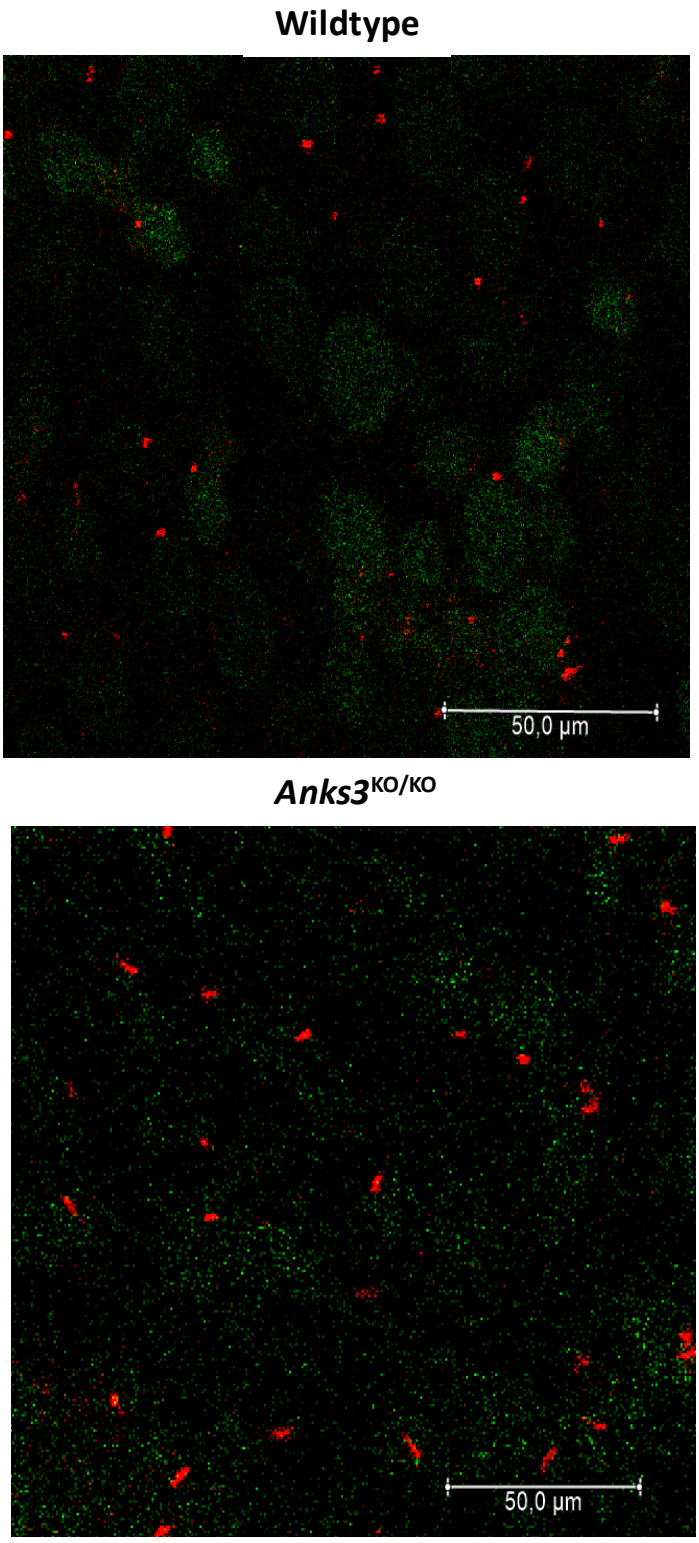

Figure 32- Immunohistochemistry of cilia in cleared Ank3$^{KO/KO}$ tissue using the expansion microscopy technique. Cilia, stained with an anti-acetylated tubulin antibody, were observed in both the wildtype and Anks3$^{KO/KO}$ embryos (green- nuclear stain with sytox green, red- acetylated tubulin).

4.2.2.3- *Anks3*^{KO} upregulates proliferative pathways and downregulates DNA replication and repair pathways in embryonic kidneys

Gene expression profiling was carried out on the embryonic kidneys of E17.5 day old *Anks3*$^{KO/KO}$ embryos and wildtype littermates using the Clariom^{TM} D array for rats. The expression of 26 pathways were significantly different in the *Anks3*$^{KO/KO}$ kidneys vs. wildtype. Interestingly, a number of pathways related to DNA replication and damage response, including 'DNA Replication', 'Nucleotide Excision Repair', 'Mismatch Repair' and 'Proteasome', (table 18) were significantly downregulated in *Anks3*$^{KO/KO}$ kidneys. In contrast, pathways related to proliferation, including 'Pathways in cancer', 'Proteoglycans in cancer', 'cAMP-', 'PI3K-Akt-', 'Ras-' and 'Ca^{2+} signalling', were upregulated (figure 33). These results fit well to the recently discovered association between cilia function and DNA damage response and proliferation. Other important pathways in embryogenesis were also upregulated including Notch, Wnt and MAPK, but did not reach statistical significance.

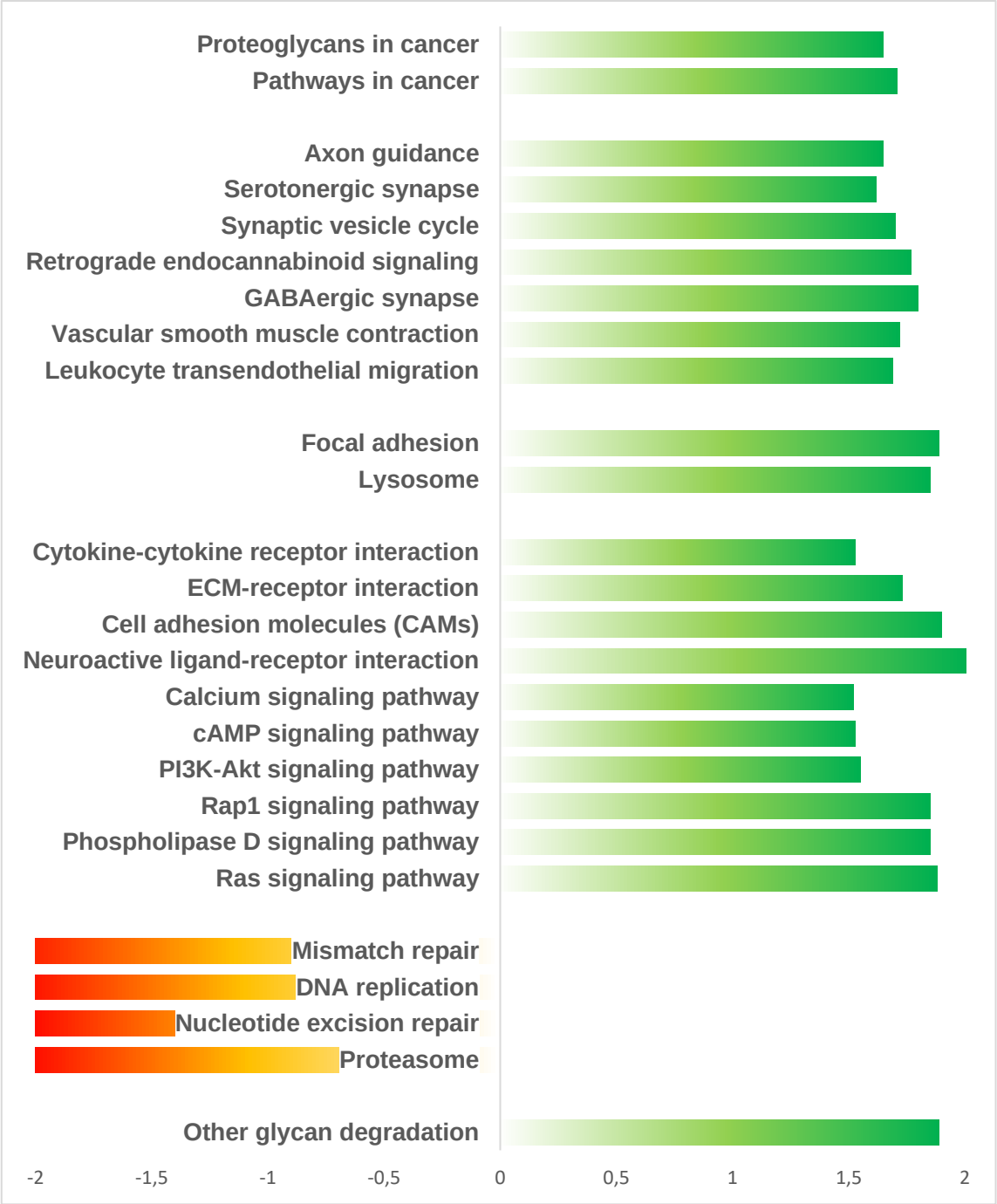

Figure 33- Pathway expression changes in E17.5 Anks3$^{KO/KO}$ rats. Significantly (p<0.05) changed pathways in E17.5 Anks3$^{KO/KO}$ rat embryos compared to wildtype embryos, showing downregulation of DNA damage response/ repsir pathways and upregulation of pathways involved in proliferation, cell-cell interactions and cancer

4.2.2.3- Heterozygous *Anks3*$^{KO/WT}$ causes a mild NPHP-like phenotype in aged rats

The heterozygous *Anks3*$^{KO/WT}$ rats developed normally and could only be distinguished from their wildtype rats, with regard to the kidney function and structure, by a slight decrease in plasma glucose levels up to an age of eight months, as shown in table 15. However, when

aged more than a year, *Anks3*$^{KO/WT}$ rats often developed thickening of the intertubular interstitium and narrowing of the tubular lumen in the renal medulla. Additionally, in some cases we found small medullary cysts and mild cortical fibrosis (figure 34).

Table 17- Clinical data from 8 month old Anks3$^{KO/WT}$ *and Anks3*$^{KI/KI}$ *rats with wildtype comparisons. Urine parameters are designated with u- and plasma parameters designated with p-.*

Clinical Parameter	**Wildtype** Mean ± SD	***Anks3*$^{KO/WT}$** Mean ± SD	***Anks3*$^{KI/KI}$** Mean ± SD
24 Hour Metabolic Cage			
Urine (ml)	30.5 ± 9.0	25.1 ± 10.2	18.6 ± 2.6
Water Intake (ml)	47.8 ± 9.5	43.1 ± 14.0	33.9 ± 2.6
Urinary Osmolarity (osmo/L)	1029 ± 283.7	1119.5 ± 336.1	1710 ± 370.6
Urine			
u-Urea (mg/24 h)	855.1 ± 96.4	799.9 ± 151.8	970.9 ± 91.5
u-Creatinine (mg/24 h)	20.3 ± 1.7	20.0 ± 2.8	19.2 ± 2.5
u-Protein (mg/24 h)	9.3 ± 3.7	11.6 ± 4.0	27.9 ± 29.4
u-Albumin (mg/24 h)	632 ± 689.9	303.1 ± 296.9	10894.3 ± 17221.8
u-Glucose (mg/dl)	3.2 ± 2.9	6.4 ± 9.5	12.0 ± 10.5
Blood Plasma			
p-Urea (mg/dl)	38.3 ± 1.2	33.9 ± 1.8	33.9 ± 4.1
p-Creatinine (mg/dl)	0.38 ± 0.01	0.31 ± 0.03	0.32 ± 0.05
p-Cholesterine (mg/dl)	94.0 ± 5.0	87.9 ± 11.0	123.1 ± 34.3
p-Triglycerides (mg/dl)	140.2 ± 26.2	148.7 ± 24.5	144.3 ± 50.8
p-Protein (mg/ml)	66.2 ± 2.6	58.9 ± 2.0	71.3 ± 5.4
p-Glucose (mg/dl)	282.5 ± 37.0	173.9 ± 36.8	148.1 ± 9.0

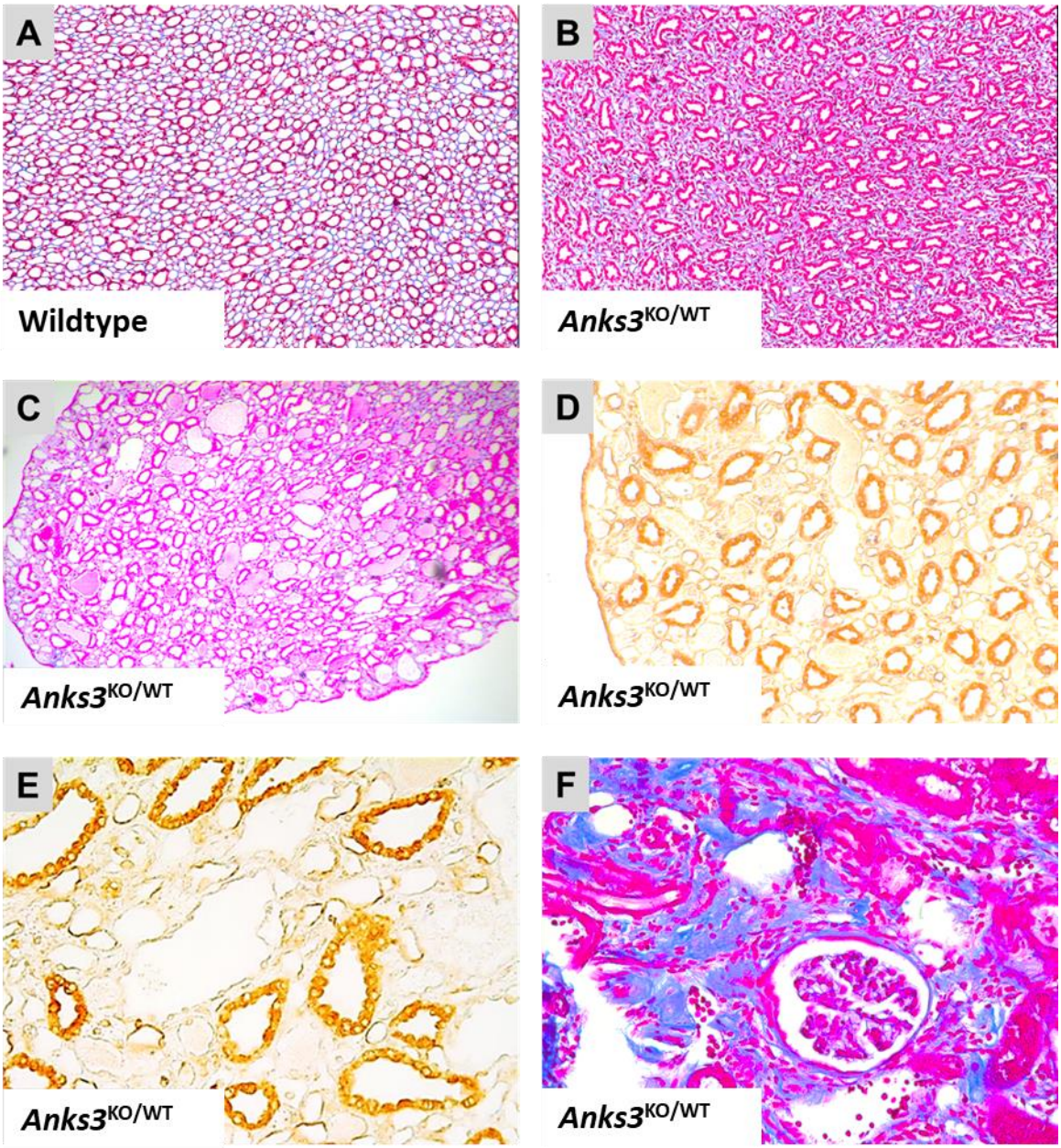

Figure 34- Renal phenotype of aged Anks3$^{KO/WT}$ rats. A-C- H&E staining of wildtype renal medulla (A) and Anks3$^{KO/WT}$ renal medulla showing thickening of the intertubular interstitium and narrowing of the tubular lumen of 8 month old rats (B) and small cysts in 16 month old rats (C). D,E- Immunohistochemistry showing ANKS3 expression in the collecting ducts but not in the cystic or dilated tubules. F- 8 month old Anks3$^{KO/WT}$ renal cortex showing mild fibrosis (Azan staining).

4.2.3- Phenotype of the Anks3-SAM$^{p.I35E}$ rats

4.2.3.1- The *Anks3*-SAMp$^{.I35E}$ mutation is involved in urine concentration but does not result in renal disease

Rats carrying the *Anks3*^{KI} mutation develop normally, even in the homozygous state. Since the *Anks3*^{KI} mutation in the SAM domain has been shown to prevent homopolymerisation but does not disturb binding to the ANKS6-SAM domain, we conclude that ANKS3 homopolymerisation is not essential for embryonic development or kidney morphogenesis. To obtain metabolic data and clinical data from 24 hour urine we placed old male *Anks3*$^{KI/KI}$ rats and wildtype comparisons into metabolic cages for 24 hours. In addition, the clinical plasma parameters were determined (table 15). Of note, the *Anks3*$^{KI/KI}$ rats showed significantly decreased urine excretion along with increased urine osmolarity and decreased water intake. Urinary concentrations of urea and creatinine were increased, however, the 24 hour excretion was unaffected. The urea and creatinine concentrations in the plasma were slightly decreased, which might be caused due to increased water reabsorption (table 15). In some cases in 12 month old animals urinary albumin was increased which is not unusual in these rats.

In chapter 4.1 we showed that both ANKS3 and ANKS6 co-localise with AQP2 in renal collecting duct cells. As AQP2 is an important mediator of water reabsorption in renal tubules we investigated whether ANKS3 is involved in the regulation of AQP2 expression. As shown in figure 35 both the RNA and protein AQP2 levels were slightly increased in *Anks3*$^{KI/KI}$ rats when compared with wildtype littermates (figure 35). This could represent one mechanism by which urine concentration is affected in *Anks3*$^{KI/KI}$ rats. In this context it is noteworthy that Delestré et al. (69) found increased AQP2 expression when *Anks3* was downregulated in 4 day old mice. Moreover, polyuria is an early sign of NPHP.

Histological evaluation did not show any sign of renal defects, even when the rats were aged more than a year (figure 36 top). The percentage of fibrotic tissue in the kidney cortex was calculated and found to be unchanged in the *Anks3*$^{KI/KI}$ rats (figure 36 bottom).

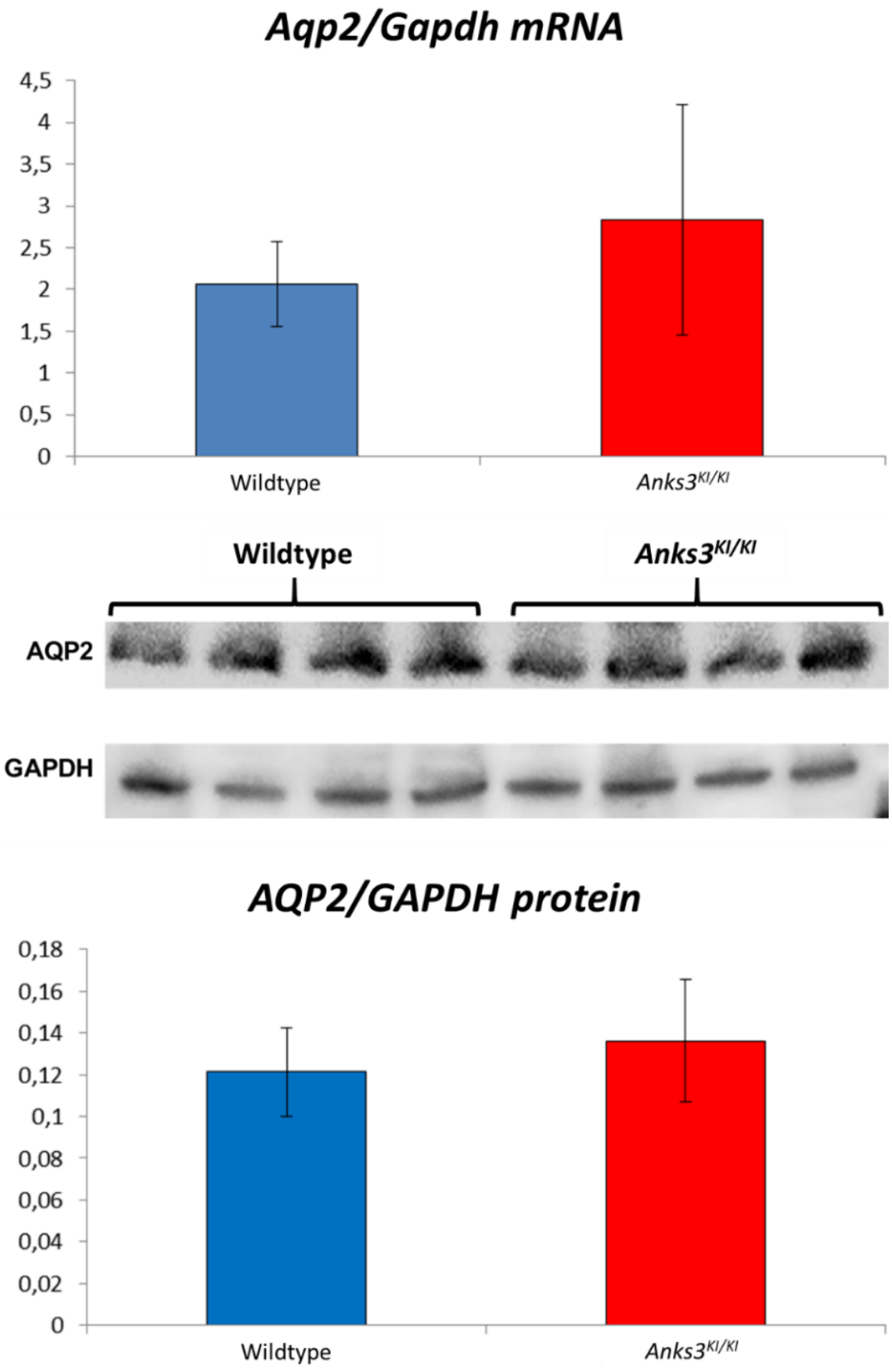

Figure 35- Expression of Aqp2 mRNA and protein in Anks3$^{KI/KI}$ rats. Top- qPCR data showing a slight increase in Aqp2 mRNA expression in Anks3$^{KI/KI}$ rats. Bottom- Western blot data showing slightly increased AQP2 protein expression in Anks3$^{KI/KI}$ rats (4 animals per group).

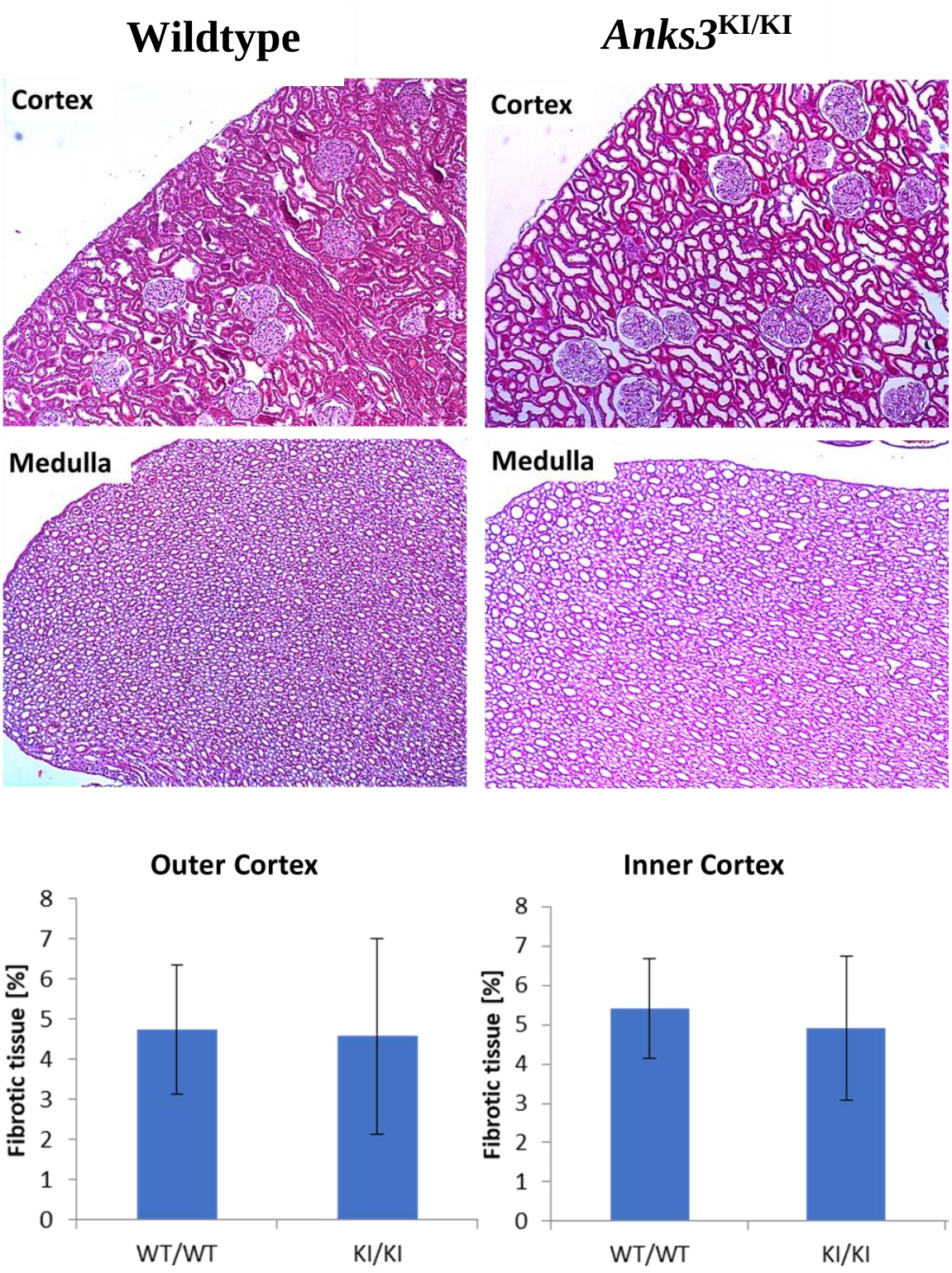

Figure 36- Renal histology and fibrosis quantification in Anks3$^{KI/KI}$ rat kidneys. Top- Azan staining of Anks3$^{KI/KI}$ kidneys showed no histological abnormalities (10x objective). Bottom- Percentage of fibrotic tissue in the kidney cortex with no difference between Anks3$^{KI/KI}$ animals and wildtype comparisons (6 animals per group).

4.2.3.2- The *Anks3*-SAM$^{p.I35E}$ mutation downregulates metabolic pathways and upregulates pathways associated with the cell cycle and cilia in adult rats

We determined the mRNA expression profile of kidney tissue from eight month old *Anks3*$^{KI/KI}$ rats and wildtype controls using the Clariom^{TM} D array for rats. It is obvious from the data that the *Anks3*^{KI} mutation affects quite a different set of pathways in the adult rats than *Anks3*^{KO} in the embryos. Unlike the *Anks3*$^{KO/KO}$ embryos, pathways related to 'DNA replication' and 'DNA damage response' and signalling pathways related to proliferation and survival are unchanged in the *Anks3*$^{KI/KI}$ rats (table 18). It is noteworthy that important pathways known to be related to cilia function and cell cycle regulation, such as Notch, Hippo and Wnt signalling, are significantly upregulated in the *Anks3*$^{KI/KI}$ rats. Additionally, the pathways 'microRNA in cancer' and 'RNA transport' are also upregulated. Moreover, many metabolic pathways related to mitochondria function are significantly downregulated as well as the pathway 'collecting duct acid secretion' (figure 37). Since we found ANKS3 is expressed in the intercalated cells of the collecting duct, a possible role for ANKS3 in the regulation of collecting duct acid secretion is reasonable. However, since the altered pathways did not have pathological consequences, they seem to be well tolerated.

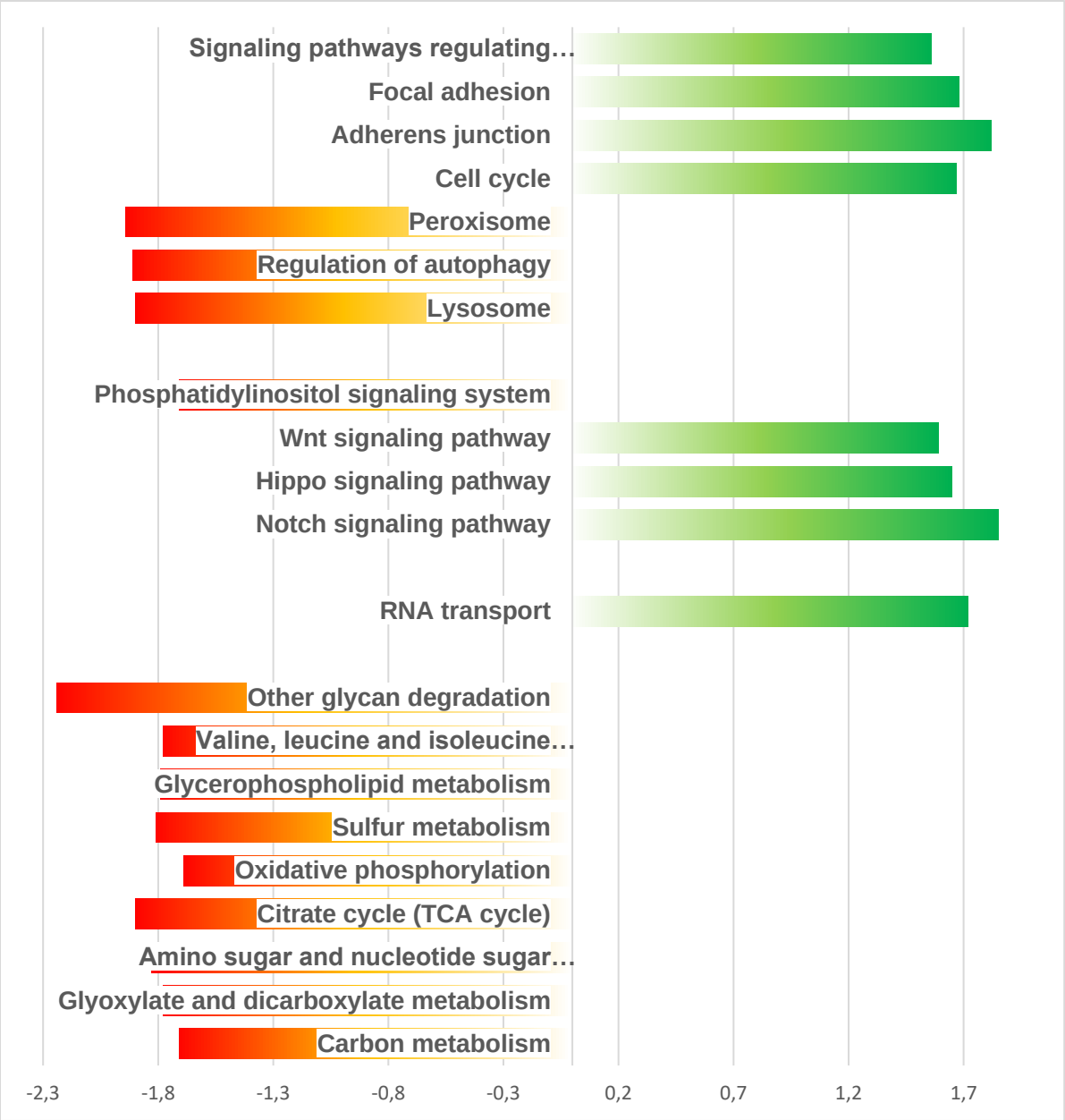

Figure 37- Pathway Expression Changes in Anks3$^{KI/KI}$ vs Wildtype Rats. Significantly ($p<0.05$) changed patways in 8 month old Anks3$^{KI/KI}$ rats compared to wildtype rats showing downregulation preferently of metabolic pathways and upregulation of key pathways involved in ciliopathies (Wnt, Hippo, Notch), RNA transport, cell cycle. and cell-cell interactions.

4.2.3.3- The *Anks3*-SAM$^{p.I35E}$ mutation retards cyst growth in TGR*Anks6* rats

As shown previously, ANKS6 binding to the ANKS3-SAM domain inhibits ANKS3 homopolymerisation. The *Anks6*$^{p.R823W}$ mutation prevents this binding, so increased homopolymerisation of ANKS3 might contribute to the ADPKD phenotype in the *Anks6*$^{p.R823W}$ rats. Hence, we aimed to study the effect of the *Anks3*^{KI} mutation, which prevents ANKS3-SAM domain homopolymerisation, on the ADPKD phenotype of TGR*Anks6* rats. To this end, we crossed the TGR*Anks6* line with the *Anks3*^{KI} line to generate rats with heterozygous *Anks6*$^{p.R823W}$ and homozygous *Anks3*$^{KI/KI}$ mutations. In these rats ANKS6 cannot bind to ANKS3 anymore and so cannot inhibit ANKS3 self-polymerisation. However, due to the presence of the homozygous *Anks3*$^{KI/KI}$ mutation, ANKS3 polymerisation is prevented. Since the *Anks3*$^{KI/KI}$ rats did not display any pathological phenotype and showed increased water resorption in the renal tubules, we hypothesised that the *Anks3*^{KI} mutation may have a protective effect in the TGR*Anks6* PKD model.

The TGR*Anks6*-*Anks3*$^{KI/KI}$ double mutant rats were sacrificed at 11-12 days (developing kidney) and at four weeks (mature kidney) after birth. As shown in figure 38, we observed a remarkable protective effect of *Anks3*$^{KI/KI}$ on cyst growth. In developing TGR*Anks6*-*Anks3*$^{KI/KI}$ kidneys the inability of ANKS3-SAM to self-polymerise prevented renal hypertrophy and cyst growth. TGR*Anks6*-*Anks3*$^{KI/WT}$ rats had a reduced degree of cystic disease (figure 38).

The protective effect of homozygous *Anks3*$^{KI/KI}$ on cyst growth persisted even in the four week old kidney. In the TGR*Anks6*-*Anks3*$^{KI/WT}$ rats the heterozygous *Anks3*$^{KI/WT}$ mutation only slowed cyst growth but did not prevent it, which indicates a dose dependent effect (figure 39).

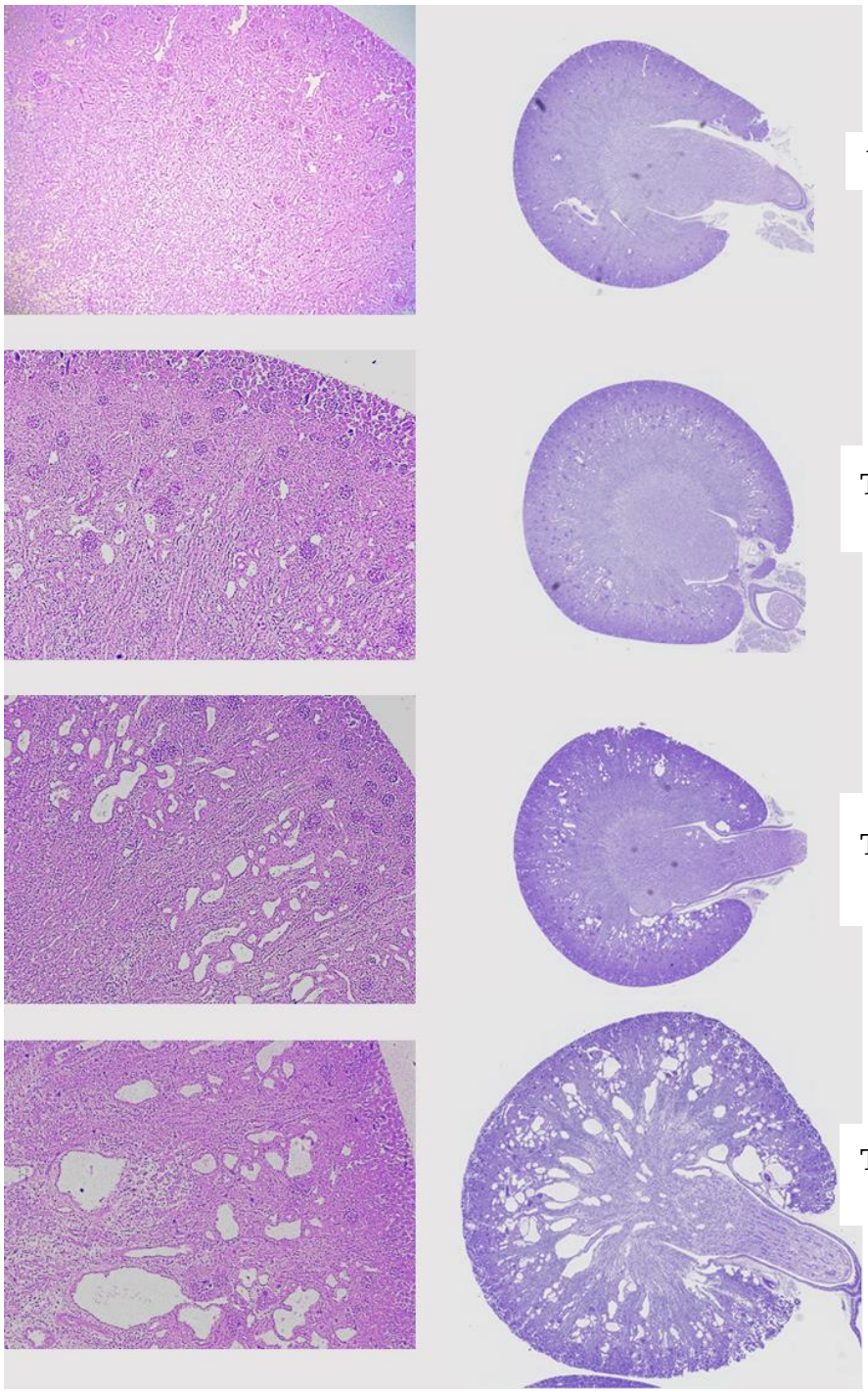

Figure 38- Anks3^{KI} *mutation retards cyst growth in 11-day old TGRAnks6-Anks3*^{KI} *rats. H&E stained kidney sections showing dose dependently reduced cyst growth in the developing kidneys of TGRAnks6 rats also carrying the Anks3*^{KI} *mutation.*

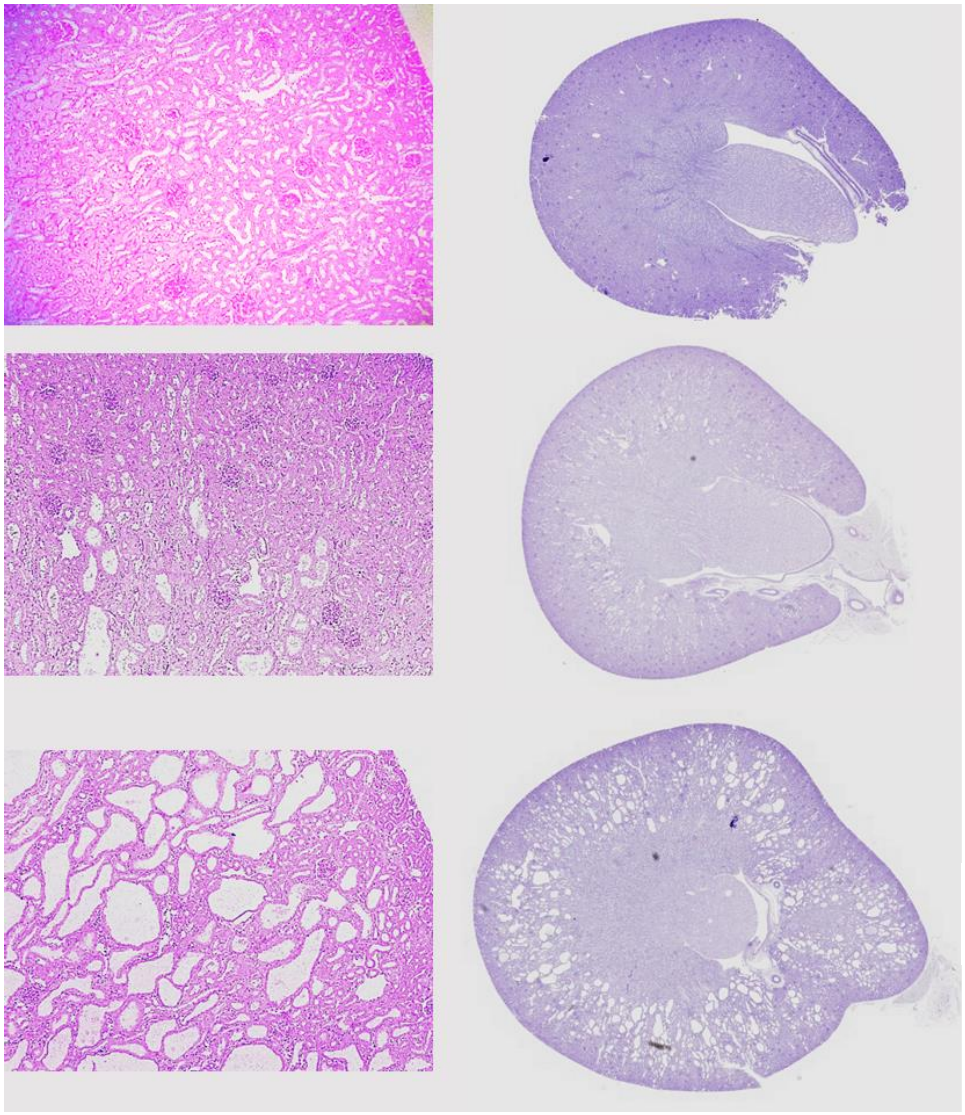

Figure 39- Anks3^{KI} *mutation retards cyst growth in 4 week old TGRAnks6-Anks3*^{KI} *rats. H&E stained kidney sections showing dose dependently reduced cyst growth in the mature TGRAnks6 rats also carrying the Anks3*^{KI} *mutation.*

As a parameter for renal hypertrophy the kidney/body weight (KW/BW) ratios were determined in addition to the cyst score as a parameter for disease severity. The cyst score was calculated by comparing the size of the cysts to the glomeruli (0=no cysts, 1= <2 glomeruli, 2= 2-4 glomeruli, 3= 4-6 glomeruli, 4= >6 glomeruli). In agreement with the histology data, both KW/BW and cyst scores were significantly reduced due to *Anks3*$^{KI/KI}$ (figure 40). The data also demonstrated the remarkable dose effects of the ANKS3-SAM self-polymerisation on cyst growth when homozygous and heterozygous *Anks3*^{KI} rats were compared.

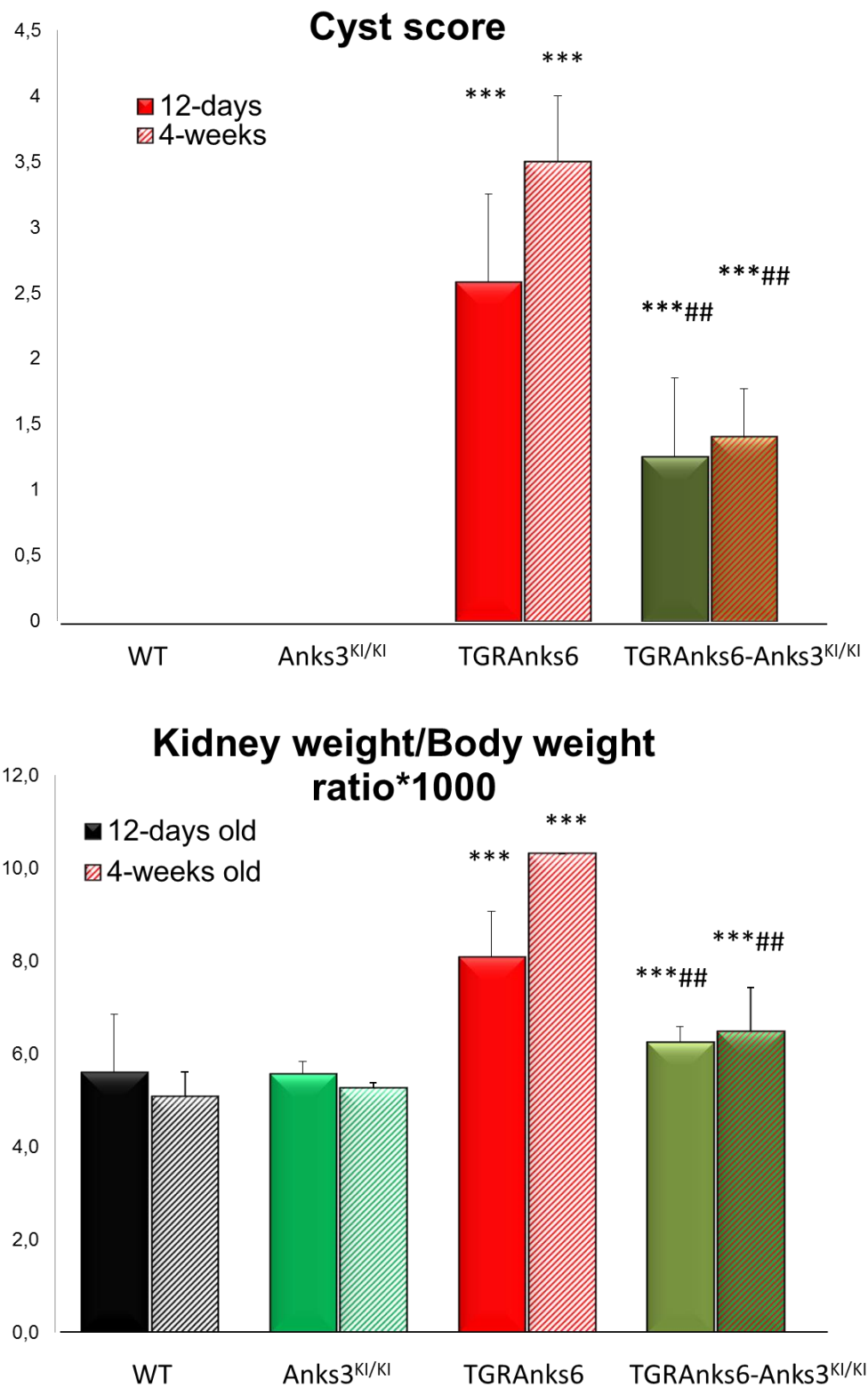

*Figure 40- Anks3^{KI} mutation retards cyst score and renal hypertrophy. Defective Anks3 homopolymerisation due to the Anks3^{KI} mutation decreases kidney weight to body weight ratio and cyst scores in 12 day and 4 week old TGRAnks6-Anks3^{KI} rats compared to the TGRAnks6rats. ***p<0,001 vs WT, ##p<0,01 vs. TGR.*

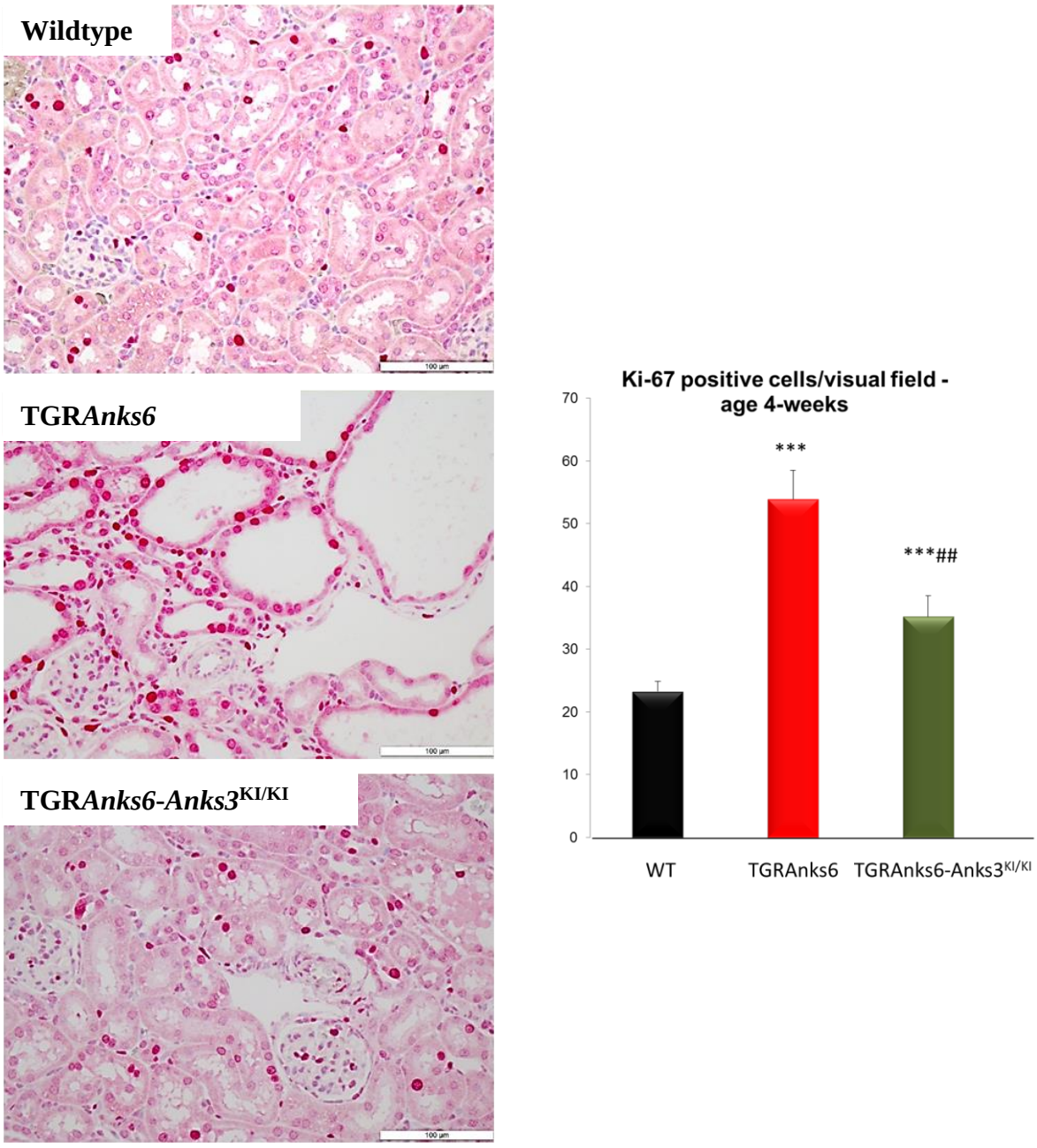

*Figure 41- Anks3^{KI} mutation reduces cell proliferation in 4 week old TGRAnks6-Anks3$^{KI/KI}$ rats. Immunohistological staining for KI-67 in the kidneys of wildtype (WT), TGRAnks6 and TGRAnks6-Anks3$^{KI/KI}$ rats shows an increased number of proliferating cells in the TGRAnks6 rats compared to WT. Number of Ki-67positive cells per visual field is significantly decreased in TGRAnks6-Anks3$^{KI/KI}$ rats vs. TGRAnks6. *** p<0.001 vs WT, ## p<0.01 vs TGRAnks6).*

Additionally, sections from four week old rats were stained for KI-67, a proliferation marker, and the number of positively stained cells per visual field were counted. As expected, the TGR*Anks6* rats had a significant increase in the number of proliferating cells compared to wildtype rats. The TGR*Anks6-Anks3*$^{KI/KI}$ rats had a significant reduction compared to the TGR*Anks6* rats, though there were still significantly more KI-67 positive cells than in wildtypes (figure 41).

4.2.3.4- The *Anks3*-SAM$^{p.I35E}$ mutation reverses the majority of pathways altered in the TGR*Anks6* rats and upregulates DNA replication and repair pathways

Gene expression profiling was performed on renal tissue from 11-12 day old rats TGR*Anks6* and TGR*Anks6-Anks3*$^{KI/KI}$ with wildtype controls using the RaGene 2.0 ST rat microarray. As shown in figure 42 the *Anks3*^{KI} mutation reversed the majority of pathways which were altered by the *Anks6*$^{p.R823W}$ mutation. While in kidneys of TGR*Anks6* rats expression of 131 pathways is significantly different compared to wildtypes, in the TGRA*nks6-Anks3*$^{KI/KI}$ rat kidneys only 20 pathways are different from wildtypes.

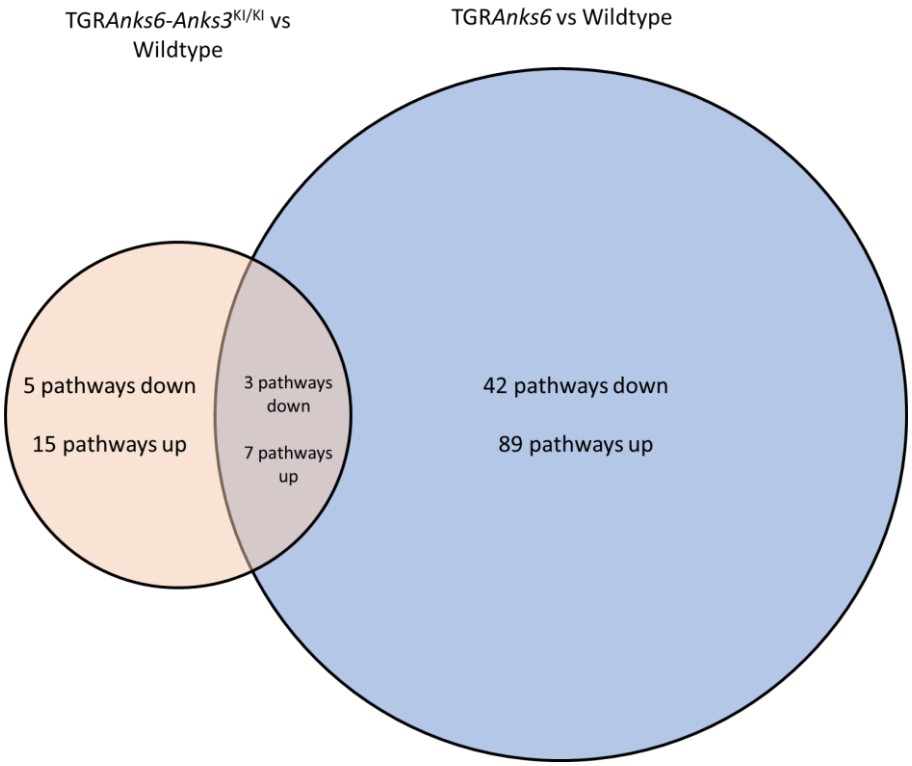

Figure 42- Venn diagram showing pathways up and downregulated in TGRAnks6 and TGRAnks6-Anks3$^{KI/KI}$ *rats versus wildtype.*

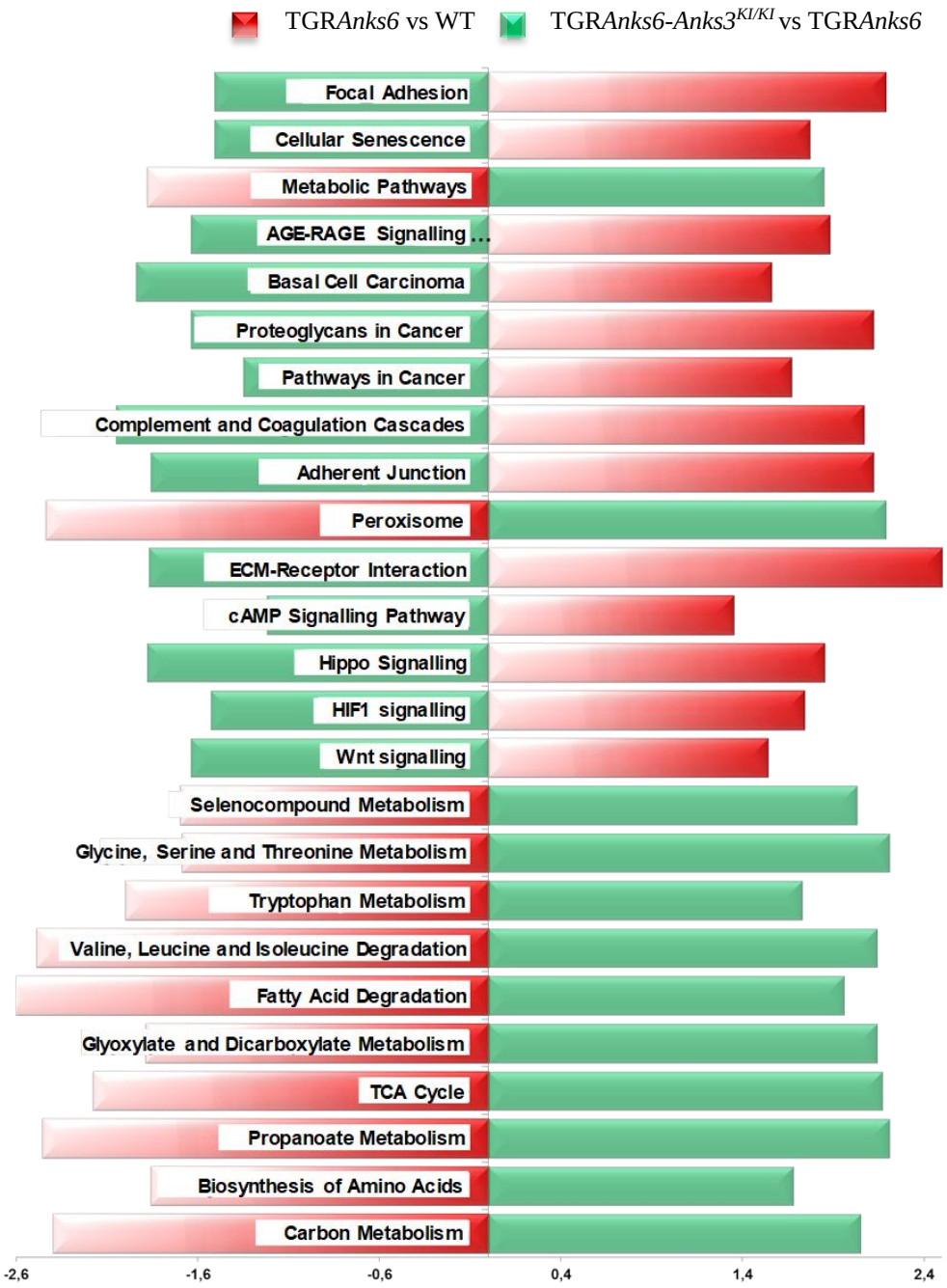

Figure 43- Pathways differently regulated in both TGRAnks6 vs wildtype (WT) and TGRAnks6-Anks3$^{KI/KI}$ rats vs TGRAnks6.

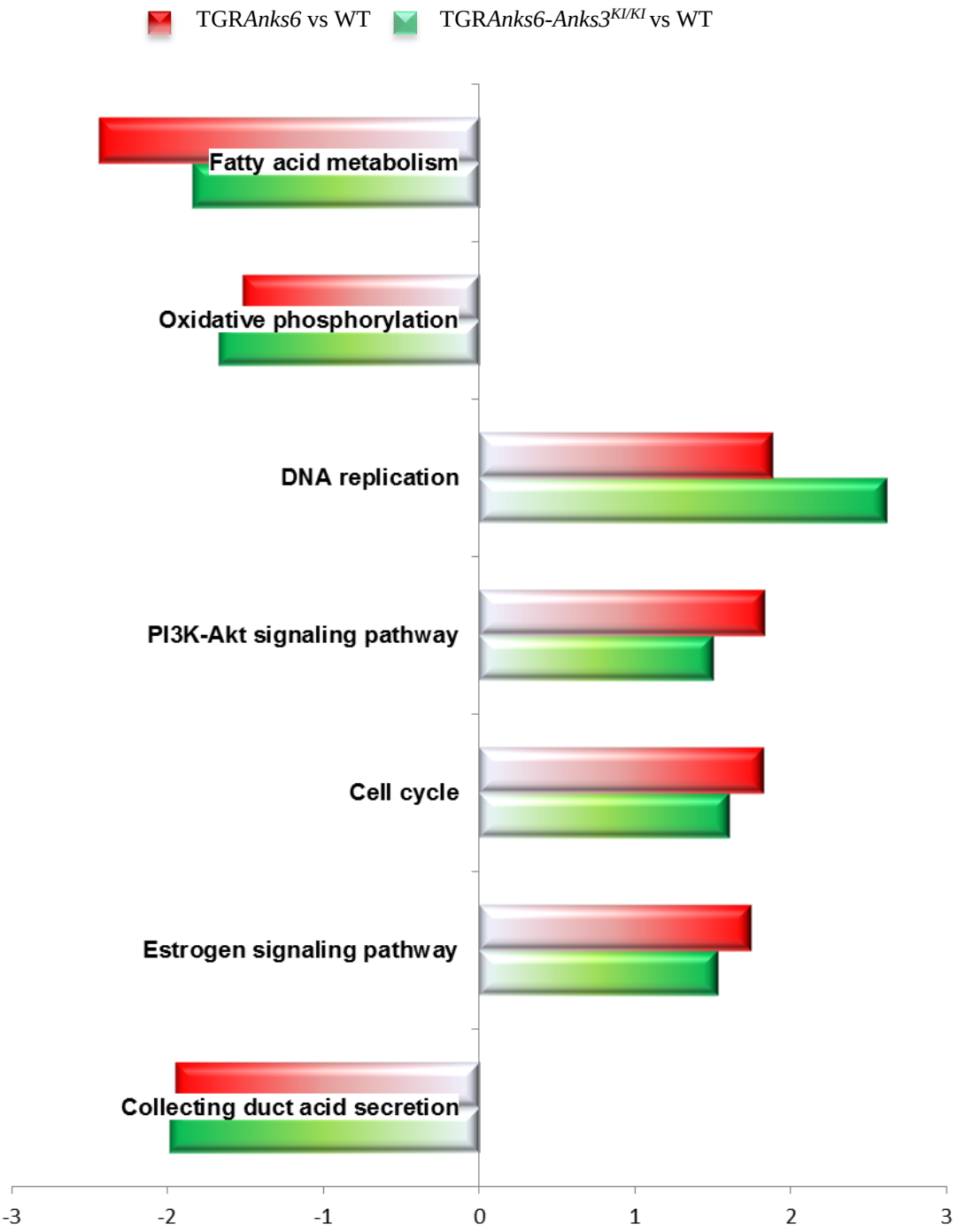

Figure 44- Pathways similarly up or downregulated in both TGRAnks6 and TGRAnks6-Anks3$^{KI/KI}$ rats when compared to wildtype rats (WT).

The *Anks3*^{KI} mutation reversed important pathways which were upregulated in the TGR*Anks6* rats such as Wnt, Hippo, HIF1 and cAMP signalling and cancer-associated pathways, which are known to be involved in cyst growth, returning them to normal. In the TGR*Anks6* kidneys metabolic pathways related to mitochondrial function (TCA cycle, fatty acid degradation, carbohydrate, lipid and amino acid metabolism) were downregulated which was reversed by the *Anks3*^{KI} mutation in the TGR*Anks6-Anks3*$^{KI/KI}$ rats (figure 43). However, 10 pathways were altered similarly in both the TGR*Anks6* and TGR*Anks6-Anks3*$^{KI/KI}$ kidneys indicating that the inability of the ANKS3-SAM domain to form homopolymers due to the *Anks3*^{KI} mutation has no influence on these, in the context of PKD (figure 44). These pathways included 'fatty acid metabolism', 'oxidative phosphorylation' and 'collecting duct acid secretion', which were downregulated and 'DNA replication', 'PI3K-Akt signalling' and 'cell cycle', which were upregulated in both genotypes.

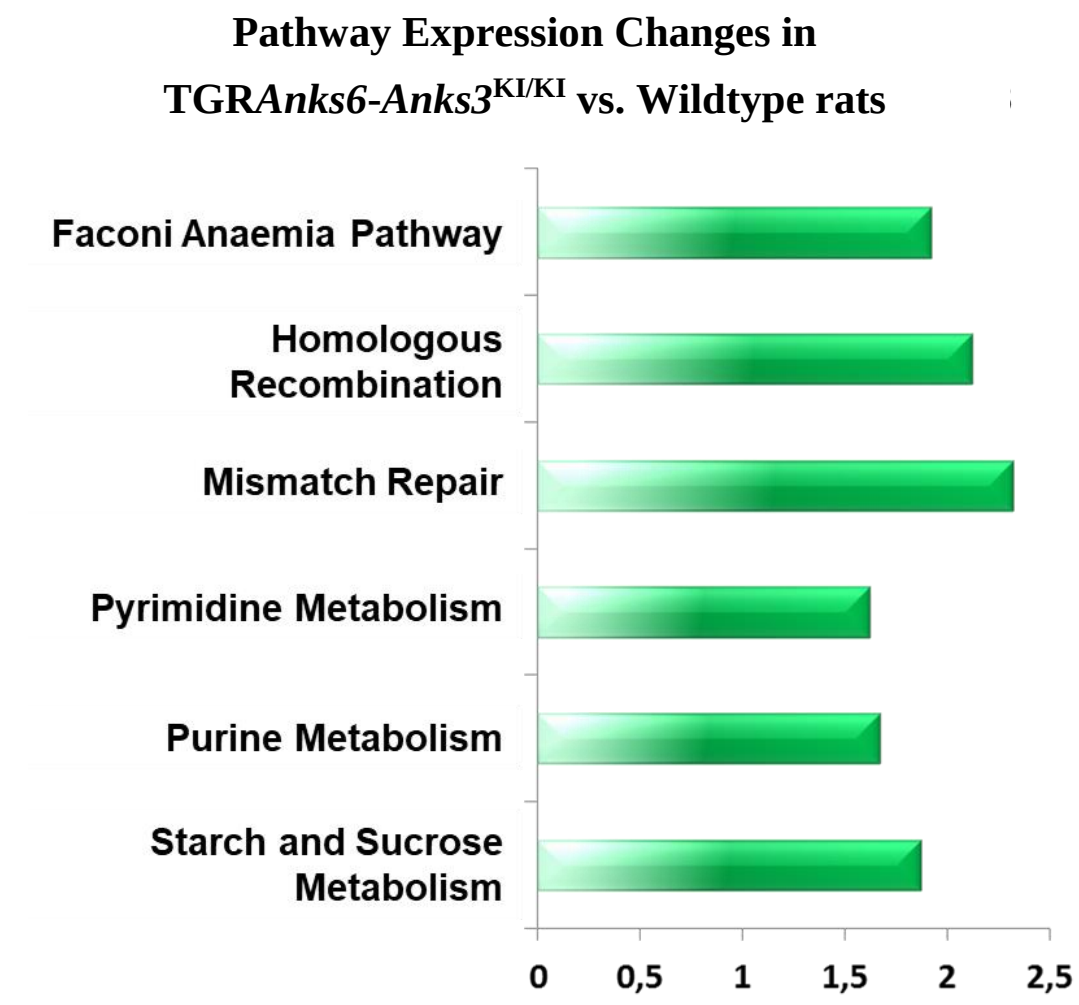

Figure 45- Pathway expression changes in TGRAnks6-Anks3$^{KI/KI}$ vs. wildtype rats. Pathways only upregulated in TGRAnks6-Anks3$^{KI/KI}$ not in TGRAnks6 rats when compared to wildtype rats.

Table 18- Comparison of changes in DNA damage response pathways between TGRAnks6, TGRAnks6-Anks3$^{KI/KI}$, Anks3$^{KI/KI}$ and Anks3$^{KO/KO}$ with wildtype comparisons

Pathway	TGR*Anks6* vs WT	TGR*Anks6*/*Anks3*^{KIKI} vs WT	TGR*Anks6*/*Anks3*^{KIKI} vs TGR*Anks6*	*Anks3*^{KIKI} vs WT adult	*Anks3*$^{KO/KO}$ vs WT embryo
DNA replication	1,88**	2,61**	1,69**	0,98	-2,09**
Fanconi anemia pathway	1,31	1,92**	1,48**	-0,9	-1,93**
Nucleotide excision repair	1,25	1,5**	0,91	0,8	-2,04**
Mismatch repair	1,16	2,32**	1,76**	-0,81	-2,17*
Homologous recombination	1,06	2,12**	1,77**	0,88	-1,77*
Base excision repair	0,98	1,68**	1,14	0,86	-1,25
Aminoacyl-tRNA biosynthesis	-1,21	1,69**	1,88**	0,82	0,82

**p<0.05, **p<0.01 green – upregulated , red - downregulated*

The 10 pathways altered only in the TGR*Anks6-Anks3*$^{KI/KI}$ rats included upregulation of 'starch and sucrose metabolism' and interestingly 'pyrimidine metabolism', 'purine metabolism', 'mismatch repair' and 'homologous recombination' which belong to the DNA replication and repair machinery (figure 45 and table 18).

5- DISCUSSION

ANKS3, an Ank and SAM domain containing protein was first identified as a physical binding partner of the PKD associated proteins ANKS6 and BICC1 by Leettola et al. in 2014 (66) by in vitro studies using isolated SAM domains of these three proteins. They also demonstrated that the ANKS3-SAM domain can self-polymerise forming large complexes. ANKS3 self-polymerisation was prevented by ANKS6 binding to the ANKS3-SAM domain. Furthermore, they demonstrated that the *Anks6*$^{p.R823W}$ mutation, which causes ADPKD in rats, prevents ANKS6 binding to ANKS3. This may may result in hyperpolymerisation of ANKS3. These findings were confirmed in both cellular and in vivo studies by Bakey et al. (60) and Delestre et al. (69) in 2015. Around the same time the interaction of ANKS3 and ANKS6 with NPHP-associated proteins was reported (59, 61, 68). The current information indicates that ANKS3 might be a player in both PKD and NPHP, however the in vivo function of ANKS3 in mammals is currently unresolved.

The main aims of this thesis were to determine the in vivo function of *Anks3* and its SAM domain in rats and the role of ANKS3-SAM domain self-polymerisation in the *Anks6*$^{p.R823W}$ model of ADPKD. We addressed the following questions in detail: **1.** Which renal cells coexpress ANKS3 and ANKS6 in the developing and adult kidneys, of both wildtype and PKD/Mhm(cy/cy) rats? **2.** What is the role of ANKS3-SAM domain polymerisation, in the TGR*Anks6* model of ADPKD, previously generated in our group (58)? **3.** What is the pathophysiological effect of *Anks3* knockout?

To this end we generated and characterised several *Anks3* mutant rat lines using the CRISPR/Cas9 system.

The present thesis, for the first time, provides the following evidence: **1)** A renal spatial-developmental expression pattern of ANKS3-ANKS6 co-expression in wildtype and PKD/Mhm(cy/cy) rats. **2)** Blocking ANKS3-SAM domain self-polymerisation is protective in the TGR*Anks6* rat model of ADPKD by normalising most of the pathways dysregulated in PKD, including Wnt, Hippo and cAMP as well as numerous metabolic pathways related to mitochondrial function. **3)** ANKS3 and its SAM domain have an essential role in mammalian development, since the knockout causes embryonic lethality due to laterality and organ patterning defects which primarily involve the downregulation of DNA damage response pathways and the upregulation of pathways involved in cell proliferation. Cilia formation still occurs.

5.1- Defective ANKS3-SAM domain self-polymerisation retards cyst growth in TGR*Anks6*$^{p.R823W}$ PKD rats

The *Anks6*$^{p.R823W}$ mutation changes the binding properties of ANKS6 to ANKS3. It is important to note that the *Anks6*$^{p.R823W}$ is the only mutation identified in this protein to cause an ADPKD-like phenotype (54). The other *ANKS6* mutations identified in both human patients and animal models cause a NPHP phenotype (59-63). The NPHP phenotype is relatively clearly linked to the interaction of ANKS6 with other NPHP proteins at the cilia. While the exact pathways are not entirely elucidated, ANKS6 does fit well into the overall picture of NPHP proteins. However, the *Anks6*$^{p.R823W}$ mutation is one of only a very few mutations, outside of the classical *PKD1* and *PKD2* (79), to cause the distinctive large renal cysts and fibrosis of ADPKD. This makes the *Anks6*$^{p.R823W}$ mutation very interesting for studying a distinct role of ANKS6 outside of the NPHP2-3-9 complex. Additionally, it is useful to study the common molecular mechanisms the PKD/Mhm rat shares with the classical *PKD1*/*PKD2* ADPKD.

Whether the loss of ANKS6-ANKS3 binding in the PKD/Mhm rats had any role in cystic development was unknown. However, as ANKS3 and BICC1 are the only known binding partners of the ANKS6-SAM domain, and in vitro work showed that ANKS6 disrupts the formation of ANKS3 homopolymers (66), it was reasonable to hypothesise a role of ANKS3 homopolymers in the *Anks6*$^{p.R823W}$ PKD rat phenotype. This raised the possibility that uncontrolled ANKS3 polymerisation may be a factor in the development of the PKD phenotype. Subsequent research released during this project showed that ANKS6, ANKS3 and BICC1 form very large cytoplasmic clusters. In these clusters, a lack of ANKS6 results in increased ANKS3 polymerisation and downregulation of BICC1 RNA processing, which provides a likely pathological pathway (72). As BICC1, an RNA binding protein, has a known role in the regulation of *PKD2* translation (74) and the Wnt and cAMP pathways (80, 81), it was possible that this linked the *Anks6*$^{p.R823W}$ mutation and ADPKD. Several mouse models of PKD with mutations in *Bicc1* exist. The *jcpk* mouse, with a truncated BICC1 protein, develops a severe PKD phenotype with cysts along the entire tubule (64). A missense mutation in *Bicc1* in *bpk* mice causes a large terminal extension which inhibits BICC1-SAM domain polymerisation and its localisation to the P-bodies, however the inhibitory effect of BICC1 on DVL2 is retained. The mutation results in the development of an ARPKD-like phenotype with massive cysts initially arising from the proximal tubules, similar to the PKD phenotype in *Anks6*$^{p.R823W}$ rats, and later also found in the collecting

ducts. Homozygous *bpk* mice die shortly after birth. This PKD phenotype is not related to defects in cilia formation (82). However, *Bicc1* knockout is associated with randomisation of left-right asymmetry (83). Also *Bicc1*^{KO} mice (*Bicc1*^{tm1Emdr}) develop an ARPKD phenotype and survive for a few weeks (84).

One of the initial points we wished to clarify was if any changes occured in the spatial or temporal expression pattern of ANKS6 or ANKS3 in the PKD/Mhm rats as well as looking for co-expression of the proteins. Of particular interest were any differences between the neonatal kidney, which in rats continues developing until the age of three weeks, and the fully developed adult kidney. In the wildtype kidneys we did indeed see a switch in the expression patterns of ANKS6 and ANKS3 between the developing and mature kidney. During renal development both proteins localised separately in the cortex and not at all in the medulla. In the adult kidney they strongly co-localise in the outer cortical distal tubules and medullary collecting ducts. However, in the corticomedullary region only ANKS6 is expressed in the S3 proximal tubule segment and only ANKS3 is expressed in the distal tubules. In the homozygous *Anks6*$^{p.R823W}$ PKD rats there is no difference in spatial expression between the developing and adult kidney. In the developing kidney ANKS6 and ANKS3 are already strongly co-expressed in the medullary collecting ducts and in cortical tubules similar to the adult kidney. As the PKD/Mhm rats do not exhibit developmental defects it would indicate that the function of the ANKS6 disrupted in these rats is not related to morphogenesis or other developmental processes. It is more likely to be related to the change in the balance of proliferation and apoptosis during kidney development.

RNA expression profiling of renal tissue from 11-12 day old TGR*Anks6* rats, the age at which cyst growth begins, revealed that numerous pathways were dysregulated. Important signalling pathways known to be involved in ciliopathies were upregulated including Wnt, Hippo and HIF-1 as well as pathways associated with increased proliferation such as cell cycle, PI3K-Akt, DNA replication and cancer associated pathways. Mitochondria associated pathways, including oxidative phosphorylation, TCA cycle, fatty acid metabolism and a large number of other metabolic pathways, were all downregulated. As it was recently shown that BICC1 is important in the regulation of metabolic processes, disturbances in BICC1 function might be involved (85).

Since we demonstrated that both proteins were not co-expressed in normal developing kidneys but strongly co-expressed in distal tubules and medullary collecting ducts in the adults, we assume that their interaction might not be necessary during renal development but

required in the mature kidney. However, in the homozygous *Anks6*$^{p.R823W}$ developing kidneys their expression is dysregulated by unknown mechanisms and both proteins are strongly co-expressed and co-localise with AQP2 in the medullary collecting ducts. Of note, BICC1 is also expressed in inner medullary collecting duct cells (86), indicating that they might act in a concerted fashion to control AQP2 via regulation of AC6. This will be dicussed later. In contrast to the healthy adult kidney where ANKS3 recruits ANKS6 to BICC1 clusters and large assemblies are formed (72), the ANKS6$^{p.R823W}$-SAM domain cannot bind to the ANKS3-SAM domain and hyperpolymerisation of ANKS3 might reduce the size of BICC1 clusters and consequently BICC1 function. Of note, BICC1 controls PC2 protein levels via miRNA and through modulation of DVL2 activity, the switch from the canonical Wnt pathway to the non-canonical planar cell polarity pathway, required for ciliogenesis. Moreover, BICC1 directly regulates the cAMP pathway and thus may affect AQP2 levels via AC6 therefore we hypothesised that hyperpolymerisation of ANKS3 could be a factor in the development of the ADPKD phenotype. Consequently we developed a knockin rat line expressing a mutant Anks3 protein which retains its ability to bind to ANKS6 via its SAM domain but loses its ability to form homopolymers. If it were the case that cyst formation was related to increased ANKS3 homopolymer formation, then rats co-expressing this altered ANKS3 protein with the ANKS6$^{p.R823W}$ protein should have either a reduction in, or complete elimination of, cysts. The mutation chosen, *Anks3*-SAM$^{p.I35E}$, was based on in vitro work performed by the group of Prof. James Bowie (66). They showed that missense mutations in any of three key residues in the mid-loop would result in the loss of ANKS3 polymer formation but leave the end-helix unaffected and able to bind ANKS6 (66). Of the three residues, we chose the one that seemed to be more efficient at reducing polymer formation than the other two. This was possibly due to it introducing steric overlap in the binding site whereas the others removed ionic interactions.

Homozygous *Anks3*$^{KI/KI}$ rats did not develop any pathological features in the kidney or in other organs throughout life. This strongly indicates that ANKS3-SAM homopolymer formation does not play an essential role in the body, at least in rats. This is a very useful feature in a potential clinical target as any major side effects of inhibiting this function would not be dangerous, in theory. The only impressive and significant changes in renal function we observed in these rats was a decrease in urine excretion and water consumption, which correlated with an increased urine osmolarity and a slight decrease in the plasma concentration of clinical parameters. Further, we have shown a trend towards increased AQP2 expression in the *Anks3*$^{KI/KI}$ rats very similar to that seen in *Anks3* knockdown mice

(69). Thus, we assume that increased water reabsorption by the renal tubules results in increased plasma volume leading to reduced water intake. This would be consistent with the decrease in *Aqp2* expression seen in the TGR*Anks6* rats. AQP2 is a water-channel protein found in connecting tubule cells and collecting duct principal cells. Arginine vasopressin, acting via the vasopressin V2 receptor, localises AQP2 from vesicles to the membrane and upregulates *Aqp2* mRNA and protein expression in order to increase osmotic water permeability in these cells (87, 88). The importance of AQP2 for urine concentration and body water homeostasis is highlighted in *Aqp2* knockout mice and in other clinical conditions in which upregulation or downregulation of AQP2 expression in kidneys is closely associated with water-balance disorders (89, 90). Increased AQP2 expression could be related to increased water reabsorption from the urine explaining the reduced urine excretion per day in the *Anks3*$^{KI/KI}$ rats. It has been shown that tolvaptan, a vasopressin V2 receptor antagonist, slows progression of ADPKD by antagonising the vasopressin-cAMP axis and thus AQP2 (91). However, in the *Anks3*$^{KI/KI}$ rats neither the vasopressin pathway nor the cAMP pathway was altered vs. wildtype rats. It is thus interesting to note that both tolvaptan and the *Anks3*^{KI} mutation inhibit cyst growth in PKD models while having opposite effects on AQP2 expression and thus water reabsorption. This may indicate that changes in renal water reabsorption is not the key factor in the therapeutic effect the *Anks3*^{KI} mutation. Analysis of the TEMPO3:4 clincal trial of tolvaptan already indicated that while decreased water reuptake reduced total kidney volume in the short term of one to three weeks, the long term effect on disease progression over 2 or 3 years was consistant with inhibition of proliferation through correction of the cAMP pathway (92). Although no pathophysiological changes were observed in these rats, RNA expression profiling of the kidneys of adult *Anks3*$^{KI/KI}$ rats revealed significant changes in a number of pathways when compared to wildtype littermates. Pathways known to be related to PKD, including Wnt, Hippo, Notch and the cell cycle, were upregulated while numerous metabolic pathways related to mitochondrial function, including TCA cycle and oxidative phosphorylation pathways, were downregulated. This does not appear to be due to a switch to the Warburg-like phenotype of oxidative glycolysis seen in ADPKD (93), as there was no significant change in the expression of the associated glycolysis pathways, but appears to be part of an overall decrease in metabolic pathway activity. This does not appear to be detrimental to the animals carrying the mutation. Obviously, counterregulatory mechanisms were able to compensate these changes.

In order to test the effect of ANKS3-SAM domain homopolymerisation on PKD progression in the TGR*Anks6* model we crossed *Anks3*^{KI} rats with TGR*Anks6* rats to obtain TGR*Anks6-Anks3*$^{KI/KI}$ rats in the F2 generation which were compared to TGR*Anks6* and wildtype littermates. Renal histology of TGR*Anks6-Anks3*^{KI} rats revealed a remarkable, significant and dose dependent protective effect of the Anks3^{KI} mutation on cyst growth. At the age of 10 days, TGR*Anks6* rats had already generated a large number of cysts, which correlated with renal hypertrophy and an increased number of KI67 positive cells indicating increased proliferation. In contrast, in the TGR*Anks6-Anks3*$^{KI/KI}$ rats, in which ANKS3 homopolymerisation was blocked, only some dilated tubules were observed. Additionally, the kidney/body weight ratio and the number of KI67 positive cells were comparable to wildtype rats. TGR*Anks6* rats with heterozygous *Anks3*$^{KI/WT}$ developed an intermediate phenotype. At the age of four weeks the protective effect of the *Anks3*$^{KI/KI}$ mutation was still present. However, we observed that the *Anks3*$^{KI/KI}$ mutation did not primarily affect the number of altered tubules but considerably reduced cyst growth. It is reasonable that this effect might be related to the urine concentration effect of the *Anks3*$^{KI/KI}$ mutation, which might reduce fluid accumulation in the tubules. Our data indicates that ANKS3-SAM domain homopolymerisation plays a role in cyst growth rather than cyst initiation.

Although we cannot explore the underlying mechanisms yet, these results strongly support our hypothesis that increased ANKS3-SAM homopolymerisation, due to the inability of ANKS6 to bind to ANKS3, contributes to the cystic phenotype of the TGR*Anks6* rats. This possibly occurs via unregulated inhibition of BICC1 function including its translational regulation of numerous proteins critical in PKD, such as PC2, DVL2, AC6 and MYC. Recently it has been shown that ANKS3 polymers can inhibit cytoplasmatic clustering of BICC1, via its C-terminal domain, in the absence of ANKS6 (72).

We have to take into account that ANKS6-ANKS3-BICC1 complexes might still function to a certain extent, since the Ank domains also contribute to the formation of these complexes, so that the ANKS6 mediated scaffolding of BICC1-ANKS3 complexes is partly independent of SAM domain polymerisation (72). In addition, we cannot eliminate the possibility that the *Anks3*^{KI} mutation is not as effective at disrupting polymerisation in vivo as it is in vitro. The *Anks3*^{KI} mutation introduces a steric overlap with a charged residue in the hydrophobic region of the mid-loop binding region of the SAM domain (66). Given this, it does not seem likely that stable enough interactions could form between ANKS3 molecules to allow the formation of polymer strands. However, the possibility remains that

under specific in vivo conditions this may occur. Another possibility is that the *Anks6*$^{p.R823W}$ mutation disrupts ANKS6 function outside the ANKS6-ANKS3-BICC1 complex. Given the nature of the phenotype and what is known of ANKS6, this could involve its role at the cilia. While it has been shown in vitro that the ANKS6-SAM domain is not required for its interaction with the NPHP2-3-9 complex at the cilia (61), ANKS3 also interacts with NPHP proteins at the cilia (68). If ANKS3 and ANKS6 interact at the cilia then the *Anks6*$^{p.R823W}$ mutation would still cause the loss of this interaction while the *Anks3*^{KI} mutation would not recover it. While a direct ANKS6-ANKS3 interaction at the cilia has not been shown they have both been shown to localise there and interact with NEK8/NPHP9. The ANKS3-NEK8/NPHP9 interaction was not demonstrated be a direct interaction and is weaker than either the ANKS3-NPHP1-4-8 or ANKS6-NEK8/NPHP9 interaction (68). As such ANKS3 may interact with NEK8/NPHP9 via the ANKS6-SAM domain to modulate the function of the complex. This could explain the partial recovery caused by the *Anks3*^{KI} mutation, without the need for a further unknown interacting partner of ANKS6. The final potential explanation for the phenotype is that ANKS3-ANKS6 binding not only inhibits ANKS3 polymer formation but also traps ANKS6 in a dimer with ANKS3. This dimer formation could inhibit ANKS6 function in other regions, such as the cilia, or change its localisation. Therefore, in the TGR*Anks6-Anks3*$^{KI/KI}$ rats, Anks6 may be overactive in other areas which would not be corrected by the *Anks3*^{KI} mutation.

We compared the RNA expression profile of kidneys from 11 day old TGR*Anks6*, TGR*Anks6-Anks3*$^{KI/KI}$ and wildtype rats. In TGR*Anks6* rats we found 131 pathways differently expressed vs. wildtype rats. Many signal transduction pathways (including Wnt, Hippo and cAMP), apoptosis, cell cycle, immune system and cancer pathways were upregulated and the majority of metabolic pathways were downregulated. These changes are what would be expected in an ADPKD-like phenotype and are consistent with the previous literature on ADPKD. By contrast, in the TGR*Anks6-Anks3*$^{KI/KI}$ rat kidneys, only 20 pathways were differently regulated compared to wildtype rat kidneys. Thus, most of the pathways altered in the TGR*Anks6* rats were returned to normal by the *Anks3*$^{KI/KI}$ mutation.

Importantly, even pathways in adult *Anks3*$^{KI/KI}$ rats which were upregulated and play an important role in ciliopathic diseases, such as Wnt and Hippo signalling and cellular senescence, or downregulated, including a vast number of metabolic pathways, were normalised in the TGR*Anks6* rats by the *Anks3*$^{KI/KI}$ mutation. However, the underlying mechanisms are still to be defined. Although we studied the RNA expression profile at the

start of the disease, which of the altered pathways in the TGR*Anks6* rats are drivers of the disease and which are secondary to the disease is unknown. Of note, seven pathways altered in the TGR*Anks6* rats were not affected by the *Anks3*$^{KI/KI}$ mutation. This included pathways related to the mitochondrial function such as oxidative phosphorylation and fatty acid metabolism, as well as PI3K-Akt signalling, focal adhesion, cell cycle, DNA replication and collecting duct acid secretion pathways. However, even if pathways such as the cell cycle are upregulated in both TGR*Anks6* and TGR*Anks6-Anks3*$^{KI/KI}$ vs. wildtypes, there are important differences between both genotypes. The DNA damage checkpoints ATM/Chek2 are downregulated in TGR*Anks6* rats but upregulated in TGR*Anks6-Anks3*$^{KI/KI}$ rats. Moreover, pathways related to DNA damage response such as mismatch repair, homologous recombination and purine and pyrimidine metabolism were upregulated only in TGR*Anks6-Anks3*$^{KI/KI}$ rats vs. TGR*Anks6* and wildtype rats. Since these pathways were not affected in the *Anks3*$^{KI/KI}$ rats, it seems that both the loss of ANKS3-SAM domain homopolymerisation and the loss of ANKS6-ANKS3-SAM domain binding is required for the participation of *Anks3* in DNA damage response. However, another possible explanation could be that *Anks3* only contributes to the DNA damage response during periods of high proliferative stress such as embryogenesis or certain disease conditions, such as PKD. It has recently been shown that ANKS3 also directly interacts with NEK7, resulting in post-translational modification of ANKS3. In addition, ANKS3 prevents NEK7 from localising to the nucleus (75). *Nek7* has been characterised best for its role in cell cycle progression. Very recently it has been shown that *Nek7* protects cells from excessive telomer damage under oxidative stress and its recruitment to telomeres is dependent on ATM and is increased in the G2/M phase (94). Whether *Anks3* might be involved in these pathways is unclear. However, it may be speculated that diminished ANKS3-NEK7 interaction due to mutations might increase nuclear localisation of NEK7. Additionally, *Nek8/Nphp9*, another interaction partner of *Anks3* and *Anks6*, is involved in the DNA damage response. *Nek8/Nphp9* contributes to repairing many types of DNA damage including inter-strand crosslinks due to γ irradiation, mitomycin C mediated alkylation, and replication fork stalls caused by hydroxyurea (95). A possible involvement of *Anks3* in DNA damage response is further supported by our findings that a number of DNA damage response related pathways are strongly downregulated in *Anks3*^{KO} embryos, which will be discussed later. Consequently, it seems that preventing the ANKS3-SAM domain self-polymerisation and the loss of ANKS3-ANKS6-SAM domain interactions improves DNA damage and repair pathways in the TGR*Anks6* PKD model, possibly via affecting ANKS3-NEK7/8 interactions. The close relation between cilia

function, genome stability, cell cycle control and mitochondrial function and their impact on ciliopathic disease progression has recently been established. It might be that DNA damage response represents a central defence mechanism in PKD.

An important pathway which is corrected by the *Anks3*$^{KI/KI}$ mutation in the TGR*Anks6* ADPKD model is the Wnt pathway which plays an important role in switching the cell from proliferation to establishing planar cell polarity allowing cilia formation. BICC1 downregulates the activity of DVL2, an important player in this process, and thus the canonical Wnt/β-catenin pathway related to increased proliferation (83). Loss of BICC1-SAM domain function results in hyperactivation of the canonical Wnt pathway in both human patients and mouse models, with an associated cystic renal disease in both cases (81, 83). The SAM domain dependent inhibition of DVL2 by BICC1 was not due to a direct interaction of the proteins but does involve recruitment of DVL2 into cytoplasmic puncta (83). As such, it is not unreasonable to believe that ANKS3 may be part of this regulation, possibly by sequestering BICC1 in different cytoplasmic foci away from DVL2. Furthermore, figure 47 (appendix) shows that in the canonical Wnt pathway the majority of effectors are downregulated, including MYC.

Another pathway which is corrected by the *Anks3*$^{KI/KI}$ mutation is the cAMP signalling pathway, which is the target of the vasopressin V2 receptor antagonists and somatostatin analogs, as well as its associated MAPK and PI3K-Akt pathways. As the downregulation of cAMP production has been shown to be clinically effective in slowing cyst growth (92), the return of cAMP and its associated pathways towards normal seems a likely mechanistic explanation for the repression of cyst growth in these animals. It should also be noted at this stage that BICC1 has been shown to regulate cAMP production via silencing of AC6 mRNA through miRNA. In experimental models, knockout of BICC1 resulted in increased AC6, and thus cAMP, expression (80). As increased ANKS3 homopolymer formation was shown to repress BICC1 function in vivo it seems reasonable that this repression could occur in the TGR*Anks6* rats which is then fixed by the introduction of the *Anks3*$^{KI/KI}$ mutation. As seen in figure 46 (appendix), AC6 mRNA levels are increased in the TGR*Anks6-Anks3*$^{KI/KI}$ rats compared to the TGR*Anks6* rats. This could be due to miRNA silencing which does not lead to degradtion of the AC6 mRNA. Feedback loops triggered by a drop in cAMP levels could cause an increase in AC6 mRNA without a corresponding increase in AC6 protein. In the figure the inhibitory proteins GNAI3 and CAMK2B are downregulated while GNAS and CALM1 are upregulated, supporting the idea of silencing combined with a feedback loop.

This is further supported by a general downregulation of the downstream effects of cAMP via PRKACA. This protein regulates a large number of downstream effects including cell survival and hedgehog signalling.

The first stage in determining whether targetting ANKS3 homopolymer formation could be a viable strategy in treating ADPKD would be to see if the effect could be replicated in experimental models with *PKD1* and *PKD2* mutations. Currently we are performing the experiment in rats which overexpress a mutant PC2 protein. If the loss of ANKS3 polymerisation has a general anti-cystic effect we may see a reduction in cyst growth in these animals. Theoretically this could be the case through changes in BICC1 regulation of *PKD1* and *PKD2* at the mRNA level or changes in the pathways described above.

5.2- ANKS3-SAM domain loss is embryonically lethal due to ciliopathic-like developmental defects

The ANKS6-ANKS3-SAM domain interaction was blocked by the *Anks6*$^{p.R823W}$ mutation, which causes an ADPKD like phenotype in rats (66). As such, it was expected that ANKS3, and specifically it's SAM domain, could also be involved in PKD. However, during this thesis it had been shown that ANKS3, like ANKS6, interacts with NPHP associated proteins and knockout of *anks3* in zebrafish causes ciliopathic-like developmental disturbances (68). However, the in vivo function of ANKS3 in mammals remained entirely unclear. To investigate this, we developed an *Anks3*^{KO} rat, an *Anks3* rat with a SAM domain deletion still harbouring the 3' flanking C-terminal end (*Anks3*$^{\Delta SAM}$) and a rat carrying *Anks3*, truncated at position 453 in the SAM domain, thus lacking exons 11-16. It was highly interesting that all three lines developed a comparable phenotype which was lethal in the second half of pregnancy in homozygous embryos. Heterozygous rats occasionally displayed a very modest NPHP-like phenotype when aged. We never observed a PKD like phenotype in any of the lines. However, in contrast to the heterozygous *Anks3*$^{KO/WT}$, the heterozygous *Anks3*$^{\Delta SAM}$ rats showed some increase in urine concentration, similar to the *Anks3*^{KI} rats.

Hence we could show that ANKS3 has an essential function during embryogenesis which appears dependent on the SAM domain. The homozygous rats primarily died in the second half of pregnancy. The phenotype was variable and included cranio-facial defects, severe cardiac malformations, haemorrhages and defects in left-right asymmetry. The kidneys were often smaller and showed severe disturbances in glomerulo- and tubulogenesis. The presence

of cardiac and brain malformations and left-right asymmetry defects in the rats is consistent with the two reported human cases carrying *Anks3* mutated at amino acid 147 (70). This suggests that the role of ANKS3 in development is relatively similar in both humans and rats. Thus, the data gathered during this research should be applicable in humans. The severe cardiac defects and pale organs in several homozygous embryos, indicates that cardiac insufficiency is the most likely cause of prenatal death in these embryos and is a possible reason for their smaller size. In other animal models of ciliopathy associated genes, such as the *Anks6*^{streaker} mouse, cardiac defects are often related to heterotaxy resulting in a 50 % mortality rate due to heart failure in the homozygotes (61). In the *Anks3*$^{KO/KO}$ embryos the heart defects appear to be at least partially independent of left-right asymetry defects as they occur in all embryos investigated. The *Anks3*^{KO} phenotype partially overlaps with the phenotype of *Nek8/Nphp9*^{KO} and *Invs/Nphp2*^{KO} mice which developed cardiac defects, including atrial/ventricular septal defects, independent of whether the embryo had aberrant or correct left-right patterning (96, 97). Thus, it seems likely that ANKS3 has a specific role in the development of the heart, though whether this is related to NEK8/NPHP9 or INVS/NPHP2 is unclear as the phenotypes are distinct.

In human patients, the cardiac phenotype in the *Anks3*$^{KO/KO}$ rats seems to most resemble the dilated cardiomyopathy seen very rarely in BBS (41, 98) and commonly in Alström syndrome (99) (a very rare ciliopathy similar to BBS), though the phenotype in the rats is more severe. In human Alström patients, dilated cardiomyopathy frequently occurs within the first few weeks after birth and then resolves. It can then rapidly reoccur in later life, typically with a poor outcome for the patient. Unfortunately due to the rarity of the disease the exact molecular mechanisms behind the phenotype are unknown. However, it is known that the ALMS1 protein localises to the centrosome and basal body of the cilia. Of ANKS3's known partners, mutations in ANKS6 and NPHP1 and NPHP3 have been associated with dilated or hypertrophic cardiomyopathy in very rare cases in humans (59, 100, 101). The specific cardiac phenotype in *Anks3*$^{KO/KO}$ embryos is distinct from those reported for the human patients with *Anks3* mutations at amino acid 147 (70). This could be due to the human patients having only a single amino acid exchange rather than the complete knockout and they may therefore have a less severe disease. The *Anks3* mutation in the human patients is located in the Ank domains which may also be the reason for the differences from our SAM domain knockout. It is also possible that due to the embryonicly lethal nature of the phenotype in *Anks3*$^{KO/KO}$ rats, that human foetuses with a similar mutation could miscarry and thus may go undetected.

The other most striking features of the *Anks3*^{KO} phenotype were the craniofacial defects and brain malformations. The cleft palate and shortened jaw are both common features of MKS which is also associated with severe brain defects (39). Due to differences between rat and human brain anatomy and the highly variable nature of the MKS and *Anks3*^{KO} phenotypes, it is difficult to say whether the brain defects seen in our rats parallel those seen in human MKS. However, in the *Anks3*^{KO} rats we did not observe occipital encephalocele (protrusion of the brain tissue or meninges through the unsealed skull) which is the most common neurological defect associated with MKS. This suggests that the 2 phenotypes are distinct though there may be some overlap with the other MKS abnormalities of microcephaly (reduced skull circumference) and anencephaly (missing parts of the brain or skull). Cleft palate, shortened jaw and brain abnormalities are also associated with OFD (102, 103). It is interesting to note that all of the genes which BBS and MKS share (*Bbs2* and *Bbs4*, *Mkks*, *Mks1* and *Cep290)*, and the Alström syndrome 1 gene (*Alms1*), encode proteins which act at the centrosome or basal body at the cilia. This is consistent with the known localisation of the NPHP1-4-8 complex, ANKS3 is associated with (104). However, *Mkks*, *Mks1* and *Cep290* (105, 106) are required for ciliogenesis and *Alms1* and, *Bbs2* and *Bbs4* knockouts result in stunted cilia (107, 108). This is in contrast to knockouts of *Nphp1*, *Nphp4* or *Rpgrip1l/Nphp8* and our *Anks3*^{KO} rats which do not result in changes in ciliogenesis (104). This suggests that the underlying mechanisms of the *Anks3*^{KO} cranio-facial and heart phenotypes are distinct from those seen in these human diseases and are more likely to involve its interaction with the NPHP1-4-8 complex and possibly NEK8/NPHP9.

One of the interesting aspects of the *Anks3*^{KO} phenotype is that a PKD-like renal phenotype was not observed. In very old heterozygous *Anks3*^{KO} rats a few cysts were occasionally seen in the medulla and corticomedullary region. This is quite surprising as renal cysts are a common feature in mutated *Anks3*, *Anks6* or *Bicc1* animal models (mouse, rat or zebrafish) (54, 61, 68, 109-111). It also makes the *Anks3*^{KO} phenotype distinct from many human ciliopathies including NPHP and MKS (35, 39). However, the lack of renal cysts is consistent with the phenotype of the two human patients with mutant *ANKS3* (70). The reduced size of the kidneys occasionally observed in the homozygous *Anks3*$^{KO/KO}$ embryos is likely related to disturbances in renal development. Reduced kidney size is a feature of NPHP rather than PKD.

Global oedema and focal haemorrhages frequently seen in homozygous *Anks3*$^{KO/KO}$ embryos is likely secondary to cardiac failure. Foetal oedema is an indicator of severe anaemia (112)

and thus, in this case, supports cardiac defects as the primary cause of death in these embryos. The haematomas, frequently seen in the *Anks3*^{KO} and *Anks3*$^{\Delta SAM}$ embryos, are likely due to changes in cell-cell and cell-matrix binding. Changes in the cell-matrix and cell-cell interactions as well as cilia function is hypothesised to play a role in the increased cerebrovascular events seen in ADPKD (113). This also is consistent with a proposed role of NPHP1, NPHP4 and NPHP8 at the tight junctions (104) which could be altered by the loss of ANKS3. Of note, oedema and focal haemorrhages are also frequently seen in *Nek8/Nphp9*^{KO} mice. Situs inversus is common in ciliopathic models and results from a loss of function of either the primary or motile cilia at the embryonic node (7). The occurance of situs inversus in our *Anks3*^{KO} model points to an early role of ANKS3 in developement.

Neither the *Anks3*^{KI} nor the *Anks6*$^{p.R823W}$ mutation, which are assumed to decrease and increase ANKS3 polymer formation respectively, cause lethal developmental defects (55). This suggests that the *Anks3*^{KO} phenotype is not related to the ANKS3-ANKS6-SAM domain interaction or the ability of ANKS3 for self-polymerisation. However since both the *Anks3*-SAM domain deletion with an intact C-terminal end and the *Anks3* truncation, which lacks the SAM domain and a C-terminal end, cause a comparable embryonic phenotype to the *Anks3*$^{KO/KO}$, it is very likely that these disturbances are primarily mediated via the SAM domain function. Of note, the knockout of *Anks6* or *Bicc1* does result in a developmental ciliopathy in animal models (59, 83), however in contrast to the *Anks3* knockout, this was associated with cystic and enlarged kidneys. *Bicc1* knockout resulted in 50 % embryonic lethality due to situs ambiguous and ventricular septal defects. The remaining knockouts died shortly after birth due to cystic kidneys (83). *Anks6* knockdown models in zebrafish and Xenopus primarily showed renal and laterality defects (59). Point mutations in *Bicc1* and *Anks6* are also primarily associated with various cystic renal phenotypes. Neither *Anks6* nor *Bicc1* have been associated with the dilated cardiomyopathy, craniofacial defects or brain malformations seen in the *Anks3*^{KO} rats, further supporting a distinct mechanism of action (55, 59, 61, 64, 83, 111). Both ANKS6 and BICC1 are directly or indirectly involved in ciliogenesis and cilia function. ANKS6 locates to the cilia and interacts with the NPHP2-3-9 complex (59). BICC1 was only found in the cytoplasm and regulates the RNA and protein levels of important PKD associated proteins including PC2, which localise to the cilia (73, 74). BICC1 also regulates DVL2, which has an important function in switching the cell from the proliferative canonical β-catenin/Wnt pathway to the non-canonical planar cell polarity Wnt pathway, which is required for ciliogenesis (83). However, at least one paper also found BICC1 in the cilia (114).

The distinct embryonic phenotypes of *Anks3*^{KO}, *Anks6*^{KO}, and *Bicc1*^{KO} animals suggests that the embryonic phenotype of Anks$^{KO/KO}$ is more likely to be associated with a loss of the ANKS3 interaction with the NPHP1-4-8 complex than with ANKS6 or BICC1 (68). *Nphp1* and *Nphp4* are primarily associated with cystic renal phenotypes (mostly NPHP). However, *NPHP1* and *NPHP4* mutations have been associated with BBS in some rare cases (115, 116). The ANKS3 interaction partner with the greatest similarity in phenotype when knocked out is RPGRIP1L/NPHP8. Mice with a homozygous knockout of *Rpgrip1l*/*Nphp8* develop thin ventricle walls very similar to the *Anks3*^{KO} rats (117). They also display similar craniofacial defects to the *Anks3*^{KO}, including shortened jaw and cleft palette, and severe brain malformations associated with MKS including exencephaly. Data shows that the neurological phenotype in the *Rpgrip1l*/*Nphp8*^{KO} mice is related to the role of RPGRIP1L/NPHP8 in Shh signalling (118). Additionally, it is interesting to note that *Shh*^{KO} mouse embryos develop enlarged atria very similar to those seen in our *Anks3*^{KO} rat embryos (119). The overlap between these features in the *Anks3*^{KO} and *Rpgrip1l*/*Nphp8*^{KO} animals strongly suggests a common mechanism, possibly Shh signalling.

The phenotype of the *Anks3*^{KO} rats and those with in-frame deletions in the ANKS3-SAM domain is consistent with a loss of ANKS3 activity at the cilium. While this domain has only been shown to interact with ANKS6 and BICC1 (66, 72), it has not been established which ANKS3 domains are required for its interaction with the NPHP1-4-8 complex (68). As we already explored the effect of changes in ANKS3-ANKS6-BICC1 binding with the TGR*Anks6* and *Anks3*$^{KI/KI}$ rats, loss of this interaction is unlikely to explain the phenotype. This, together with the strong overlap with the *Rpgrip1l*/*Nphp8*^{KO} phenotype, suggest that the ANKS3-SAM domain is essential for its interaction with the NPHP1-4-8. This is unlike the interaction of ANKS6 with the NPHP2-3-9 where the ANKS6-Ank domains alone are apparently capable of binding NEK8/NPHP9 and stimulating its activity (61). It is possible that the deletions result in the protein being unable to fold correctly causing it to be flagged for degradation and thus producing the same effect as the knockout. However, similarly truncated versions of ANKS3 have been expressed successfully in vitro (66). Another point worth considering is that ANKS3 has primarily been studied in the kidney and kidney cells. This is because ANKS3 has mainly been shown to interact with proteins associated with renal phenotypes. As such, there are potentially tissue specific partners in the heart, brain and other organs which have not been identified. However, the very strong phenotypic overlap with *Rpgrip1l*/*Nphp8*^{KO} suggests that its interaction with ANKS3 is key.

Of interest, the pathways which are significantly differently expressed between the *Anks3*$^{KO/KO}$ and wildtype embryos differ considerably from those which are differently expressed between, TGR*Anks6*, *Anks3*$^{KI/KI}$, TGR*Anks6-Anks3*$^{KI/KI}$ and wildtype rats. While in the TGR*Anks6*, *Anks3*$^{KI/KI}$ and TGR*Anks6-Anks3*$^{KI/KI}$ rats numerous metabolic pathways and pathways typically altered in PKD like Wnt, Hippo and HIF1 pathways (120-122) are affected, in the *Anks3*$^{KO/KO}$ embryos almost all aspects of the "Genetic Information Processing" category are differently expressed vs. wildtype. This is consistent with metabolic profiling in *Anks3* depleted IMCD cells which showed increased DNA damage and reduced concentrations of nucleotides (123). In that study they were unable to determine if increased damage caused nucleotide depletion or vice versa. Our results show downregulation of the machinery for pyrimidine synthesis as well as all types of DNA repair, which strongly suggests impaired DNA damage response leads to increased DNA damage. Several ciliopathic genes have been linked to increased DNA damage including *Nf423*, *Cep164*, and, as previously discussed, the known *Anks3* partners, *Nek8/Nphp9* and *Nek7*. In addition, numerous pathways altered in the *Anks3*^{KO} embryos were related to increased proliferation. These results support our hypothesis that *Anks3* has important functions in DNA replication and damage response, which become critical under conditions of high proliferative stress such as embryonic development and specific disease conditions including PKD. Defective ANKS3-SAM domain polymerisation is protective in this context.

Altogether, in the course of this thesis we provided the research community with three novel mutated *Anks3* rat models, which, for the first time, allow the study of specific aspects of *Anks3* function in vivo in a mammalian model and will contribute to further elucidation of the molecular pathways of PKD and other ciliopathies, and their interaction.

Based on our studies we draw the following conclusions:

1. Developmental regulated spatial ANKS3 and ANKS6 expression pattern in the kidney is altered due to the *Anks6*$^{p.R823W}$ mutation and is associated with ADPKD. Disruption of the ANKS6-ANKS3-SAM domain interaction in homozygous *Anks6*$^{p.R823W}$ rats is associated with significantly lower *Aqp2* expression, which may promote diuresis in the developing kidney.

2. Defective ANKS3 polymerisation retards cyst growth and reverses most of the altered pathways, including metabolic pathways and signalling pathways (Hippo, Wnt and cAMP), in the TGR*Anks6* rat and is associated with increased AQP2 expression and urine concentration.

3. *Anks3* has important functions in DNA replication and damage response, which become critical under conditions of high proliferation stress such as the embryonic state and specific disease conditions including PKD. Defective ANKS3-SAM domain polymerisation is protective in this context

4. The ANKS3-SAM domain, but not ANKS3 polymerisation, is required for proper morphogenesis in embryos.

5. Our *Anks3* mutations never caused a PKD phenotype, unlike *Anks6*.

REFERENCES

1. Kempeneers C, Chilvers MA. To beat, or not to beat, that is question! The spectrum of ciliopathies. Pediatric Pulmonology. 2018.
2. Mitchison HM, Valente EM. Motile and non-motile cilia in human pathology: from function to phenotypes. The Journal of Pathology. 2017;241(2):294-309.
3. Marshall WF. Basal bodies platforms for building cilia. Current Topics in Developmental Biology. 2008;85:1-22.
4. Wei Q, Ling K, Hu J. The essential roles of transition fibers in the context of cilia. Current Opinion in Cell Biology. 2016;35:98-105.
5. Gonçalves J, Pelletier L. The ciliary transition zone: finding the pieces and assembling the gate. Molecules and Cells. 2017;40(4):243-53.
6. Elliott KH, Brugmann SA. Sending mixed signals: Cilia-dependent signaling during development and disease. Developmental Biology. 2019;447:28-41.
7. Babu D, Roy S. Left-right asymmetry: cilia stir up new surprises in the node. Open Biology. 2013;3(5):130052.
8. Huangfu D, Anderson KV. Cilia and Hedgehog responsiveness in the mouse. Proceedings of the National Academy of Sciences of the United States of America. 2005;102(32):11325-30.
9. Qin H, Wang Z, Siener S, Rosenbaum J. Intraflagellar Transport Protein 27 Is a Small G Protein Involved in Cell-Cycle Control. Current Biology. 2007;17(3):193-202.
10. Robert A, Margall-Ducos G, Guidotti JE, Brégerie O, Celati C, Bréchot C, et al. The intraflagellar transport component IFT88/polaris is a centrosomal protein regulating G1-S transition in non-ciliated cells. Journal of Cell Sciences. 2007;120(4):628-37.
11. Inoko A, Matsuyama M, Goto H, Ohmuro-Matsuyama Y, Hayashi Y, Enomoto M, et al. Trichoplein and Aurora A block aberrant primary cilia assembly in proliferating cells. The Journal of Cell Biology. 2012;197(3):391-405.
12. Bergmann C, Guay-Woodford LM, Harris PC, Horie S, Peters DJM, Torres VE. Polycystic kidney disease. Nature Reviews- Disease Primers. 2018;4(1):50.
13. Dalgaard OZ. Bilateral polycystic disease of the kidneys: a follow-up of two hundred and eigthy-four patients and their families. AMA Arch Intern Med. 1958;102(2):332.
14. Iglesias CG, Torres VE, Offord KP, Holley KE, Beard CM, Kurland LT. Epidemiology of adult polycystic kidney disease, Olmsted County, Minnesota: 1935-1980. American Journal of Kidney Diseases. 1983;2(6):630-9.
15. Lemos FO, Ehrlich BE. Polycystin and calcium signaling in cell death and survival. Cell Calcium. 2018;69:37-45.
16. Yuan S, Zhao L, Brueckner M, Sun Z. Intraciliary calcium oscillations initiate vetabrate left-right assymetry. Current Biology. 2015;25:556-67.
17. Delling M, Indzhykulian AA, Liu X, Li Y, Xie T, Corey DP, et al. Primary cilia are not calcium-responsive mechanosensors. Nature. 2016;531:656-60.
18. Malekshahabi T, Rad NK, Serra AL, Moghadasali R. Autosomal dominant polycystic kidney disease: Disrupted pathways and potential therapeutic interventions. Journal of Cellular Physiology. 2019:Epub ahead of print.
19. Chang MY, Ong ACM. Targeting new cellular disease pathways in autosomal dominant polycystic kidney disease. Nephrology, Dialysis, Transplantation. 2018;33(8):1310-6.
20. Potts JW, Mousa SA. Recent Advances in Management of Autosomal-Dominant Polycystic Kidney Disease. American Journal of Health-System Pharmacy. 2017;74(23):1959-68.
21. Chebib FT, Torres VE. Recent Advances in the Management of Autosomal Dominant Polycystic Kidney Disease. Clinical Journal of the American Society of Nephrology. 2018.

22. Nowak KL, You Z, Gitomer B, Brosnahan G, Torres VE, Chapman AB, et al. Overweight and obesity are predictors of progression in early autosomal dominant polycystic kidney disease. Journal of the American Society of Nephrology. 2018;29:571-8.
23. Kipp KR, Rezaei M, Lin L, Dewey EC, Weimbs T. A mild reduction of food intake slows disease progression in an orthologous mouse model of polycystic kidney disease. American Journal of Physiology: Renal Physiology. 2016;310(8):F726-F31.
24. Torres VE, Abebe KZ, Schrier RW, Perrone RD, Chapman AB, Yu AS, et al. Dietary salt restriction is beneficial to the management of autosomal dominant polycystic kidney disease. Kidney International. 2017;91:493-500.
25. Clark WF, Sontrop JM, Huang SH, Gallo K, Moist L, House AA, et al. Effect of coaching to increase water intake on kidney function decline in adults with chronic kidney disease: The CKD WIT randomized clinical trial JAMA. 2018;319(18):1870-9.
26. Bergmann C. Genetics of Autosomal Recessive Polycystic Kidney Disease and Its Differential Diagnoses. Frontiers in Pediatrics. 2018;5:221.
27. Zerres K, Rudnik-Schöneborn S, Steinkamm C, Becker J, Mücher G. Autosomal recessive polycystic kidney disease. Journal of Molecular Medicine. 1998;76:303-9.
28. Bergmann C, Senderek J, Windelen E, Küpper F, Middeldorf I, Schneider F, et al. Clinical consequences of PKHD1 mutations in 164 patients with autosomal-recessive polycystic kidney disease (ARPKD). Kidney International. 2005;67(3):829-48.
29. Wang S, Luo Y, Wilson PD, Witman GB, Zhou J. The autosomal recessive polycystic kidney disease protein is localized to primary cilia, with concentration in the basal body area. Journal of the American Society of Nephrology. 2004;15(3):592-602.
30. Onuchic LF, Furu L, Nagasawa Y, Hou X, Eggermann T, Ren Z, et al. PKHD1, the polycystic kidney and hepatic disease 1 gene, encodes a novel large protein containing multiple immunoglobulin-like plexin-transcription-factor domains and parallel beta-helix 1 repeats. American Journal of Human Genetics. 2002;70(5):1305-17.
31. Bergmann C, Senderek J, Sedlacek B, Pegiazoglou I, Puglia P, Eggermann T, et al. Spectrum of mutations in the gene for autosomal recessive polycystic kidney disease (ARPKD/PKHD1). Journal of the American Society of Nephrology. 2003;14(1):76-89.
32. Deget F, Rudnik-Schöneborn S, Zerres K. Course of autosomal recessive polycystic kidney disease (ARPKD) in siblings: a clinical comparison of 20 sibships. Clinical Genetics. 1995;47(5):248-53.
33. Lu H, Galeano MCR, Ott E, Kaeslin G, Kausalya PJ, Kramer C, et al. Mutations in DZIP1L, which encodes a ciliary-transition-zone protein, cause autosomal recessive polycystic kidney disease. Nature Genetics. 2017;49(7):1025-34.
34. Luo F, Tao YH. Nephronophthisis: A review of genotype-phenotype correlation. Nephrology. 2018;23:904-11.
35. Wolf MTF. Nephronophthisis and related syndromes. Current Opinion in Pediatrics. 2015;27(2):201-11.
36. Srivastava S, Molinari E, Raman S, Sayer JA. Many Genes- One Disease? Genetics of Nephronophthisis (NPHP) and NPHP-Associated Disorders. Frontiers in Pediatrics. 2018;5:287.
37. Tanos BE, Yang HJ, Soni R, Wang WJ, Macaluso FP, Asara JM, et al. Centriole distal appendafes promote membrane docking , leading to cilia initiation. Genes and Development. 2012;27:163-8.
38. Romani M, Micalizzi A, Valente EM. Joubert Syndrome: Congenital Cerebellar Ataxia with the Molar Tooth. The Lancet: Neurology. 2013;12(9):894-905.
39. Hartill V, Szymanska K, Sharif SM, Wheway G, Johnson CA. Meckel–Gruber Syndrome: An Update on Diagnosis, Clinical Management, and Research Advances. Frontiers in Pediatrics. 2017;5:224.
40. Forsythe E, Kenny J, Bacchelli C, Beales PL. Managing Bardet-Biedl Syndrome-Now and in the Future. Frontiers in Pediatrics. 2018;6:23.
41. Beales PL, Elcioglu N, Woolf AS, Flinter FA. New criteria for improved diagnosis of Bardet-Biedl syndrome: results of a population survey. Journal of Medical Genetics. 1999;36:437-46.

42. Kulaga HM, Leitch CC, Eichers ER, Badano JL, Lesemann A, Hoskins BE, et al. Loss of BBS proteins causes anosmia in humans and defects in olfactory cilia structure and function in the mouse. Nature Genetics. 2004;36:994-8.
43. Tan PL, Barr T, Inglis PN, Mitsuma N, Huang SM, Garcia-Gonzalez MA, et al. Loss of Bardet-Biedl syndrome proteins causes defects in peripheral sensory innervation and function. Proceedings of the National Academy of Sciences 2007;104(44):17524-9.
44. Verloes A, Lambotte C. Further delineation of a syndrome of cerebellar vermis hypo/aplasia, oligophrenia, congenital ataxia, coloboma and hepatic fibrosis. American Journal of Medical Genetics. 1989;32:227-32.
45. Doherty D, Parisi MA, Finn LS, Gunay-Aygun M, Al-Mateen M, Bates D, et al. Mutations in 3 genes (MKS3, CC2D2A and RPGRIP1L) cause COACH syndrome (Joubert syndrome with congenital hepatic fibrosis). Journal of Medical Genetics. 2010;47(1):8-21.
46. Bruel AL, Franco B, Duffourd Y, Thevenon J, Jego L, Lopez E, et al. 15 years of research on Oral-Facial-Digital syndromes: from 1 to 16 causal genes. Journal of Medical Genetics. 2017;54(6):371-80.
47. Sakakibara N, Morisada N, Nozu K, Nagatani K, Ohta T, Shimizu J, et al. Clinical spectrum of male patients with OFD1 mutations. Journal of Human Genetics. 2018.
48. Kaur A, Dhir SK, Goyal G, Mittal N, Goyal RK. Senior Loken Syndrome. Journal of Clinical and Diagnostic Research. 2016;10(11):SD03-SD4.
49. Satran D, Pierpont MEM, Dobyns WB. Cerebello-Oculo-Renal syndromes including Arima, Senior Löken and COACH syndromes: more than just variants of Joubert syndrome. American Journal of Medical Genetics. 1999;86(5):459-69.
50. Mirra V, Werner C, Santamaria F. Primary Ciliary Dyskinesia: An Update on Clinical Aspects, Genetics, Diagnosis, and Future Treatment Strategies. Frontiers in Pediatrics. 2017;5:135.
51. Stagner EE, Bouvrette DJ, Cheng J, Bryda EC. The polycystic kidney disease-related proteins Bicc1 and SamCystin interact. Biochemical and Biophysical Research Communications. 2009;383(1):16-21.
52. Kim CA, Bowie JU. SAM domains: uniform structure, diversity of function. Trends in Biochemical Sciences. 2003;28(12):625-8.
53. Mosavi LK, Cammett TJ, Desrosiers DC, Peng Z-Y. The ankyrin repeat as molecular architecture for protien recognition. Protein Science. 2004;13(6):1435-48.
54. Kaspareit-Rittinghausen J, Rapp K, Deerberg F, Wcislo A, Messow C. Hereditary polycysitc kidney disease associated with osteorenal syndrome in rats. Veterinary Pathology. 1989;26(3):195-201.
55. Schafer K, GRetz N, Bader M, Oberbaumer I, Eckardt KU, Kriz W, et al. Chararcterization of the Han:SPRD rat model for hereditary polycystic kidney disease. Kidney International. 1994;46(1):134-52.
56. Bihoreau MT, Ceccherini I, Browne J, Kranzlin B, Romeo G, Lathrop GM, et al. Location of the first genetic locus, PKDr1, controlling autosomal dominant polycystic kidney disease in Han:SPRD cy/+ rat. Human Molecular Genetics. 1997;6(4):609-13.
57. Brown JH, Bihoreau MT, Hoffmann S, Kranzlin B, Tychinskaya I, Obermuller N, et al. Missense mutation in sterile alpha motif of novel protein SamCystin is associated with polycystic kidney disease in (cy/+) rat. Journal of the American Society of Nephrology. 2005;16:3517-26.
58. Neudecker S, Walz R, Menon K, Maier E, Bihoreau MT, Obermuller N, et al. Transgenic overexpression of Anks6(p.R823W) causes polycystic kidney disease in rats. The American Journal of Pathology. 2010;177(6):3000-9.
59. Hoff S, Halbritter J, Epting D, Frank V, Nguyen TMT, Reeuwijk Jv, et al. Anks6 is a central component of a nephronophthisis module linking NEK8 to INVS and NPHP3. Nature Genetics. 2013;45(8):951-6.
60. Bakey Z, Bihoreau MT, Piedagnel R, Delestre L, Arnould C, Viliers AHd, et al. The SAM domain of ANKS6 has different interacting partners and mutations can induce different cystic phenotypes. Kidney International. 2015;88:299-310.

61. Czarnecki PG, Gabriel GC, Manning DK, Sergeev M, Lemke K, Klena NT, et al. Anks6 is the critical activator of NEK8 kinase in embryonic situs determination and organ patterning. Nature Communications. 2015;6:6023.
62. Taskiran EZ, Korkmaz E, Gucer S, Kosukcu C, Kaymaz F, Koyunlar C, et al. Mutations in Anks6 cause a nephronophthisis-like phenotype with ESRD. Journal of the American Society of Nephrology. 2014;25(8):1653-61.
63. Fu R, Chen C, He JJ. Progression of nephronophthisis-like phenotype caused by Anks6 gene mutation to end-stage renal disease in a boy. Chinese Journal of Pediatrics. 2018;56:695-7.
64. Flaherty L, Bryda EC, Collins D, Rudofsky U, Montogomery JC. New mouse model for polycystic kidney disease with both recessive and dominant gene effects. Kidney International. 1995;47(2):552-8.
65. Nakajima Y, Kiyonari H, Mukumoto Y, Yokoyama T. The Inv compartment of renal cilia is an intraciliary signal-activating center to phosphorylate Anks6. Kidney International. 2018;93(5):1108-17.
66. Leettola CN, Knight MJ, Cascio D, Hoffmann S, Bowie JU. Characterisation of the SAM domain of the PKD-related protein Anks6 and its interaction with Anks3. BMC Structural Biology. 2014;14(17).
67. Knight MJ, Leettola C, Ginery M, Li H, Bowie JU. A human sterila alpha motif domain polymerizome. Protein Science. 2011;20:1697-706.
68. Yakulov TA, Yasunaga T, Ramachandran H, Engel C, Müller B, Hoff S, et al. Anks3 interacts with nephronophthisis proteins and is required for normal renal development. Kidney International. 2015;87:1191-200.
69. Delestre L, Bakey Z, Prado C, Hoffmann S, Bihoreau MT, Lelongt B, et al. Anks3 co-localises with Anks6 in mouse renal cilia and is associated with vasopressin signaling and apoptosis In Vivo in mice. PLoS ONE. 2015;10(9):e0136781.
70. Shamseldin HE, Yakulov TA, Hashem A, Walz G, Alkuraya FS. Anks3 is mutated in a family with autosomal recessive laterality defect. Human Genetics. 2016;135(11):1233-9.
71. Kan W, Fang G, Chen L, Wang R, Deng Q. Influence of the R823W mutation on the interaction of the Anks6-Anks3: Insights from the molecular dynamics simulation and free energy analysis. Journal of Biomolecular Structure and Dynamics. 2015;34(5):1113-22.
72. Rothe B, Leettola CN, Leal-Esteban L, Cascio D, Fortier S, Isenschmid M, et al. Crystal structure of Bicc1 SAM polymer and mapping of interactions between the ciliopathy-associated proteins Bicc1, Anks3 and Anks6. Structure. 2018;26(2):209-24.
73. Rothe B, Leal-Esteban L, Bernet F, Urfer S, Doerr N, Weimbs T, et al. Bicc1 polymeriszation regulates the localisation and silencing of bound mRNA. Molecular and Cellular Biology. 2015;35(19):3339-53.
74. Tran U, Zakin L, Schweickert A, Agrawal R, Döger R, Blum M, et al. The RNA-binding protein bicaudal C regulates polycystin 2 in the kidney by antagonizing miR-17 activity. Development. 2010;137(7):1107-16.
75. Ramachandran H, Engel C, Müller B, Dengjel J, Wlaz G, Yakulov TA. Anks3 alters the sub-cellular localization of the Nek7 kinase. Biochemical and Biophysical Research Communications. 2015;464:901-7.
76. Hoffmann S. Cardiac-specific overexpression of angiotensin II type 1 receptor in transgenic rats. Methods in Molecular Medicine. 2005;112:389-403.
77. Subramanian A, Tamayo P, Mootha VK, Mukherjee S, Ebert BL, Gillette MA, et al. Gene set enrichment analysis: a knowledge-based approach for interpreting genome-wide expression profiles. Proceedings of the National Academy of Sciences of the United States of America. 2005;102(43):15545-50.
78. Ménoret S, Cin AD, Tesson L, Remy S, Usal C, Boulé JB, et al. Homology-directed repair in rodent zygotes using Cas9 and TALEN engineered proteins. Scientific Reports. 2015;5:14410.

79. Happe H, Peters DJ. Translational research in ADPKD: lessons from animal models. Nature Reviews Nephrology. 2014;10(10):587-601.
80. Piazzon N, Maisonneuve C, Guilleret I, Rotman S, Constam DB. Bicc1 links the regulation of cAMP signaling in polycystic kidneys to microRNA-induced gene silencing. Journal of Molecular Cell Biology. 2012;4(6):398-408.
81. Kraus MR, Clauin S, Pfister Y, Maïo MD, Ulinski T, Constam D, et al. Two mutations in human BICC1 resulting in Wnt pathway hyperactivity associated with cystic renal dysplasia. Human Mutation. 2012;33(1):86-90.
82. Ryan S, Verghese S, Cianciola NL, Cotton CU, Carlin CR. Autosomal recessive polycystic kidney disease epithelial cell model reveals multiple basolateral epidermal growth factor receptor sorting pathways. Molecular Biology of the Cell. 2010;21(15):2732-45.
83. Maisonneuve C, Guilleret I, Vick P, Weber T, Andre P, Beyer T, et al. Bicaudal C, a novel regulator of Dvl signaling abutting RNA-processing bodies, controls cilia orientation and leftward flow. Development. 2009;136(17):3019-30.
84. Robertis EMD. A targeted mutation of Bicc1. MGI Direct Data Submission. 2007.
85. Leal-Esteban LC, Rothé B, Fortier S, Isenschmid M, Constam DB. Role of Bicaudal C1 in renal gluconeogenesis and its novel interaction with the CTLH complex. PLoS Genetics. 2018;14(7):e1007487.
86. Fu Y, Kim I, Lian P, Li A, Zhou L, Li C, et al. Loss of Bicc1 impairs tubulomorphogenesis of cultured IMCD cells by disrupting E-cadherin-based cell-cell adhesion. European Journal of Cell Biology. 2010;89(6):428-36.
87. Yamamoto T, Sasaki S, Fushimi K, Ishibashi K, Yaoita E, Kawasaki K, et al. Vasopressin increases AQP-CD water channel in apical membrane of collecting duct cells in Brattleboro rats. American Journal of Physiology. 1995;268(6):C1546-51.
88. Yasui M, Zelenin SM, Celsi G, Aperia A. Adenylate cyclase-coupled vasopressin receptor activates AQP2 promoter via a dual effect on CRE and AP1 elements. American Journal of Physiology. 1997;272(4):F443-50.
89. Rojek A, Füchtbauer EM, Kwon TH, Frøkiær J, Nielsen S. Severe urinary concentrating defect in renal collecting duct-selective AQP2 conditional-knockout mice. Proceedings of the National Academy of Sciences. 2006;103(15):6037-42.
90. Radin MJ, Yu MJ, Stoedkilde L, Miller RL, Hoffert JD, Frokiaer J, et al. Aquaporin-2 Regulation in Health and Disease. Veterinary Clinical Pathology. 2012;41(4):455-70.
91. Veeraveedu PT, Watanabe K, Ma M, Palaniyandi SS, Yamaguchi K, Suzuki K, et al. Effects of nonpeptide vasopressin V2 antagonist tolvaptan in rats with heart failure. Biochemical Pharmacology. 2007;74(10):1466-75.
92. Torres VE, Chapman AB, Devuyst O, Gansevoort RT, Grantham JJ, Higashihara E, et al. Tolvaptan in patients with autosomal dominant polycystic kidney disease. New England Journal of Medicine. 2012;367(25):2407-18.
93. Seeger-Nukpezah T, Geynisman DM, Nikonova AS, Benzing T, Golemis EA. Unexpected relevance of the hallmarks of cancer to the pathogenesis of polycystic kidney disease. Nature Reviews- Nephrology. 2015;11(9):515-34.
94. Tan R, Nakajima S, Wang Q, Sun H, Xue J, Wu J, et al. Nek7 Protects Telomeres from Oxidative DNA Damage by Phosphorylation and Stabilization of TRF1. Molecular Cell. 2017;65(5):818-31.
95. Abeyta A, Castella M, Jacquemont C, Taniguchi T. NEK8 regulates DNA damage-induced RAD51 foci formation and replication fork protection. Cell Cycle. 2017;16(4):335-47.
96. MAnning DK, Sergeev M, Heesbeen RGv, Wong MD, Oh JH, Liu Y, et al. Loss of the ciliary kinase Nek8 causes left-right asymmetry defects. Journal of the American Society of Nephrology. 2012;24(1):100-12.
97. McQuinn TC, Miga DE, Mjaatvedt CH, Phelps AL, Wessels A. Cardiopulmonary malformations in the inv/inv mouse. The anatomical record. 2001;263(1):62-71.

98. Chakravarthy DJK, Sarma YS, Sriharibabu M, Subhramanyam K, Sivakumar T, Chandrakanth K. Bardet-Biedl syndrome presenting as dilated cardiomyopathy. Journal of Indian College of Cardiology. 2013;3(3):134-8.
99. Marshall JD, Maffei P, Collin GB, Naggert JK. Alström Syndrome: Genetics and Clinical Overview. Current Genomics. 2011;12:225-35.
100. Amiri FS, Kariminejad A. Juvenile nephronophthisis and dysthyroidism: a rare association. Clinical and Experimental Nephrology Case Reports. 2017;6(1):98-104.
101. Bergmann C, Fliegauf M, Brüchle NO, Frank V, Olbrich H, Kirschner J, et al. Loss of nephrocystin-3 function can cause embryonic lethailty, Meckel-Gruber-like syndrome, situs inversus, and renal-hepatic-pancreatic dysplasia. American Journal of Human Genetics. 2008;82(4):959-70.
102. Biswas A, Ghosh JK, Sinha MK, Basu K, Chatterjee S. Mohr-Claussen Syndrome or Oro-Facial-Digital Syndrome (OFDS) Type-II Journal of the Pakistan Medical Association. 2009;59(7):484-6.
103. Darmency-Stamboul V, Burglen L, Lopez E, Mejean N, Dean J, Franco B, et al. Detailed clinical, genetic and neuroimaging characterization of OFD VI syndrome. European Journal of Medical Genetics. 2013;56(6):301-8.
104. Sang L, Miller JJ, Corbit KC, Giles RH, Brauer MJ, Otto EA, et al. Mapping the NPHP-JBTS-MKS protein network reveals ciliopathy disease genes and pathways. Cell. 2011;145(5):513-28.
105. Weatherbee SD, Niswander LA, Anderson KV. A mouse model for Meckel syndrome reveals Mks1 is required for ciliogenesis and Hedgehog signaling. Human Molecular Genetics. 2009;18(23):4565-75.
106. Rachel RA, May-Simera HL, Veleri S, Gotoh N, Choi BY, Murga-Zamalloa C, et al. Combining Cep290 and Mkks ciliopathy alleles in mice rescues sensory defects and restores ciliogensis. The Journal of Clinical Investigation. 2012;122(4):1233-45.
107. Li G, Vega R, Nelms K, Gekakis N, Goodnow C, McNamara P, et al. A Role for Alström syndrome protein, alms1, in kidney ciliogenesis and cellular quiescence. PLoS Genetics. 2007;3(1):e8.
108. Berbari NF, Lewis JS, Bishop GA, Askwith CC, Mykytyn K. Bardet-Biedl syndrome proteins are required for teh localization of G protein-coupled receptors to primary cilia. Proceedings of the National Academy of Sciences of the United States of America. 2008;105(11):4242-6.
109. Bouvrette DJ, Sittaramane V, Heidel JR, Chandrasekhar A, Bryda EC. Knockdown of Bicaudal C in zebrafish (Danio rerio) causes cystic kidneys: a nonmammalian model of polycystic kidney disease. Comparative medicine. 2010;60(2):96-106.
110. Flaherty L, Messer A, Russell LB, Rinchik EM. Chlorambucil-induced mutations in mice recovered in homozygotes. Proceedings of the National Academy of Sciences of the United States of America. 1992;89(7):2859-63.
111. Nauta J, Ozawa Y, Jr WES, Rutledge JC, Avner ED. Renal and biliary abnormalities in a new murine model of autosomal recessive polycystic kidney disease. Pediatric Nephrology. 1993;7(2):163-72.
112. King TC. 4- Genetic and Perinatal Disease. In: King TC, editor. Elsevier's Integrated Pathology: Mosby; 2007. p. 89-110.
113. Qiu C, Yu J. The function of polycystin-1 and polycystin-2 in cadiovascular system. Journal of Cardiovascular Diseases and Diagnosis. 2013;1:110.
114. Mohieldin AM, Hymour HS, Lo ST, AbouAlaiwa WA, Atkinson KF, Ward CJ, et al. Protein composition and movements of membrane swellings associated with primary cilia. Cellular and Molecular Life Sciences. 2015;72(12):2415-29.
115. Lindstrand A, Davis EE, Carvalho CMB, Pehlivan D, Willer JR, Tsai IC, et al. Recurrent CNVs and SNVs at the NPHP1 locus contribute pathogenic allels to Bardet-Biedl syndrome. American Journal of Human Genetics. 2014;94(5):745-54.
116. Lindstrand A, Frangakis S, Carvalho CMB, Richardson EB, McFadden KA, Willer JR, et al. Copy-number variation contributes to the mutational load of Bardet-Biedl syndrome. American Journal of Human Genetics. 2016;99(2):318-36.

117. Gerhardt C, Lier JM, Kuschel S, Rüther U. The ciliary protein Ftm is required for ventricular wall and septal development. PLoS ONE. 2013;8(2):e57545.
118. Vierkotten J, Dildrop R, Peters T, Wang B, Rüther U. Ftm is a novel basal body protein of cilia involved in Shh signalling. Development. 2007;134:2569-77.
119. Tsukui T, Capdevila J, Tamura K, Ruiz-Lozano P, Rodriguez-Esteban C, Yonei-Tamura S, et al. Multiple left-right asymmetry defects in Shh-/- mutant mice unveil a convergence of the Shh and retinoic acid pathways in control of Lefty-1. Proceedings of the National Academy of Sciences of the United States of America. 1999;96(20):11376-81.
120. Plouffe SW, Hong AW, Guan KL. Disease implications of the Hippo/YAP pathway. Trends in Molecular Medicine. 2015;21(4):212-22.
121. Wang Y, Zhou CJ, Liu Y. Wnt signaling in kidney development and disease. Progress in molecular biology and translational science. 2018;153:181-207.
122. Belibi F, Zafar I, Ravichandran K, Segvic AB, Jani A, Ljubanovic DG, et al. Hypoxia-inducible factor-1α (HIF-1α) and autophagy in polycystic kidney disease (PKD). American Journal of Physiology: Renal Physiology. 2011;300(5):F1235-F43
123. Schlimpert M, Lagies S, Budnyk V, Müller B, Walz G, Kammerer B. Metabolic phenotyping of Anks3 depletion in mIMCD-3 cells- aputative nephronophthisis candidate. Scientific Reports. 2018;8(1):9022.

FIGURE AND TABLE LIST

APPENDIX

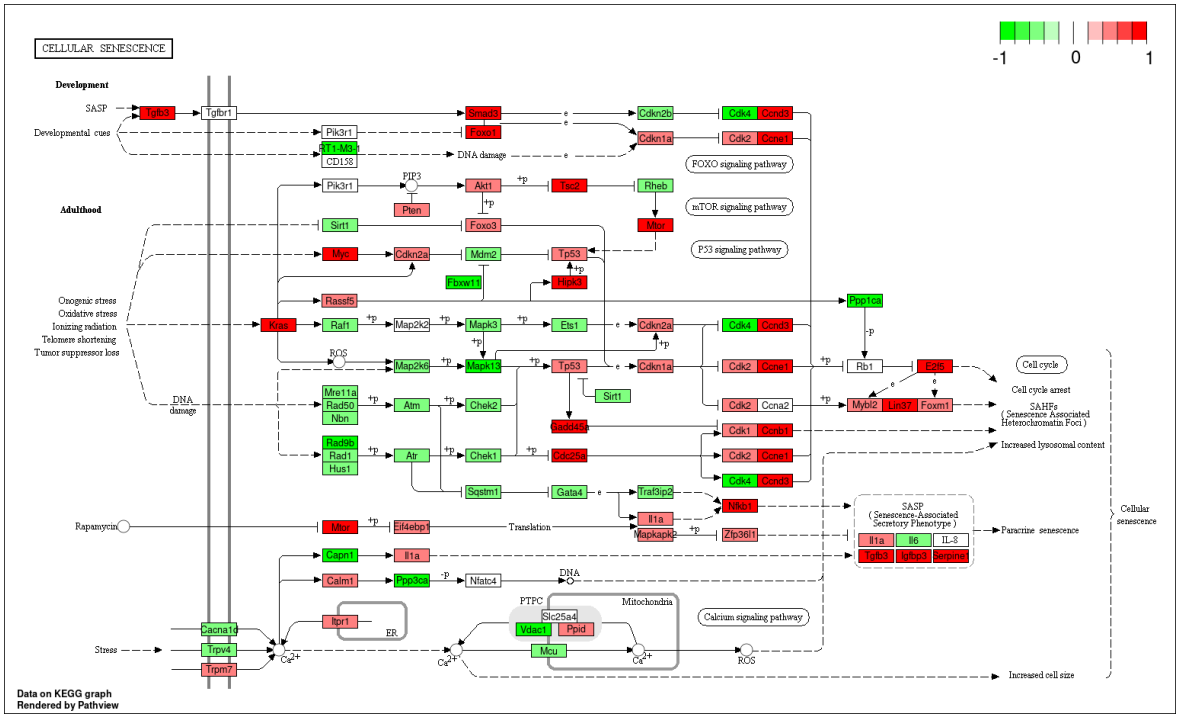

Figure 46– Changes in cellular senescence mRNA expression in TGRAnks6 vs wildtype rats.

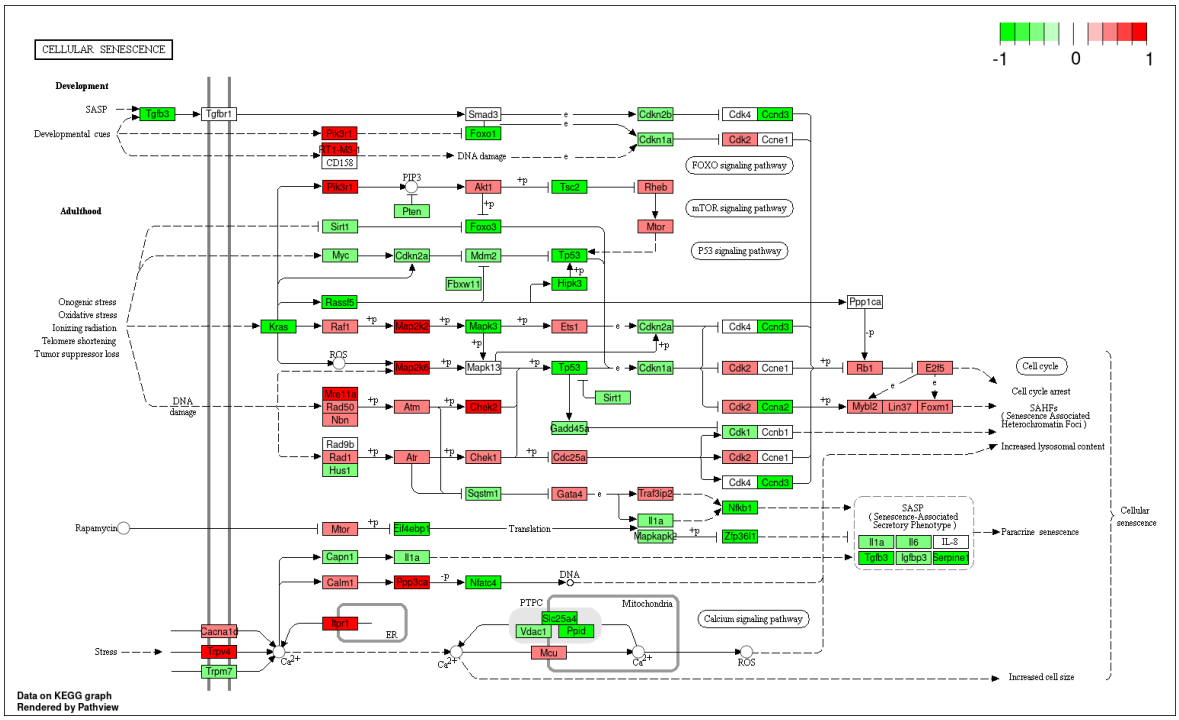

Figure 47– Changes in cellular senescence mRNA expression in TGRAnks6-Anks3$^{KI/KI}$ vs TGRAnks6 rats.

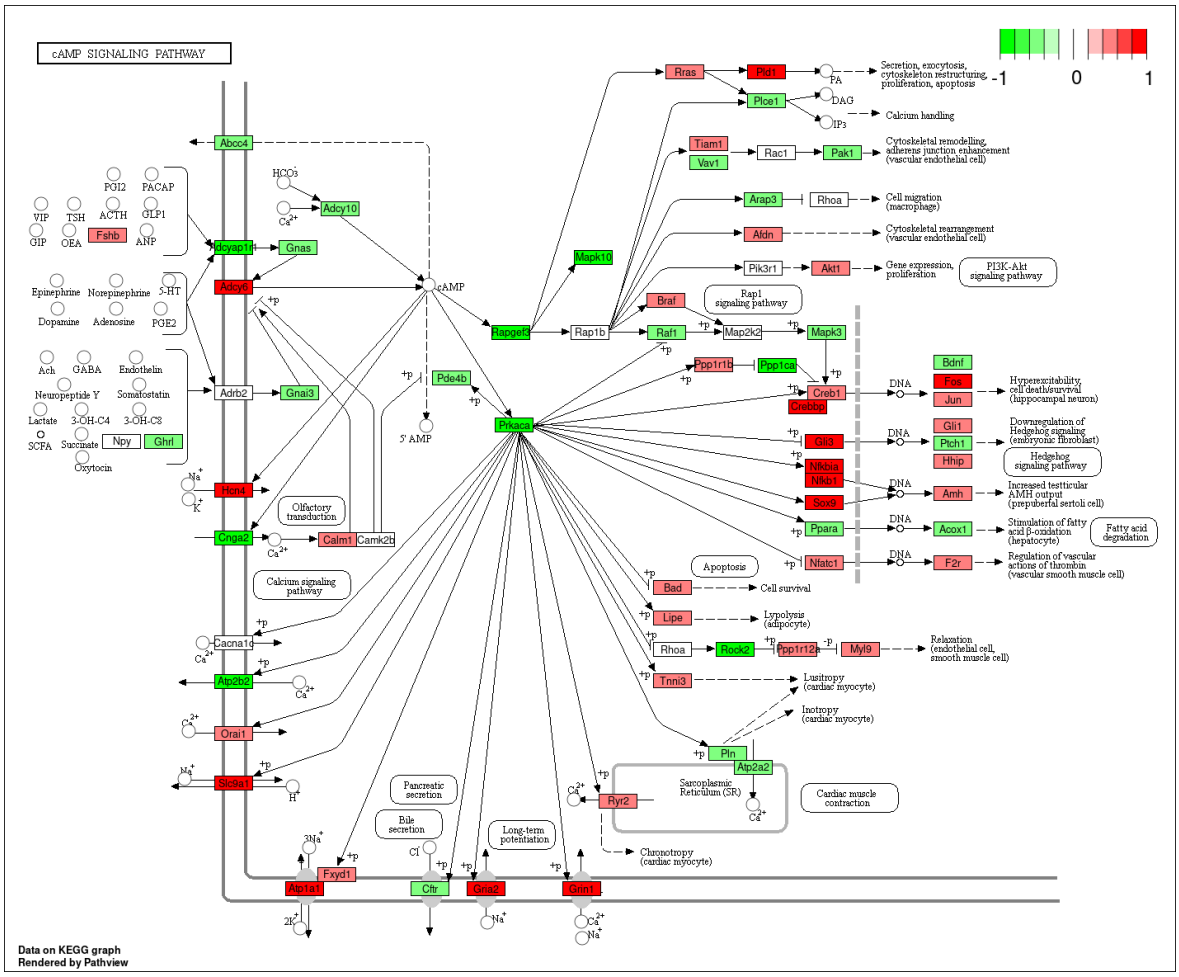

Figure 48- Changes in the cAMP signalling pathway mRNA expression in TGRAnks6 vs wildtype rats.

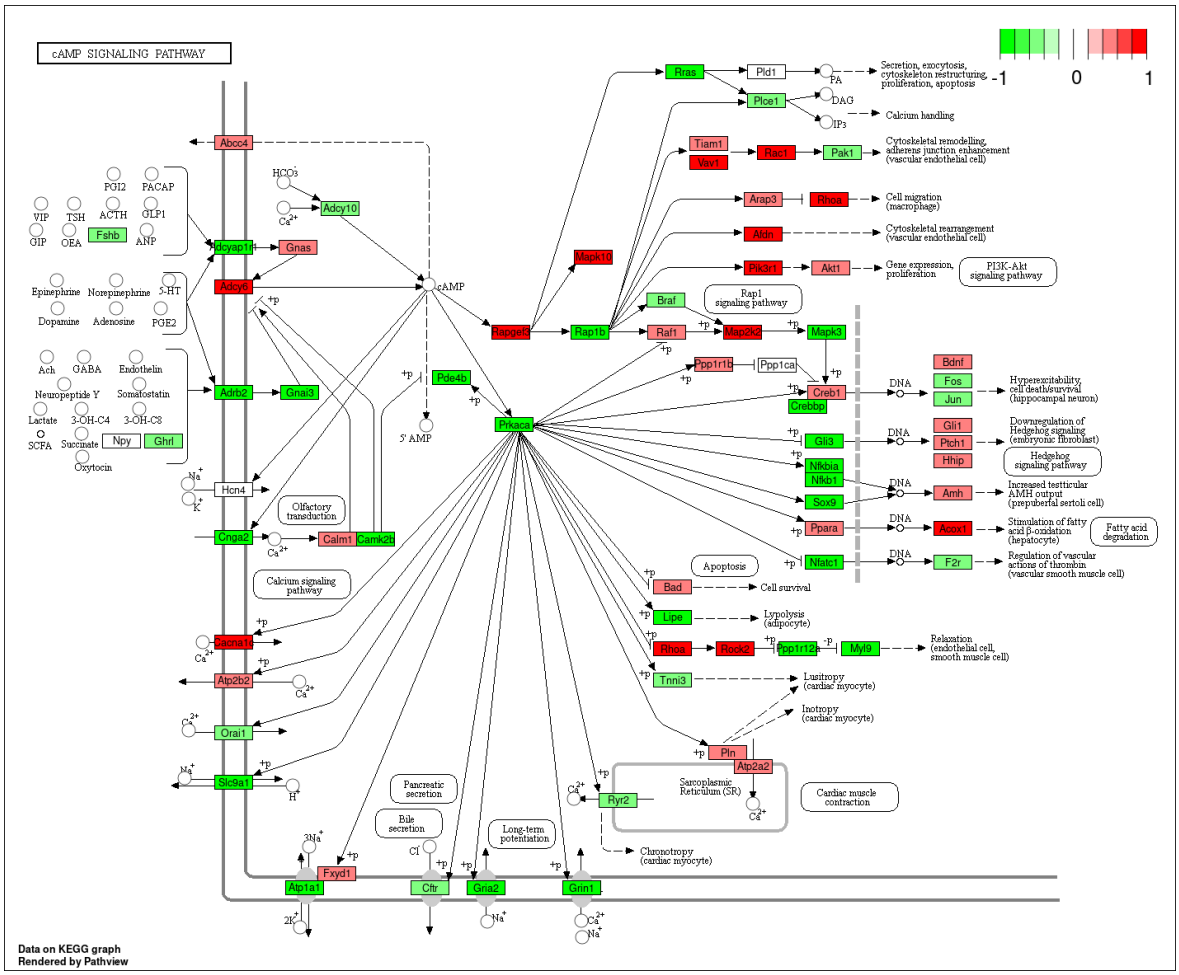

Figure 49- Changes in the cAMP signalling pathway mRNA expression in TGRAnks6-Anks3$^{KI/KI}$ vs TGRAnks6 rats.

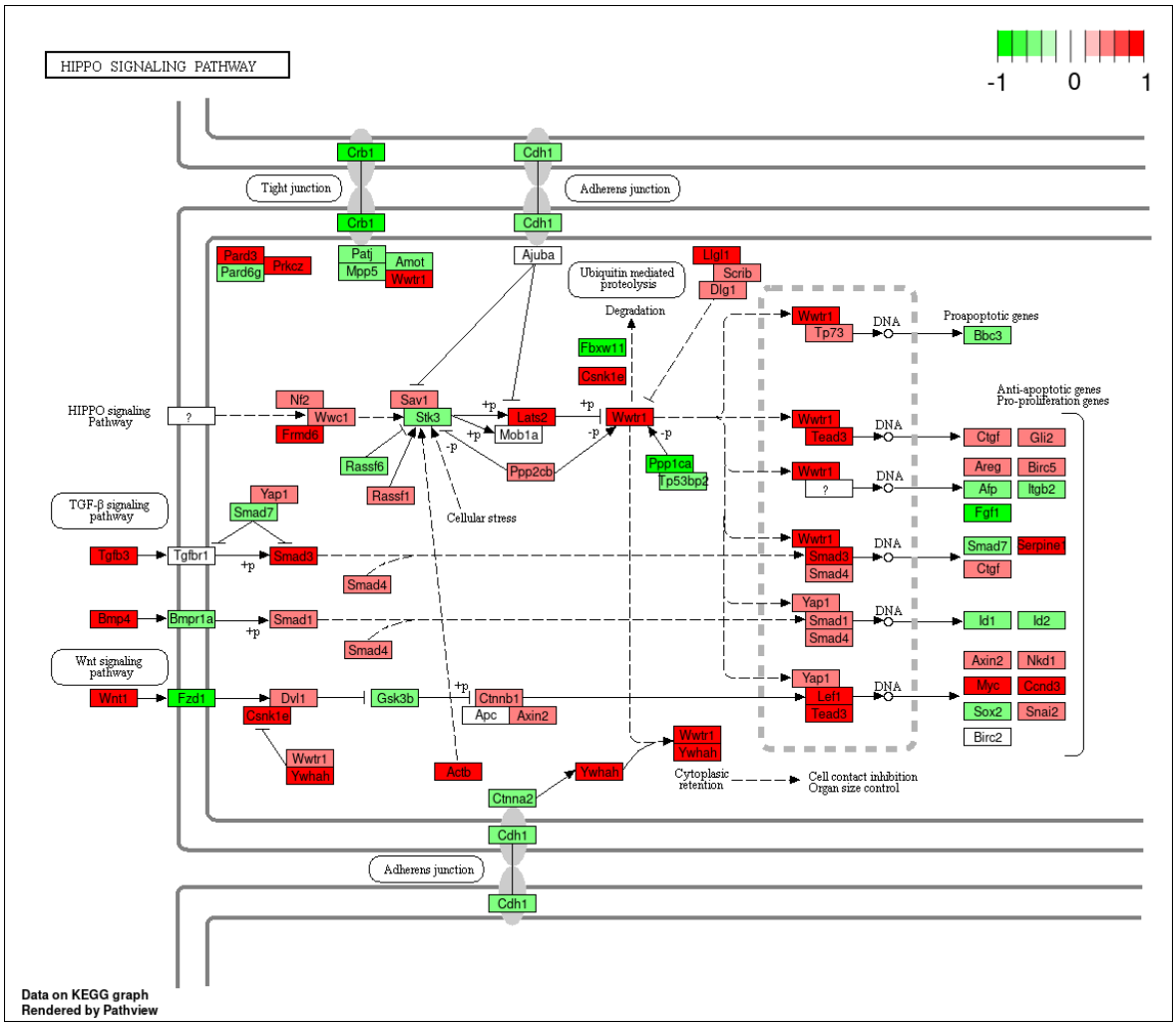

Figure 50- Changes in the Hippo signalling pathway mRNA expression in TGRAnks6 vs wildtype rats.

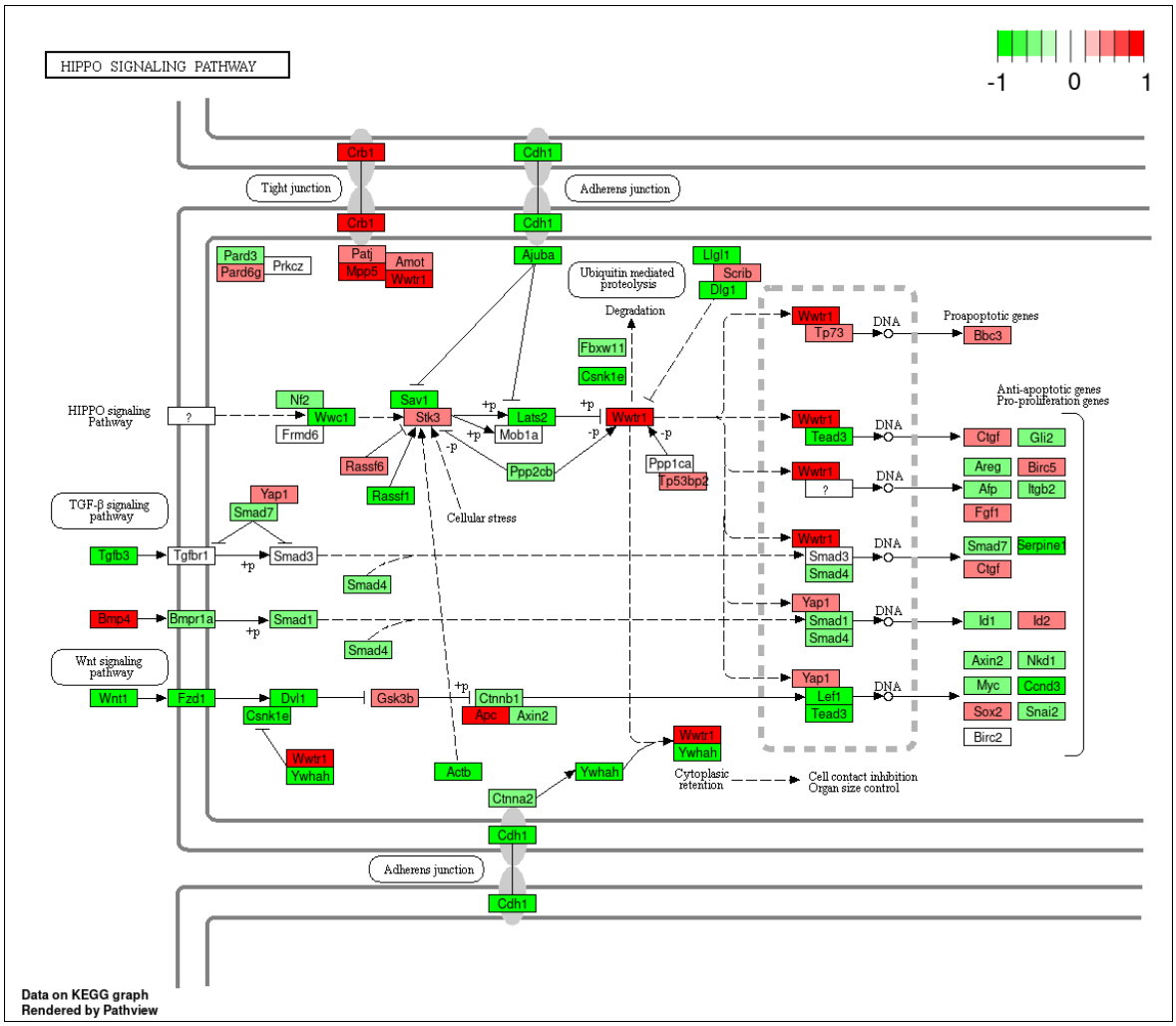

Figure 51- Changes in the Hippo signalling pathway mRNA expression in TGRAnks6-Anks3$^{KI/KI}$ vs TGRAnks6 rats.

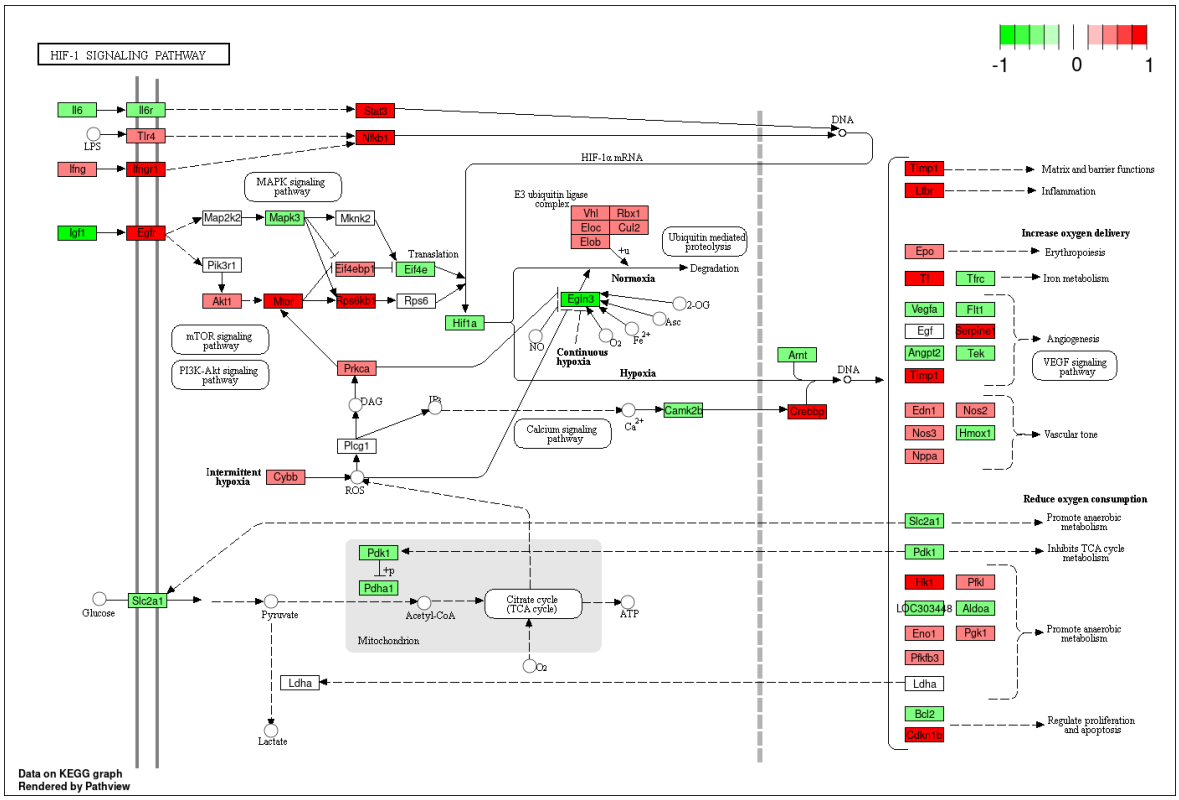

Figure 52- Changes in the HIF-1 signalling pathway mRNA expression in TGRAnks6 vs wildtype rats.

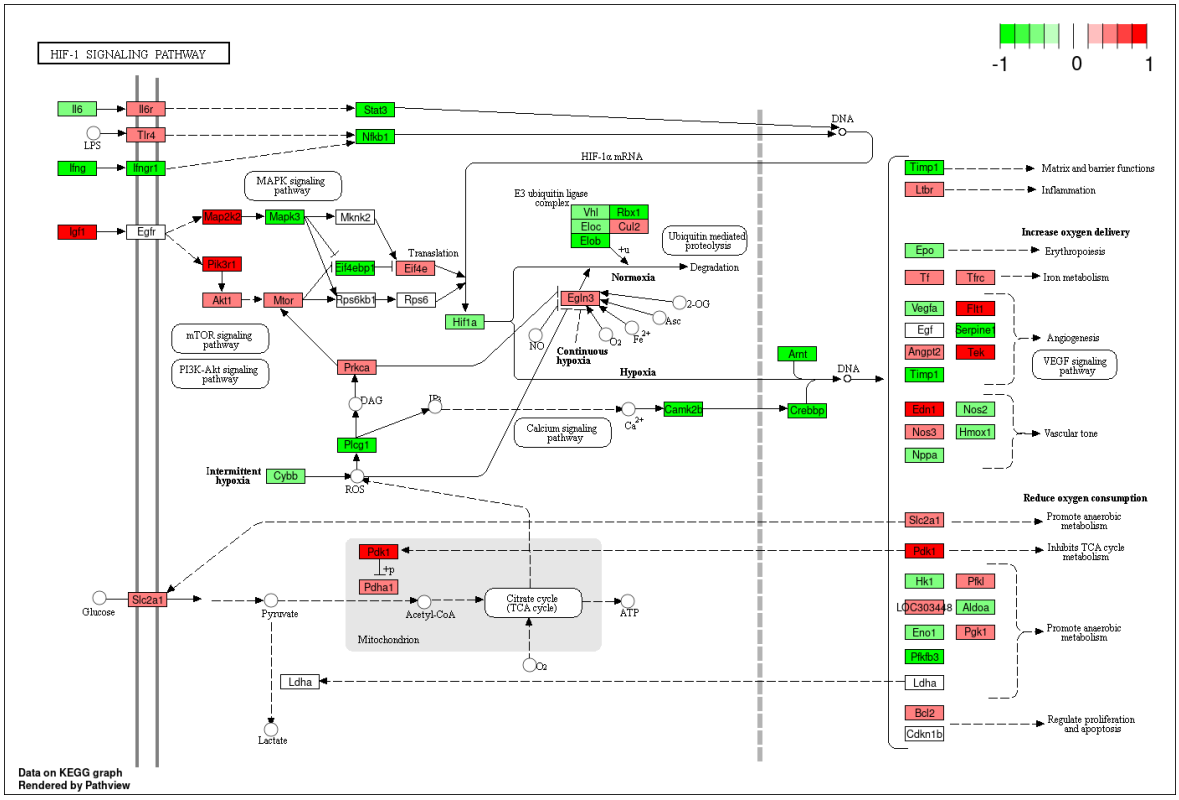

Figure 53- Changes in the HIF-1 signalling pathway mRNA expression in TGRAnks6-Anks3$^{KI/KI}$ vs TGRAnks6 rats.

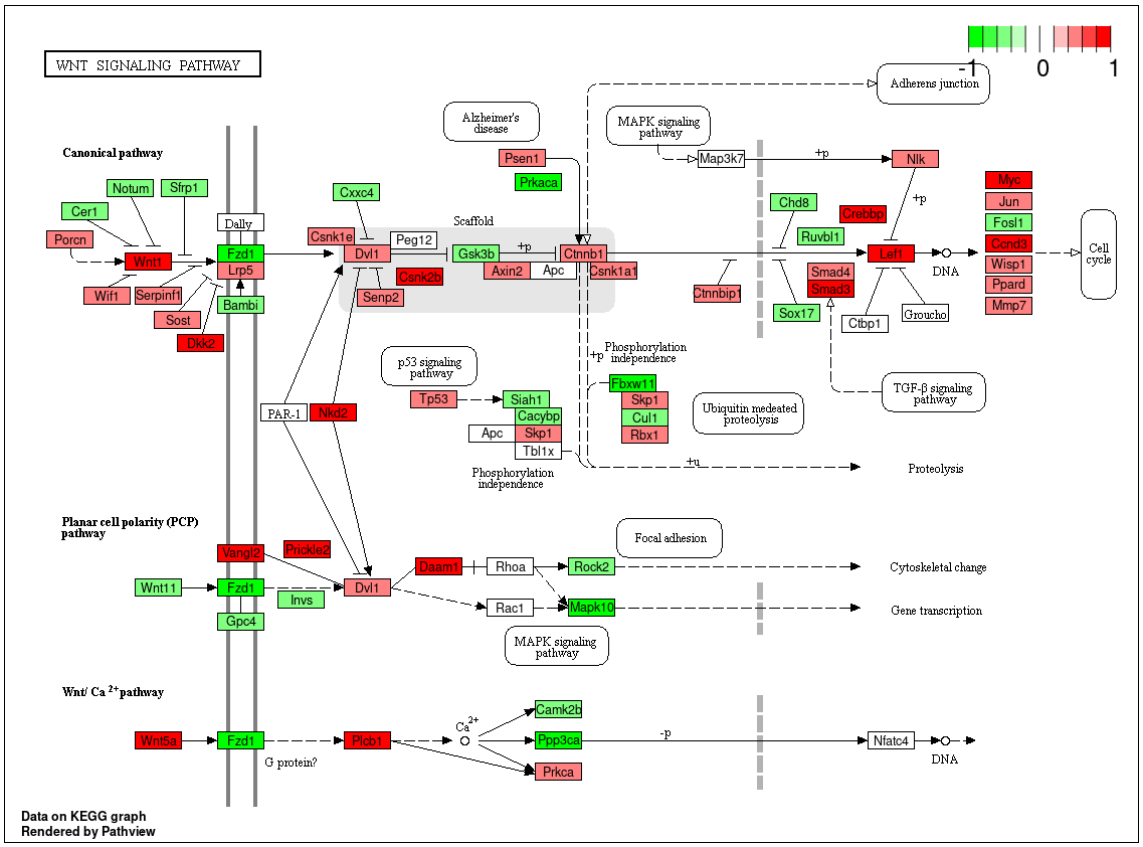

Figure 54- Changes in the Wnt signalling pathway mRNA expression in TGRAnks6 vs wildtype rats.

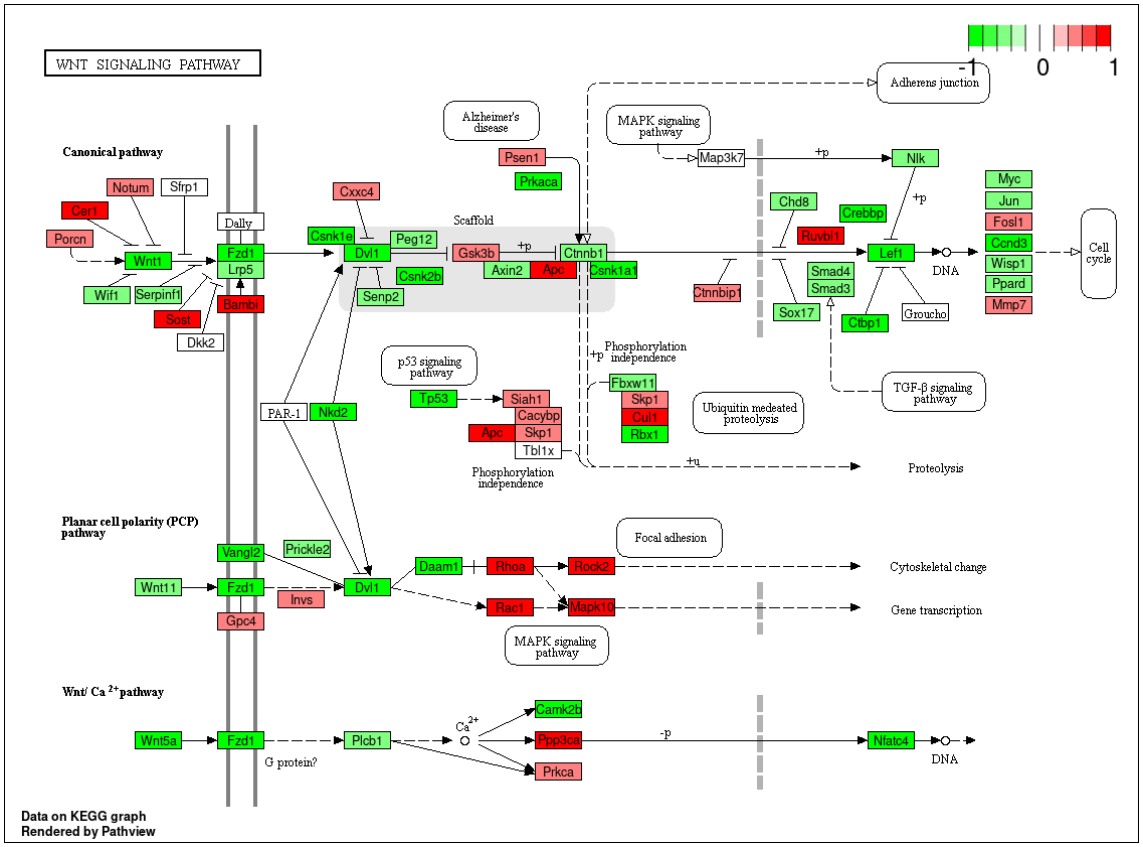

Figure 55- Changes in the Wnt signalling pathway mRNA expression in TGRAnks6-Anks3$^{KI/KI}$ vs TGRAnks6 rats.

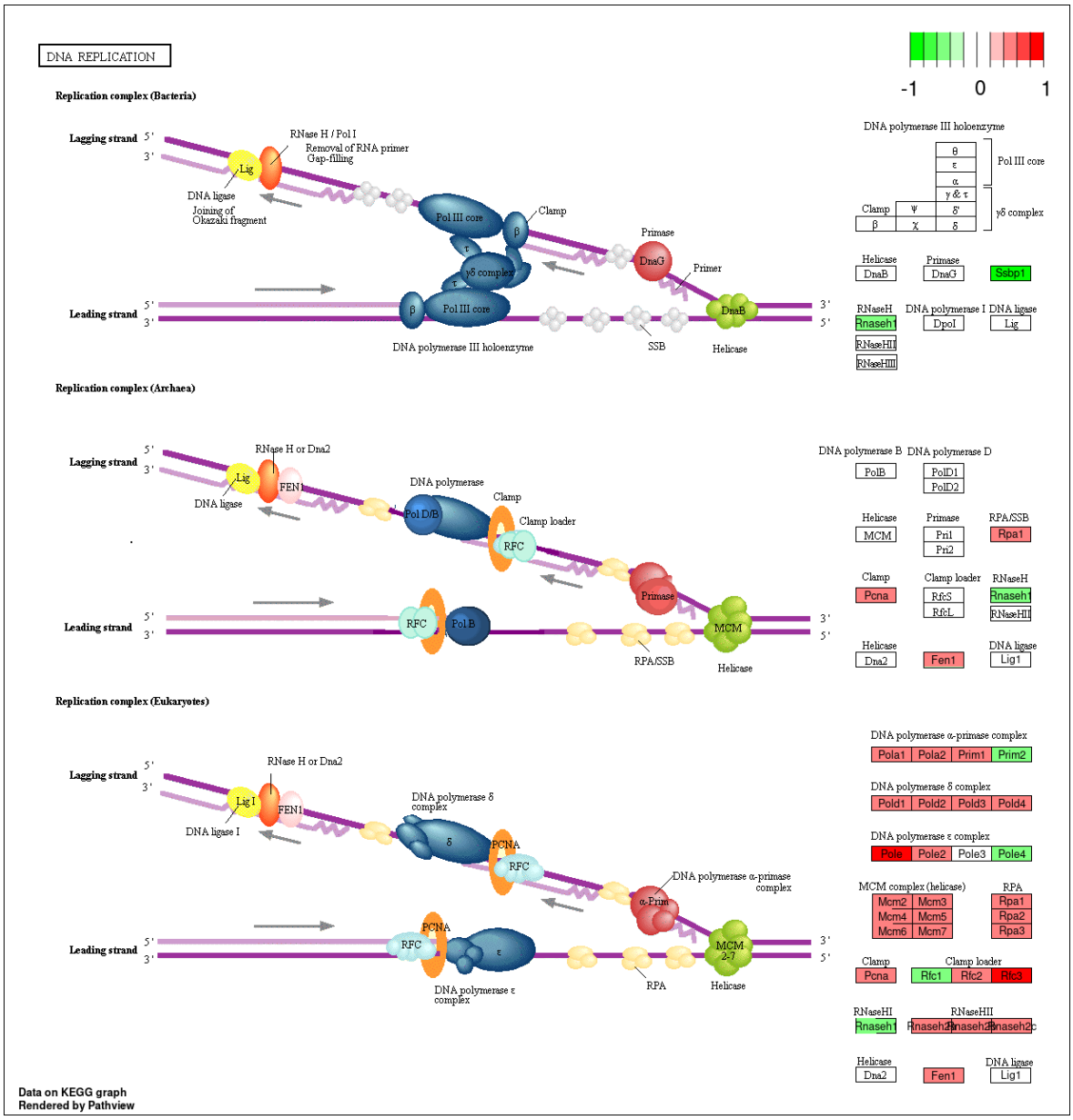

Figure 56- Changes in mRNA expression of the DNA replication machinery in TGRAnks6 vs wildtype rats.

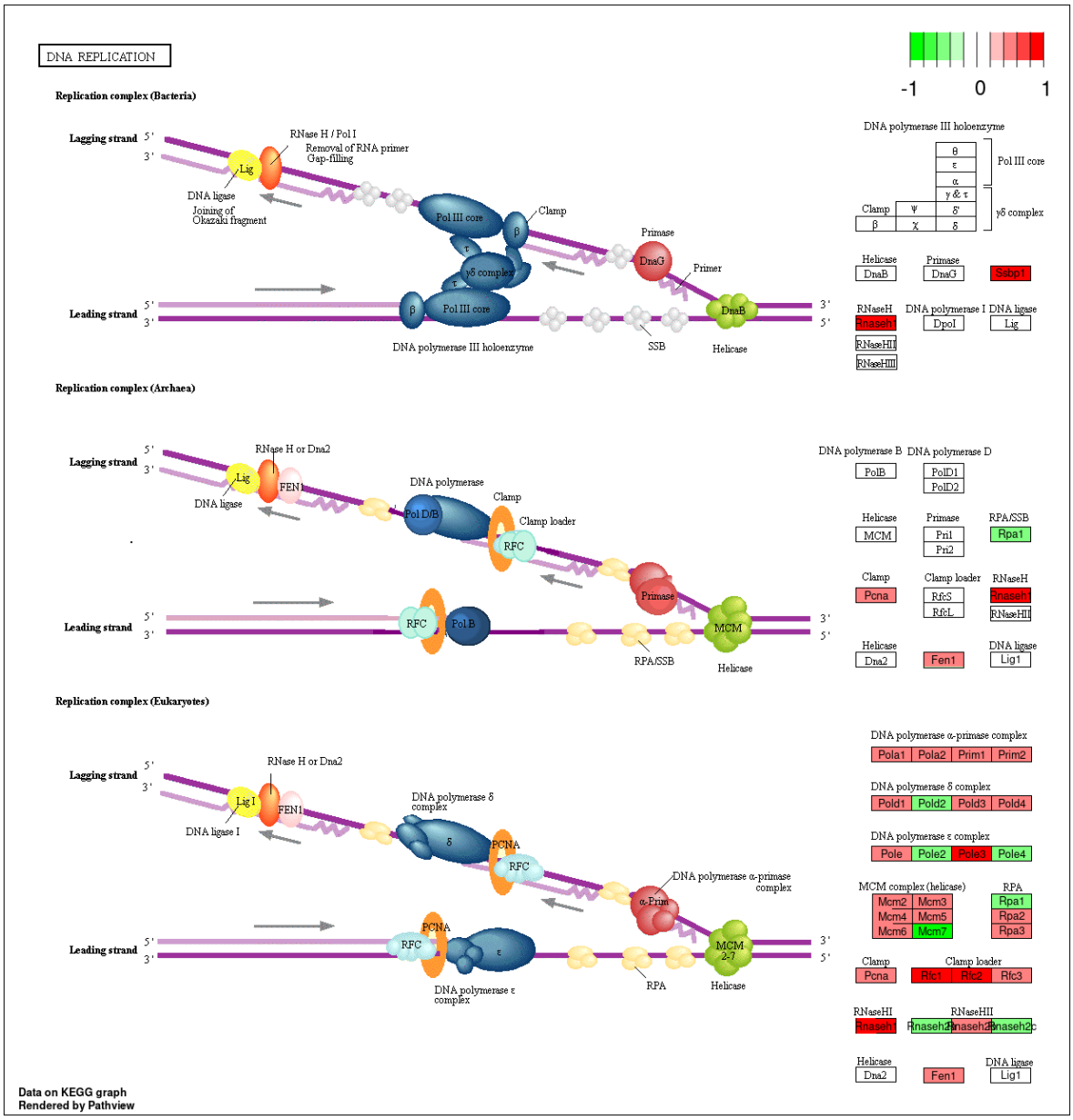

Figure 57- Changes in mRNA expression of the DNA replication machinery in TGRAnks6-Anks3$^{KI/KI}$ vs TGRAnks6 rats.

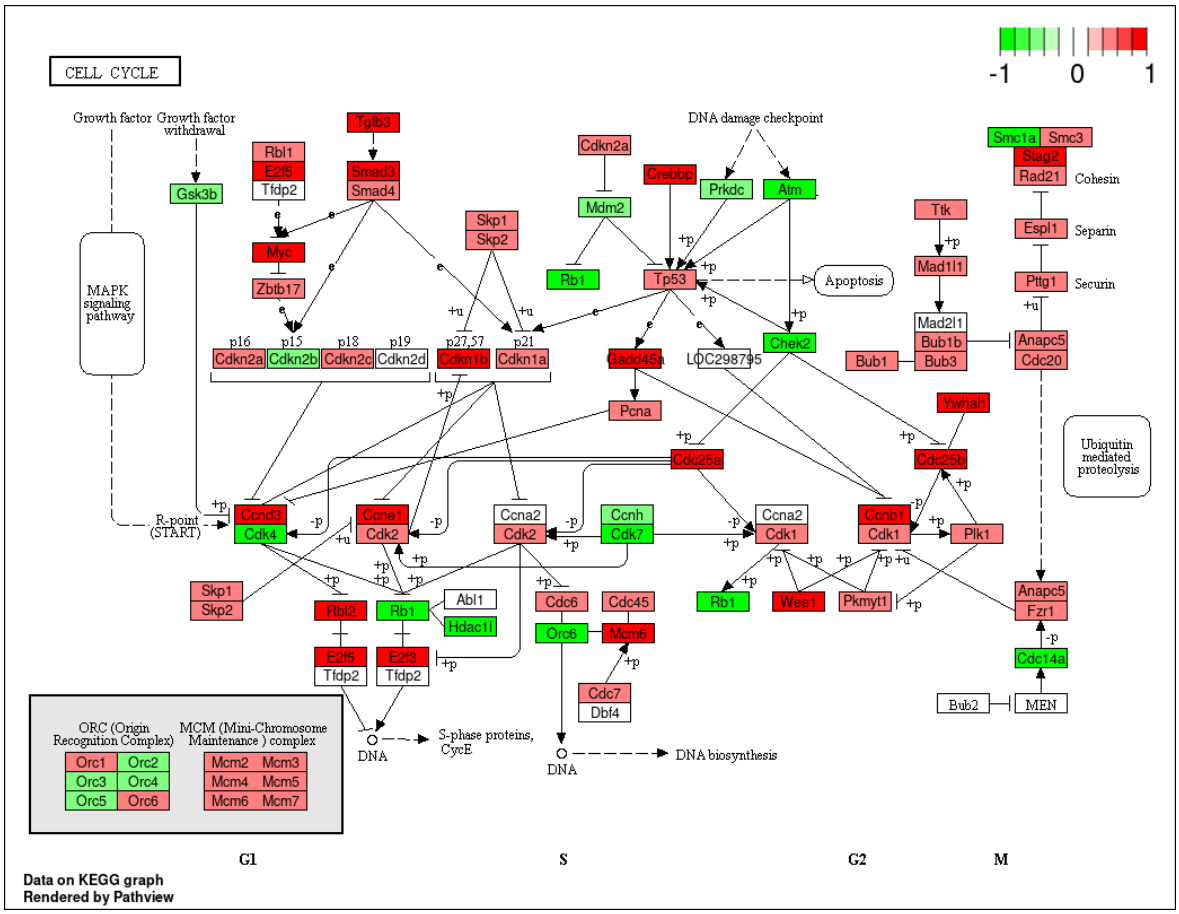

Figure 58- Changes in mRNA expression of the cell cycle machinery in TGRAnks6 vs wildtype rats.

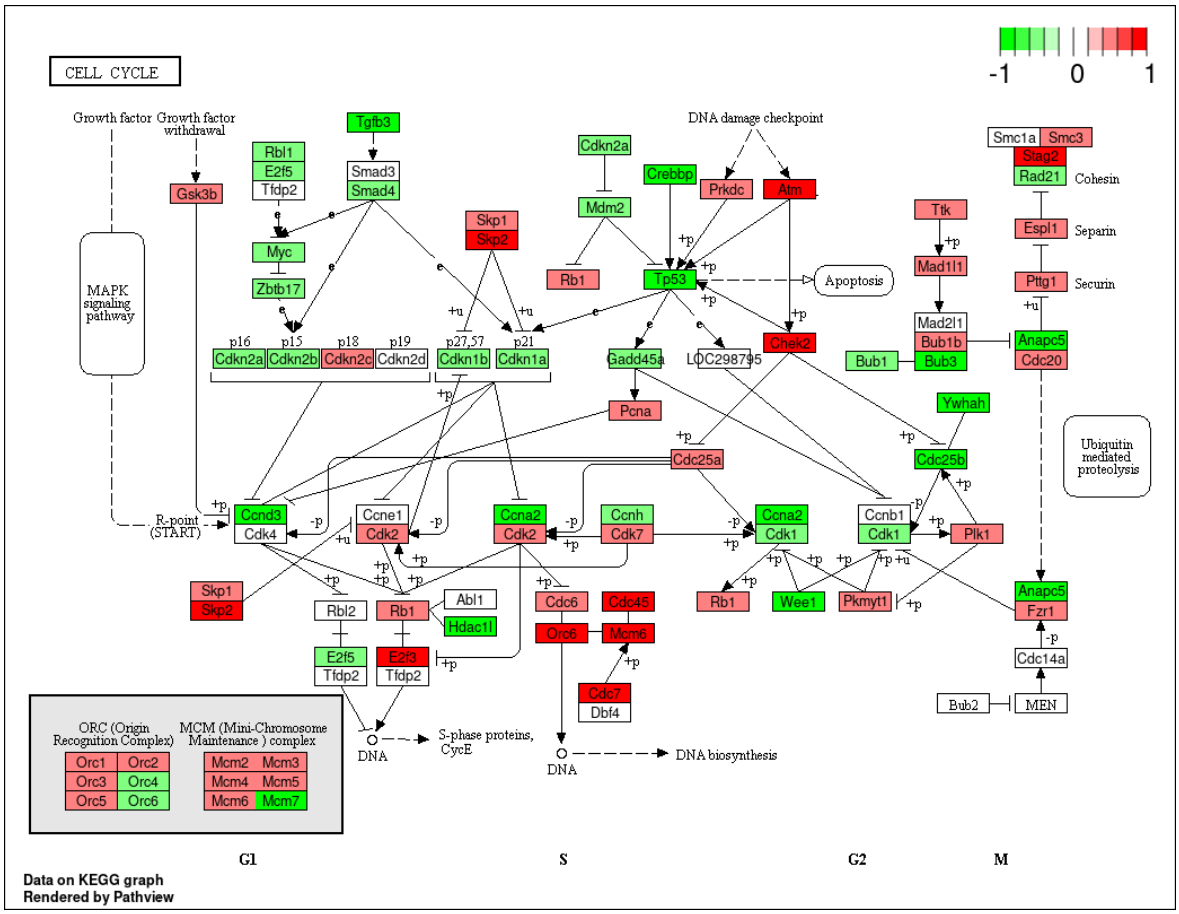

Figure 59- Changes in mRNA expression of the cell cycle machinery in TGRAnks6-Anks3$^{KI/KI}$ vs TGRAnks6 rats.

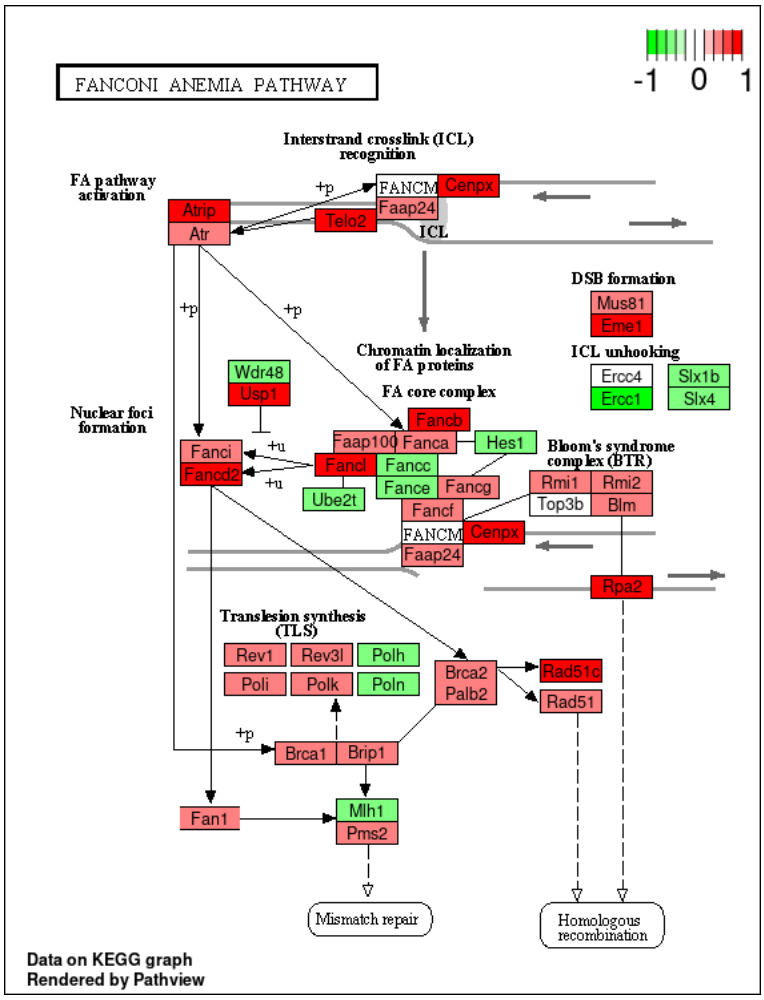

Figure 60- Changes in mRNA expression of the fanconi anaemia pathway in TGRAnks6-Anks3$^{KI/KI}$ vs wildtype rats.

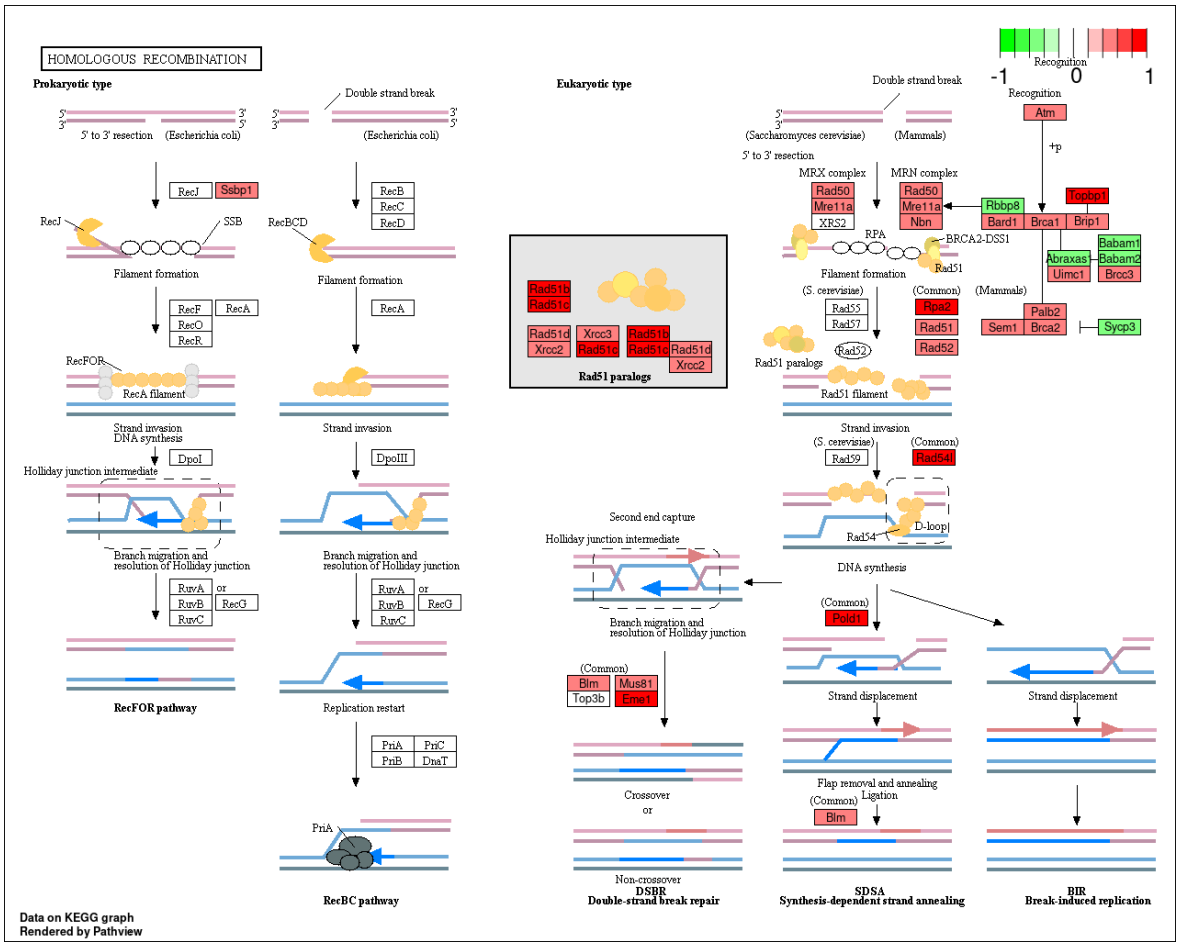

Figure 61- Changes in mRNA expression of the homologous recombination machinery in TGRAnks6-Anks3$^{KI/KI}$ vs wildtype rats.

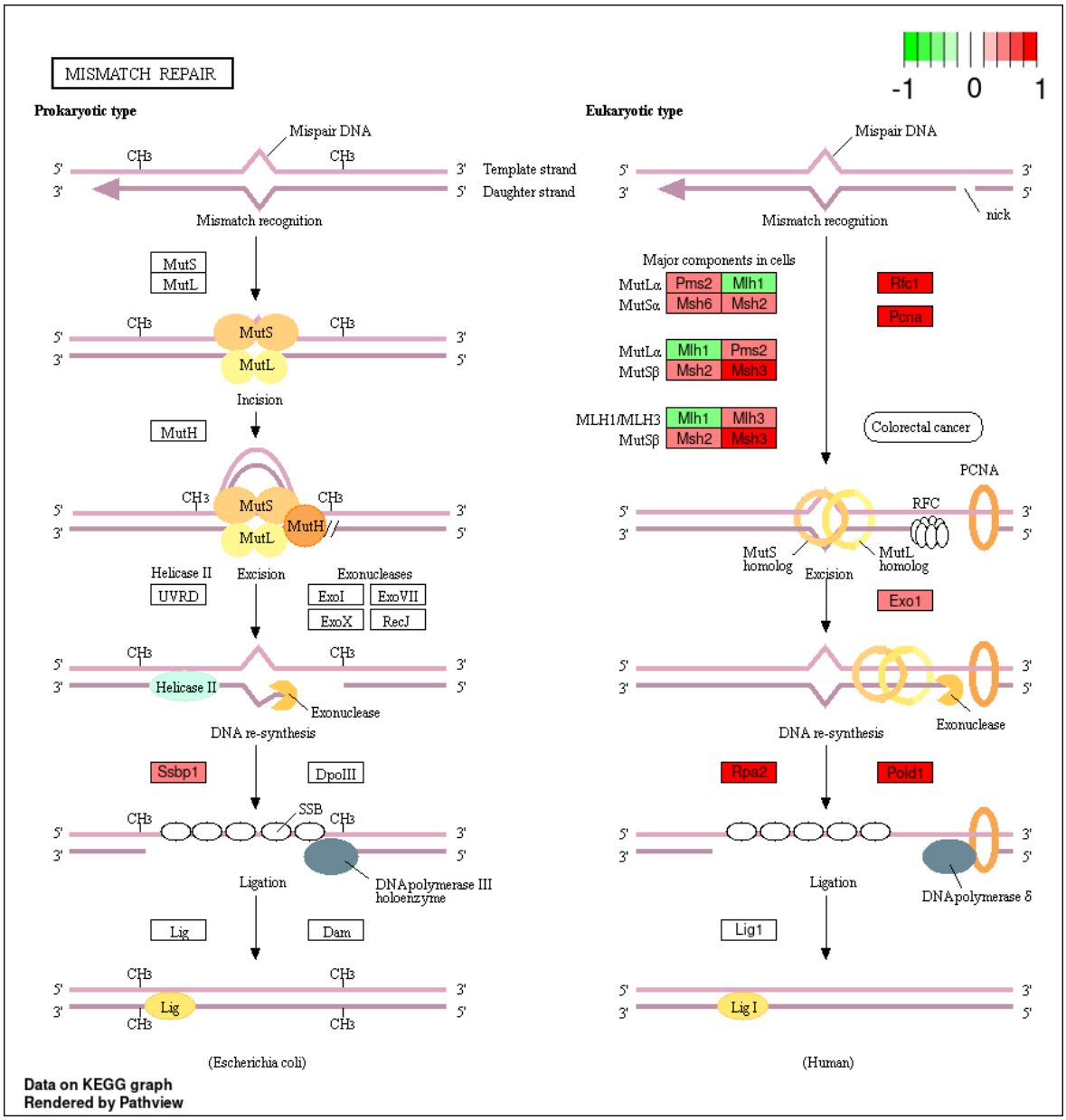

Figure 62- Changes in mRNA expression of the mismatch repair machinery in TGRAnks6-Anks3$^{KI/KI}$ vs wildtype rats.

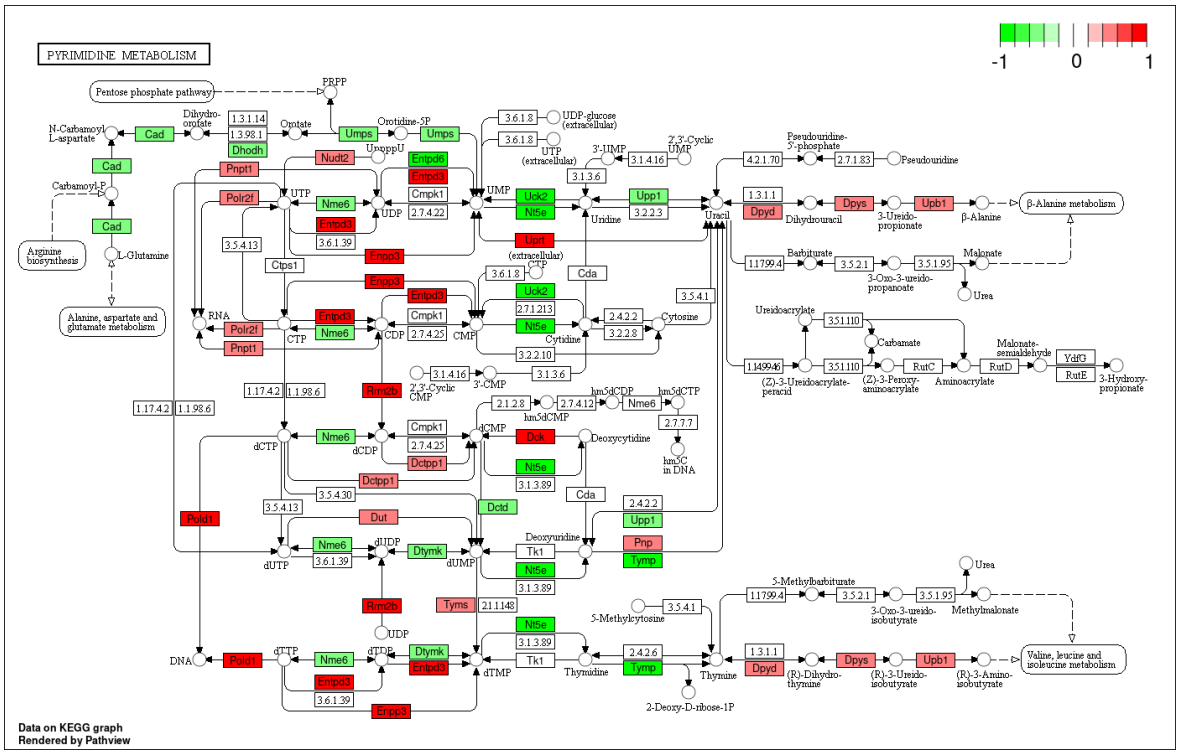

Figure 63- Changes in mRNA expression of the pyrimidine metabolism machinery in TGRAnks6-Anks3$^{KI/KI}$ vs wildtype rats.

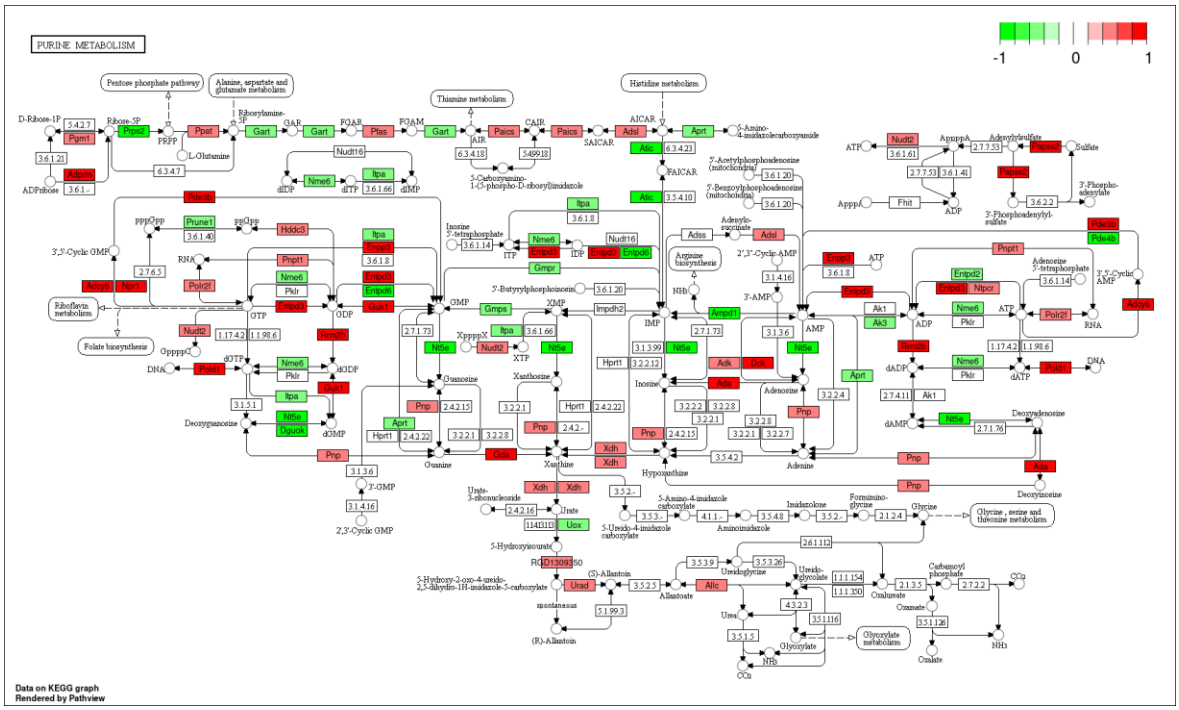

Figure 64- Changes in mRNA expression of the purine metabolism machinery in TGRAnks6-Anks3$^{KI/KI}$ vs wildtype rats.

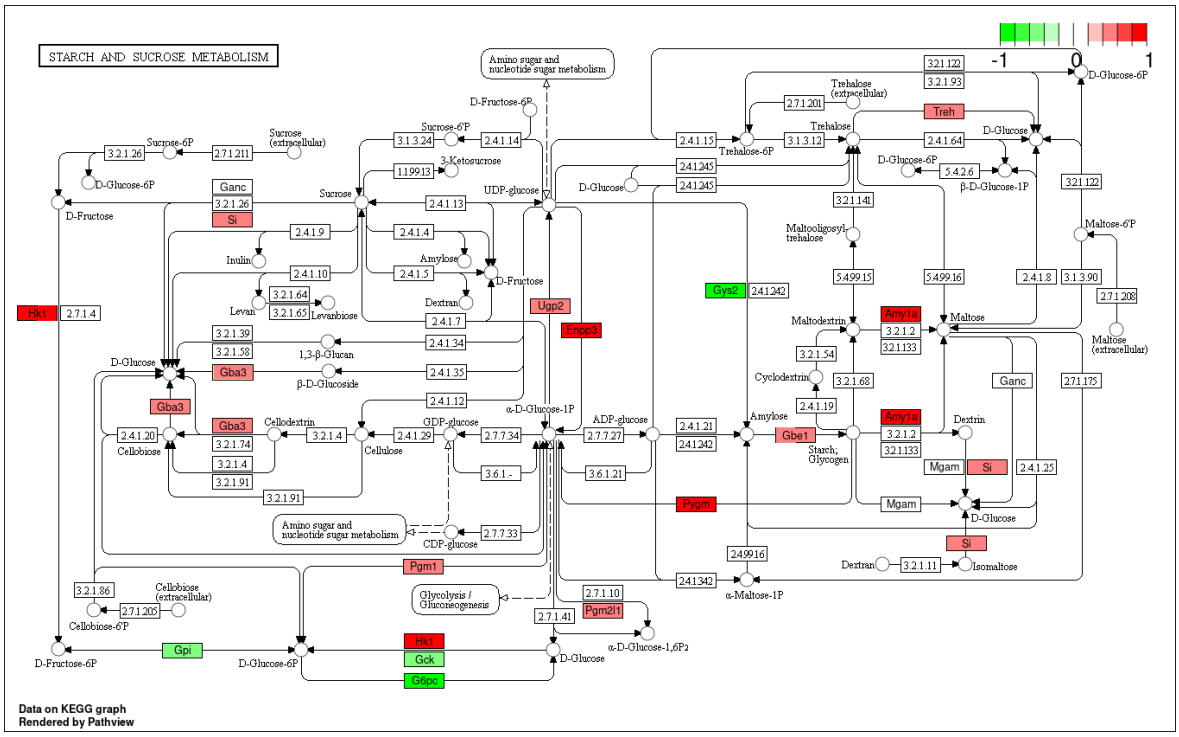

Figure 65- Changes in mRNA expression of the starch and sucrose metabolism machinery in TGRAnks6-Anks3$^{KI/KI}$ vs wildtype rats.

ACKNOWLEDGMENTS

I would like to thank the NIH for funding this project (5RO1DK100482)

I would like to thank Prof. Dr. Sigrid Hoffmann for providing me the oportunity to work on this project and for supervision throughout this project.

I would like to thank the group of Prof. James Bowie who gave input for this work from the in vitro and protein crystalography work..

I would like to thank my colleages Tamara Micakovic, Yalcin Kuzay, Sabrina Klingele, Christian Gosmann, Wiktoria Banczyk and Dian Bolhuis for experimental assistance throughout this project.

I would like to thank Matina Papagiannarou, Dr. Elisabeth Seelinger and Cathleen Fichtner for technical assistance throughout this project.

I would like to thank Carolina De La Torre and Dr. Carsten Sticht for analysis of the microarrays.

I would like to thank Alexia Giannakopoulou, Viktoria Skude and Alexander Schlund for assitance with animal work throughout this project.

I would like to thank Prof. Dr. Hermann-Josef Gröne and Prof. Dr. Gergana Dobreva for histological analysis of samples.

I would like to thank Dr. Marc Pretze for performing the MRIs of the embryos and the financial support of the German Research Foundation for the small animal 1T MRI imaging system ICON [funding code: INST 91027/11-1-FUGG] to Prof. Dr. Björn Wängler.

I would like to thank my mother, Elspeth Clark, for editing my work.